Afterload system design for functional donor heart assessment

Pigot, Harry

2024

Document Version:
Publisher's PDF, also known as Version of record

Afterload system design for functional donor heart assessment

HENRY PIGOT
DEPARTMENT OF AUTOMATIC CONTROL | LUND UNIVERSITY

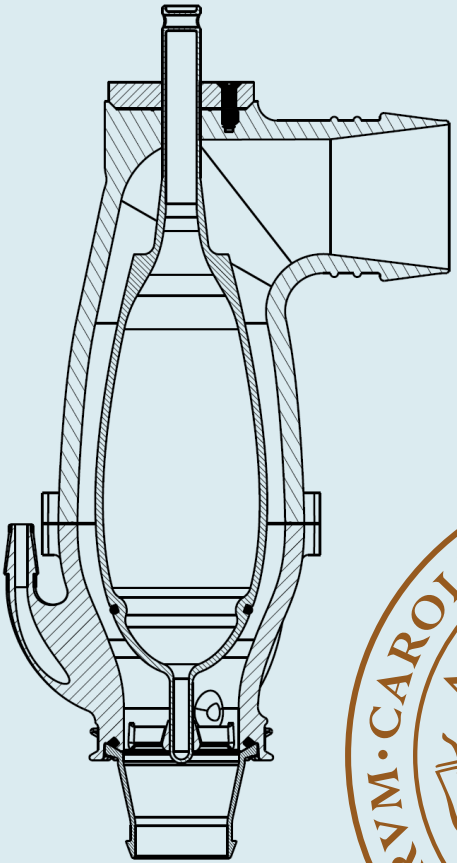

Printed by Media-Tryck, Lund 2024 NORDIC SWAN ECOLABEL 3041 0903

Department of Automatic Control
P.O. Box 118, 221 00 Lund, Sweden
www.control.lth.se

PhD Thesis TFRT-1143
ISBN 978-91-8039-921-0
ISSN 0280–5316

Afterload system design for functional donor heart assessment

Henry Pigot

LUND
UNIVERSITY

Department of Automatic Control

Cover image by Tomas Norlander.

PhD Thesis TFRT-1143
ISBN 978-91-8039-921-0 (print)
ISBN 978-91-8039-920-3 (web)
ISSN 0280–5316

Department of Automatic Control
Lund University
Box 118
SE-221 00 LUND
Sweden

Printed in Sweden by Media-Tryck.
Lund 2024

Abstract

Heart transplantation is a life-saving procedure for patients with end-stage heart failure. However, conservative acceptance criteria result in most donated hearts being discarded. Enabling clinicians to assess heart function after organ procurement can pave the way for the safe use of hearts that are currently rejected. This thesis focuses on improving techniques for the direct, controlled assessment of a recovered heart's hemodynamic performance. The first paper reviews *ex situ* working heart models and cardiac afterload devices, discussing challenges in emulating cardiac afterload and detailing an experimental method for a working porcine heart model. Paper II analyzes Windkessel models, which are the standard cardiac afterload model. It assesses their applicability and limitations, and presents a method for identifying model parameters from sampled data. The analysis concludes that complex models like the 4-element Windkessel model are not identifiable from relevant experimental data. The third paper reformulates traditional Windkessel models for a more accurate representation of hemodynamic responses. Using power as model input, the paper offers a more physiological representation of the hemodynamic response to various afterloads, aiding in afterload device design. In Paper IV, the efficacy of a pneumatic afterload device creating a range of physiological loading conditions is investigated in six porcine hearts. The experiments show the concept's utility in testing hearts under multiple conditions. Paper V introduces an actively controlled variable flow resistance, demonstrating its ability to reproduce a wide range of afterload dynamics while enforcing safe pressure limits for heart assessment. The afterload concept, outlined in Paper I, is investigated *in silico* using the methods from Paper III. A physical prototype and pilot experiments led to a patent submission for the design. These papers advance functional heart assessment by both refining Windkessel-model-based simulation tools (Papers II and III) and exploring novel afterload device concepts (Papers I, IV, and V). Together, they constitute a step towards clinical implementation of technology that can safely enable more transplantations by providing an improved basis for decision-making.

Acknowledgements

This work was made possible by the support and enthusiasm of a large group of people who I've had the pleasure of engaging with over the past several years, both as colleagues and friends. Though the list is long, there are some in particular that I'd like to highlight here.

At the Department of Automatic Control

Firstly, to my supervisor, Kristian Soltesz, thank you for your guidance and finding a great balance between setting clear expectations and giving me the freedom to direct my research. Thanks for your patience as I continually fastened in the details, for pulling me out of the weeds and keeping the important stuff in focus. I've learned to get more comfortable judging what is good enough for a given milestone, ultimately making the completion of this work possible. I'm continually impressed by your ability to connect people with complementary research interests and skill-sets to bring about exciting new projects. Trying to keep up with you has been both challenging and rewarding.

I'm also thankful for the complementary role that my co-supervisor, Professor Tore Hägglund, has played. Tore, thanks for always being there to give a second opinion and offer words of encouragement. You have been a great inspiration in my role as teacher, and I consider it a great honor to have been able to work alongside you on the Basic Course in Automatic Control.

Ylva Wahlquist, you've been a great research collaborator, office roommate, and fellow PhD student of Kristian. Thank you for all the helpful discussions, comforting commiseration, and in general for being—and giving me the chance to be—a "ball plank." Sharing the experience of being Kristian's PhD student with you has been hugely valuable, and I have appreciated your input and honesty.

The Department of Automatic Control is such a nice place to work due to the wonderful people there, and in particular thanks to Eva Westin. Eva, thank you for your unfaltering support through a variety of bureaucratic and

logistical challenges, and for always being there to lend a helping hand or kind word. Special thanks to Anders Blomdell and Alexander Pisarevskiy for their invaluable technical support, especially with firmware, circuit design, and PCB layout.

At the Department of Clinical Sciences and Igelösa Life Science

This research was made possible due to close collaboration with Professor Stig Steen and his remarkable team at Igelösa Life Science who have made foundational contributions to organ preservation technology. Stig, it has been an honor to work together with you. I have appreciated our discussions, and your enthusiastic clarifications of many physiological processes underlying our research. Your methodical and patient experimental approach has left a deep impression on me. Thank you for the opportunity to collaborate on such exciting work.

I have enjoyed stimulating exchanges with the engineers at Igelösa as well. Audrius, you have long been an engineering role-model for me. Thank you for all the insights, fruitful discussions, and technical contributions that helped make this work what it is. Petter, catching up with you in the OP or workshop and discussing our latest projects was always a pleasure; your rapid-prototyping wizardry was a big help throughout the development process. Thanks as well to Tomas for productive discussions on mechanical design, and great 3D CAD work that helped actualize important research prototypes.

Thanks to Qiuming and Erik for their essential contributions to daily experimental work as surgeon and technician, respectively. Thank you to the late Tryvge Sjöberg who, in addition to providing excellent manuscript feedback and helping make the gears turn at Igelösa, always met me with kindness and warmth. Also, thank you to Steve for proof-reading my kappa; with your experience in applied heart perfusion technologies, your input was most helpful. Thanks to Göran as well for many thought-provoking meetings during the patent process.

Ådne and Gunilla, thank you for creating such a lovely environment at Igelösa and facilitating the interdisciplinary research that I've been so fortunate to participate in. You help foster an environment for creativity and innovation that makes Igelösa so special.

Family and friends

Mom, Dad, and Hannah, your unwavering support and encouragement throughout these past 5 years, and all the years leading up to it, has meant the world to me. Thank you for always being there, through the ups and downs. You have always made me feel safe, and that I belong. As the years pass, I grow increasingly aware of what an incredible gift that is.

Josh, thanks for being my PhD-survivor confidant and arm-chair psychologist. I can't tell you how thankful I am for all our chats and visits throughout the years.

Finally, to my partner Hanna, every day is made better by having you in my life. Thank you for your love, for sharing all the trials and tribulations, for all the small day-to-day moments that are made brighter by your participation. I'm so thankful for the life we've built together.

Financial Support

This work was made possible due to funding from the Hans-Gabriel and Alice Trolle-Wachtmeister Foundation for Medical Research, the LMK Foundation, the Swedish Foundation for Strategic Research (grant SM21-0037), and the Swedish Research Council (grant 2017-04989). I have also been a member of the ELLIIT Strategic Research Area at Lund University throughout my time as a PhD student.

Contents

Nomenclature

The following terminology and abbreviations are used in accordance with the European Directorate for the Quality of Medicines & HealthCare's *Guide to the Quality and Safety of Organs for Transplantation* [*EDQM,* 2022]. They pertain to Chapters 1 and 2.

Terminology	**Description**
Recovery	The removal of a solid organ (i. e., heart) from a donor. The term is *not* used to refer to an organ that has regained function or become healthy again following some damage.
Ex situ, *in situ*; *ex vivo*, *in vivo*	The terms *in situ* and *ex situ* are preferable when referring to organ preservation strategies, as they refer to organs from an individual already declared dead (*ex situ* translating to "out of position"). Therefore, *ex situ* refers to an organ outside of a deceased donor, while *in situ* refers to an organ inside a deceased donor. However, some use *vivo* instead of *situ* (with *ex vivo* translating to "outside the living", which may be justified if considering the organ's position from the perspective of the potential recipient). In Chapters 1 and 2 I follow the *situ* convention, while in the enclosed papers we use *vivo*.

Abbreviation	**Description**
DBD	donation after brain death
DCD	donation after the circulatory determination of death
ECMO	extracorporeal circulation with membrane oxygenation
MP	machine perfusion
NIHP	non-ischemic heart preservation
NRP	normothermic regional perfusion
OCS	(TransMedics) Organ Care System
SCS	static cold storage
WLST	withdrawal of life-sustaining treatment

1

Introduction

Heart transplantation is often the only treatment option for patients with end-stage heart failure. Although the number of transplantations performed each year continues to grow in Europe, waiting lists persist due to the limited availability of donor organs [Domínguez-Gil, 2022]. One factor constraining the number of available organs is uncertainty regarding organ quality. This is especially true after transportation using today's standard method, static cold storage (SCS), during which the oxygen-starved organ incurs ischemic damage. Organ quality uncertainty leads to a conservative organ selection approach, which in turn leads to a large number of organs being discarded. Today, two thirds of potential donor hearts in Sweden are discarded, and the situation is similar globally[1] [Domínguez-Gil, 2022; *GODT,* 2023].

The advent of non-ischemic heart preservation (NIHP) technology has opened up new opportunities for evaluating donor hearts *ex situ* prior to transplantation. NIHP uses machine perfusion to keep the heart oxygenated during transportation, alleviating the typical 4-hour time constraint on out-of-body time for the organ [Steen et al., 2016; Nilsson et al., 2020; McGiffin et al., 2023]. This extra time enables transportation of the organ over larger geographical distances, as well as functional assessment of the organ. The objective of functional assessment is to provide clinicians with more information about the quality of each organ, to enable safe use of hearts that would otherwise be discarded. A flow-chart comparing the current standard of care, SCS, with the proposed method of NIHP and functional assessment is shown in Figure 1.1.

Ex situ functional assessment is performed using a working heart model where the organ beats a blood-like perfusate against a mechanical load controlled to have a flow impedance similar to the body's vasculature, and example of which is shown in Figure 1.2. The mechanical load is also known as an afterload device. By contrast, in a non-working—or Langendorff—model

[1] Comparing the number of reported heart transplants to the number of actual deceased organ donors.

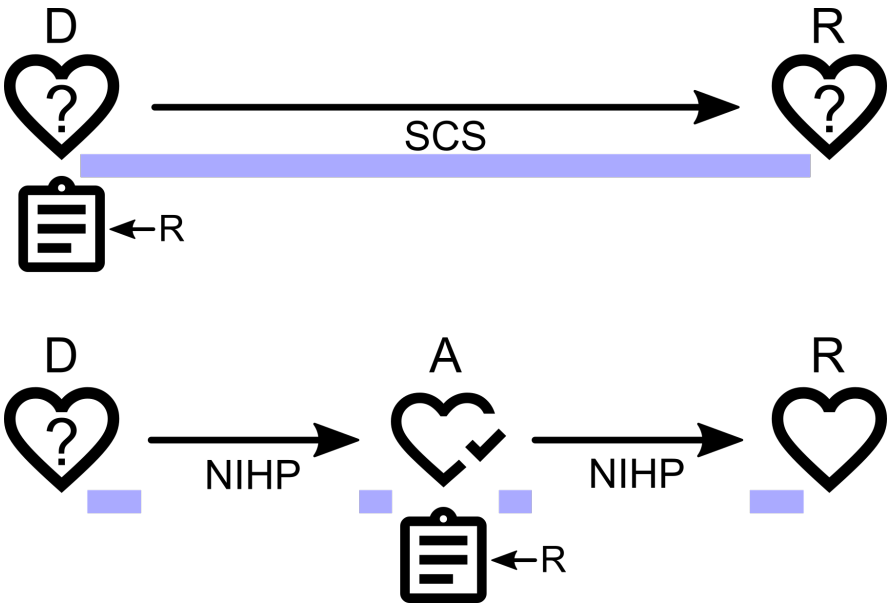

Figure 1.1 Timelines illustrating the current standard of care, static cold storage (SCS, top), and the proposed method, non-ischemic heart perfusion (NIHP) with functional assessment (bottom). The blue line indicates ischemic time, when the heart is without oxygen. The heart is recovered at the donor hospital (D). In the current standard of care, the decision to use the heart and selection of recipient (←R) done using the the limited information available at the donor hospital. The heart is then transported to the recipient hospital (R) using SCS. In the proposed method, the heart is transported to a centralized assessment center (A) using NIHP, avoiding ischemia during transport. Based on the results of a functional assessment, the recipient is chosen and their hospital initiates the transplantation procedure. The heart is transported with NIHP from the assessment center (A) to the recipient hospital (R). Alternatively, the assessment could be performed at a donor or potential-recipient hospital.

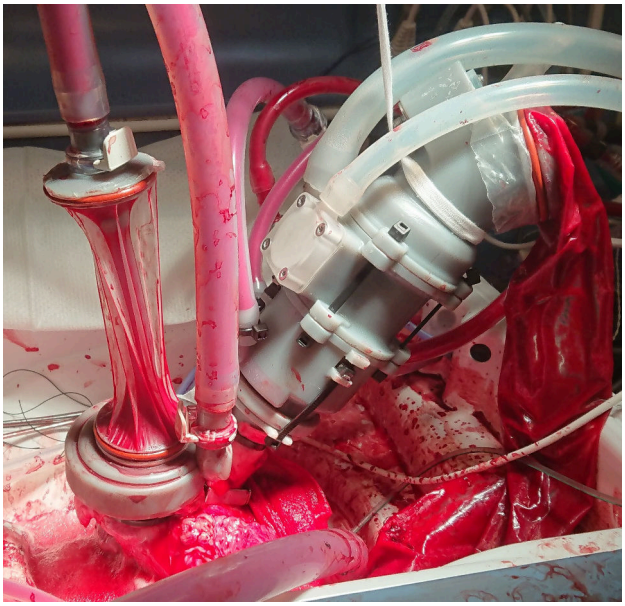

Figure 1.2 Afterload device (right, grey) that the heart (bottom) pumps blood against. The device should enable control of systolic and diastolic pressure, so the heart's pumping function can be evaluated under safe and realistic conditions. Photo from [Pigot et al., 2022].

the heart beats empty while perfusate in the aorta is externally pressurized to facilitate blood flow to the heart itself. A working heart model allows for direct observation of the hemodynamic function of the heart, i. e., the cardiac output it can produce and the associated atrial, ventricular, and arterial pressures. Different loading conditions can be used to represent different individuals (i. e., prospective heart transplant recipients) under varying exertion levels. Loading conditions may also be adjusted to account for pathologies such as hypertension, or to investigate how the heart responds to the progression of a disease that affects afterload.

Ideally, an afterload device enables independent adjustment of systolic and diastolic arterial pressures, even under varying cardiac output. Typical porcine *in vivo* aortic pressure and flow waveforms is shown in Figure 1.3, with systole and diastole marked for each cardiac cycle. Setting a lower bound on diastolic pressure (during heart relaxation) helps ensure adequate coronary perfusion, which primarily occurs during diastole and depends on the pressure gradient between the aorta and right atrium. Systolic pressure, which occurs as the heart contracts, is limited by the inotropic ability of the heart. None the less, it is important to maintain an upper bound on systolic

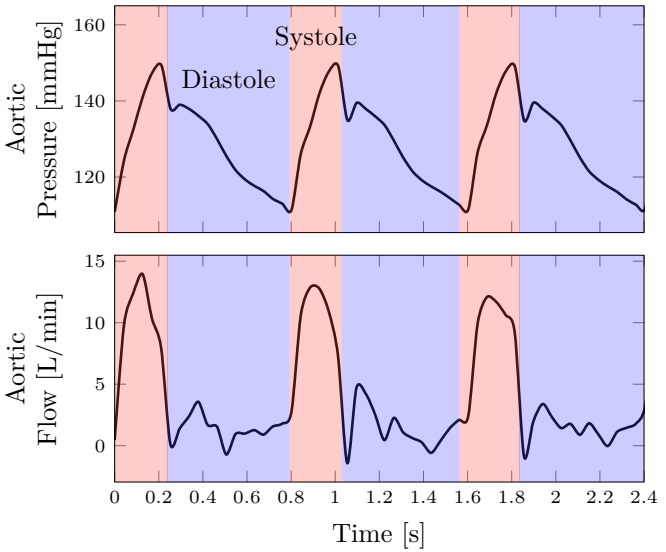

Figure 1.3 Three cardiac cycles illustrating typical porcine *in vivo* aortic pressure (top) and flow (bottom) waveforms. Systole and diastole are marked for each cycle by red and blue shading, respectively. Data from experimental results published in [Pigot et al., 2022].

pressure so as not to subject the heart to excessive stress. This is particularly important *ex situ*, where the heart lacks the protective pleura that helps prevent ventricular overdistension *in vivo*. Similarly, the denervated heart lacks feedback to the vasomotor center from baroreceptors in the aorta and carotid arteries that otherwise help regulate blood pressure [Guyton and Hall, 2006]. As such, it is desirable for an afterload device to be able to enforce both upper and lower bounds on systolic and diastolic pressures, respectively.

This thesis aims to contribute to the development of a new method for assessing the quality of donor hearts by providing modelling tools as well as presenting novel approaches to afterload device design and control. In particular, classic lumped-parameter models of cardiac afterload dynamics are evaluated and expanded upon to better facilitate *in silico* development of cardiac afterload devices. Two novel afterload device designs are investigated: one via computer simulation with the developed models and another using preclinical porcine experiments. Implementation of these methods may help increase the number of available donor hearts by providing clinicians with more information about the quality of each organ, as well as enabling the safe adoption of new, promising procedures such as the use of extended criteria donors and donation after the circulatory determination of death (DCD),

discussed further in Chapter 2. Here, I present a summary of the enclosed published works, followed by a brief overview of how heart transplantation is done today. The Background is proceeded by a book chapter, enclosed as Paper I, that elaborates on the working heart model and afterload devices. Paper I may be considered as a third part of the introductory material.

1.1 Included publications

Paper I

H. Pigot, K. Soltesz, S. Steen (in press, 2024). "Ex vivo working porcine heart model". In: *Experimental Models of Cardiovascular Diseases*. 2nd ed. Methods in Molecular Biology. Humana Press, New York, NY

The first work presented here is a book chapter which serves as a technical and methodological overview of the working heart model. The chapter includes a detailed step-by-step guide to the experimental model using pig hearts. Particular focus is given to the history and state-of-the-art of afterload devices.

Paper II

H. Pigot, J. Hansson, A. Paskevicius, Q. Liao, T. Sjöberg, S. Steen, K. Soltesz (Jan. 2021). "Identification of cardiac afterload dynamics from data". *IFAC-PapersOnLine*. 11th IFAC Symposium on Biological and Medical Systems BMS 2021 **54**:15, pp. 508–513. DOI: 10.1016/j.ifacol.2021.10.307

In the body, cardiac afterload for the left side of the heart is the result of the systemic arterial vasculature, which carries oxygenated blood to the body. For the right side of the heart, it is determined by the pulmonary arterial vasculature, which carries deoxygenated blood to the lungs. An afterload device used in a working heart model aims to mimic the vascular impedance of the body. When considering afterload designs, it is helpful to investigate the standard mathematical models of vascular impedance, so called Windkessel models. While Paper I introduces the history and implementation of these models, Paper II presents an analysis of the 2-, 3-, and 4-element Windkessel models. Each variant of the model is fitted to experimental data, and the suitability of such an approach is evaluated using sensitivity and persistence of excitation analyses. The analyses show that clinically-feasible experimental data do not meaningfully support more complex models than the standard 3-element Windkessel model.

Paper III

H. Pigot and K. Soltesz (June 2022). "The differential-algebraic Windkessel model with power as input". In: *2022 American Control Conference (ACC)*, pp. 3006–3011. DOI: 10.23919/ACC53348.2022.9867889

Traditional Windkessel models take one of arterial pressure or flow as input, and output the other. This presents a limitation when using the model as a simulation tool for designing and assessing afterload devices. As afterload changes in the body, it results in changes to both pressure and flow. This behavior is not captured by the standard Windkessel models. Take for example a model with arterial flow as the input. With flow fixed as predetermined input values, an increase in afterload will result in an increase in arterial pressure without any bound. As such, the resulting cardiac power in simulation (the product of arterial flow and pressure) is a responding variable determined by the controlled afterload parameters, and does not reflect the physical limitations of the heart as a pump.

It is more realistic to consider the heart as a power source, with both pressure and flow responding to changes in afterload. Paper III reformulates the traditional Windkessel model to use power as the input, and output both arterial flow and pressure. The model is able to capture the behavior of the standard Windkessel models while also simulating responses to changes in the heart's inotropic response, such as arrhythmias. This provides a more physiological representation of the response to various afterloads, offering a useful tool in the design and simulation of afterload devices for *ex situ* heart assessment (as in Paper V).

Paper IV

H. Pigot, K. Soltesz, A. Paskevicius, Q. Liao, T. Sjöberg, S. Steen (Sept. 2022). "A novel nonlinear afterload for ex vivo heart evaluation: Porcine experimental results". *Artificial Organs* **46**:9, pp. 1794–1803. DOI: 10.1111/aor.14307

As discussed in Paper I, existing approaches to afterload device design often rely on verbatim implementations of the Windkessel model using discrete resistive and compliant elements, and may be supported with pumps to actively maintain a lower bound on diastolic pressure. Beyond controlling the systolic and diastolic limits with an afterload device, it is desirable for the form of the arterial waveforms to follow that observed *in vivo*, which helps ensure proper valve function and coronary perfusion. The Windkessel approach aims to achieve such physiological pressure waveforms (see Paper II). However, multiple elements must be adjusted simultaneously to make independent adjustments of systolic or diastolic pressure, and an afterload

device purely based on Windkessel elements is not able to enforce hard upper and lower bounds on these pressures.

In Paper IV an alternative afterload device concept is presented and investigated experimentally using $n = 6$ pig hearts. The design uses a pressurized cuff, through which the heart forces perfusate. By controlling the pressure levels in the cuff, the device aims to enforce set systolic and diastolic limits on a beat-to-beat basis. Measured hemodynamics *in vivo* and *ex situ* were compared. The experiments show that the device is able to produce a variety of physiological afterload conditions. However, non-ideal pressure valve behavior and the lack of arterial pressure feedback in the pressure control loop requires user-input to adjust for some static errors in the set pressure levels, especially during systole.

Paper V

H. Pigot, Y. Wahlquist, K. Soltesz (Jan. 2023). "Actively controlled cardiac afterload". *IFAC-PapersOnLine*. 22nd IFAC World Congress **56**:2, pp. 6484–6489. DOI: 10.1016/j.ifacol.2023.10.863

The afterload device presented in Paper V is based on a simple operating principle and aims to address the drawbacks of the aforementioned devices. The paper investigates via simulation the use of a variable flow resistance controlled at high bandwidth to allow the reproduction of a wide variety of afterload dynamics. The addition of an auxiliary flow between the resistance and the artery allows the emulation of compliant behavior (i. e., fluid flow from the aorta into the coronary arteries during diastole). Furthermore, the device is designed to continuously enforce hard upper and lower bounds on systolic and diastolic pressures, respectively, by rapidly decreasing or increasing its resistance. A control strategy is demonstrated that reproduces Windkessel model dynamics while also enforcing pressure bounds for improved safety during heart assessment.

1.2 Patent application

A prototype of the afterload concept presented in Paper V has been developed, show in Figure 1.4, and is briefly described in Paper I. Pilot experiments with the proof-of-concept prototype informed the patent application "Afterload for Heart Evaluation", filed 2023-05-17 with Sveriges Patent- och registreringsverket. Prototype development is ongoing.

Figure 1.4 Prototype of the actively controlled afterload concept presented in Papers I and V. Photo by Johan Persson.

1.3 Other publications

A number of complimentary, but not directly related, peer-reviewed works were excluded from this collection. They are listed in Chapter 3.

2

Background

Solid organ donation can be divided into two general categories: donation after brain death (DBD) and donation after circulatory determination of death (DCD). In DBD, the donor organs continue to be perfused with oxygen-rich blood following declaration of donor death, contrasting DCD where the organs are ischemic (lacking oxygen) for a period surrounding the declaration of death. Timelines comparing DBD and DCD are shown in Figure 2.1. In 2022, 77 % of solid organ transplantations reported worldwide were DBD. Considering hearts alone, the proportion rises to 94 % [*GODT,* 2023] DBD. This difference reflects the heart's sensitivity to ischemic damage, being the most sensitive of the donated organs due to its high metabolic rate. There is a higher risk of ischemic damage with DCD, and as such the adoption of DCD heart transplantation has been much slower than for other organs.

In the following section I present DBD and DCD as they are done in Sweden, which is where the research in the enclosed papers was conducted. The DBD and DCD process in Sweden is indicative of other EU countries. In particular, I highlight how the processes differ in clinical implementation today and their role in meeting the growing demand for donor hearts.

2.1 Addressing the donor heart shortage

Despite its challenges, DCD presents an opportunity to significantly increase the number of organs available for transplantation. This potential is driving research and innovation to improve the safety and accessability of DCD transplantation. Though still less than a quarter of total donations, DCD saw exceptional growth in the European Union from 2021 to 2022—up 42.7 % to 2843—while the number of DBD organ donations grew by just 2.7 % to 9166 [*GODT,* 2023]. In the Netherlands, DCD donors accounted for 59 % of all donated organs [Domínguez-Gil, 2022]. However, the number of DCD heart transplants remains low, with only Belgium, the Netherlands, Spain, Australia, the UK, and the USA reporting DCD heart transplants in 2022

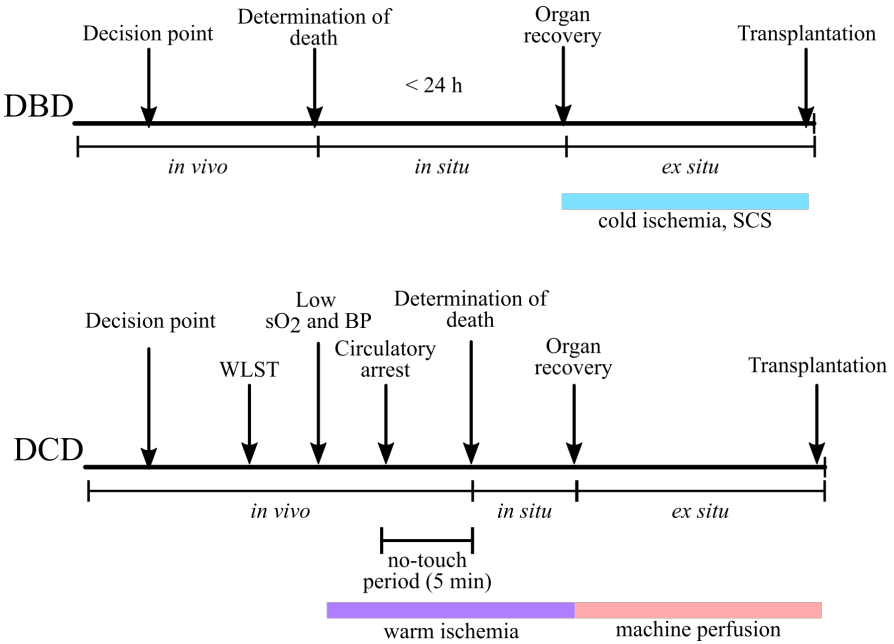

Figure 2.1 Timelines comparing the donation after brain death (DBD) and donation after circulatory determination of death (DCD) processes. In DCD, recovery should happen as quickly as possible after the no-touch period to minimize warm ischemia time. In DBD, organ transportation is typically done with static cold storage (SCS). DCD is generally done with a recipient in the same facility or is transported using a machine perfusion device to minimize further ischemia following the declaration of death; the latter is illustrated here. WLST: withdrawal of life-sustaining therapy. sO_2: blood oxygen saturation. BP: blood pressure.

[Domínguez-Gil, 2022]. In Sweden, clinical trials using DCD donors began in 2018, and in 2022 changes were made to national transplant law to make DCD donation possible as a part of standard clinical practice [*Vävnadsrådet,* 2020; *Socialstyrelsen* 2022]. However, DCD heart transplantation is still not performed in Sweden.

2.1.1 Donation after brain death

To understand the additional challenges in recovering hearts from DCD donors, it is helpful to first consider the typical DBD process. DBD occurs when donor death is determined using neurological criteria, typically in patients with traumatic brain injury or who have suffered a stroke [*EDQM,* 2022]. Although exact definitions vary from country to country, brain death

is characterized by a complete and irreversible loss of brain function. Importantly, organ-preserving treatment such as mechanical ventilation continues following the determination of death in DBD, ensuring oxygenation of the organs.

As outlined by [*Socialstyrelsen* 2022], the process of DBD organ donation starts with the decision point when further treatment of a patient is no longer deemed meaningful, i. e., for whom recovery of brain function is not plausible. Two licensed doctors collectively decide not to initiate or continue life-sustaining therapy, and the decision is documented in the patient's journal. A meeting is held to inform the next of kin. A transplant coordinator is notified of the potential donor's identity. Prior to the decision point, the doctor may communicate anonymized medical information about a potential donor to the transplant coordinator.

After the decision point, organ-preserving treatment begins with the aim of conserving organ function or improving conditions for transplantation. The treatment is usually the intensive care that the patient has already been receiving, but may be supplemented or adjusted[1]. Palliative care is provided simultaneously, and always takes precedence over organ-preserving treatment. Furthermore, organ-preserving treatment may only be given if the treatment cannot wait until after death, does not cause significant pain or harm to the donor, and does not hinder treatment for the patient's own benefit [*Riksdagen* 2022].The patient's will to donate is investigated in accordance with §3 of the transplant law [*Riksdagen* 2022]. Healthcare staff check the donor registry for the patient's preferences, and the next of kin are consulted.Consent to post-mortem organ donation automatically covers associated organ preservation treatment and medical eligibility assessment.

Once the patient's will to donate has been confirmed, assessment of a patient's medical suitability for donation may begin. The assessment is done by a doctor who is not involved in the care of any potential organ recipient and may involve reviewing medical records, collecting information about illnesses or potential contraindications, physical examination, laboratory testing, and radiographic examinations [*Socialstyrelsen* 2022; *EDQM,* 2022]. As with organ-preservation treatment, assessment may not cause significant pain or harm to the patient.

Following chapter 4 of national regulation [*SOSFS* 2022], brain death is determined using two clinical neurological examinations, and noted in the patient's records. Following the declaration, additional organ-preserving treatments may begin, as well as continuation of previous organ-preserving treatments. Such treatments are conducted with respect for the deceased

[1] Organ-preserving treatment given before the declaration of death may be referred to as *ante mortem* interventions, though that term is generally reserved for the DCD case where life-sustaining therapy is withdrawn prior to declaration of death.

and their next of kin. Ongoing preservation enables organ recovery within 24 hours following the declaration of brain death, without compromising organ quality [*Socialstyrelsen* 2022].

Organs are recovered by teams from the transplant centers where matched recipients have been identified. In DBD, the heart is oxygenated until the moment of recovery, when cardioplegia[2] is induced and the heart is cooled to limit ischemic damage. The current standard of care is to transport using static cold storage (SCS), where the heart is kept in this cold, non-beating state. The period from the induction of cold cardioplegic, followed by transportation using SCS, until the heart is warmed with oxygenated blood in the recipient is known as the cold ischemia time. By contrast, warm ischemia occurs under conditions when the heart lacks oxygen but remains at normothermic temperatures, which will be discussed below in the context of DCD. Although the effects are less damaging than warm ischemia, cold ischemia times exceeding 4 hours have been shown to result in poor post-transplant patient outcomes using hearts from donors older than 18 years [John et al., 2019]. An analysis of 30008 heart transplants performed between 2008 and 2018 showed a significant jump in 30-day patient mortality following cold ischemia times exceeding 4 hours [McGiffin et al., 2023]. In general, hearts with a cold ischemia time longer than 4 hours are not used in transplantation [*EDQM,* 2022; *Socialstyrelsen* 2022]. As such, transportation using SCS is typically limited to 4 hours.

Overall, the DBD process provides a relatively long time window for organ recovery (24 hours), with the heart being oxygenated up until the moment of recovery. However, the number of patients who die under conditions suitable for DBD—i. e., brain death while under intensive care at the hospital—is limited, motivating adoption of DCD. Furthermore, the effects of ischemia during SCS lead to uncertainty in organ quality following transportation.

2.1.2 Donation after circulatory determination of death

Donation after circulatory determination of death (DCD) occurs when donor death is declared by circulatory criteria, i. e., no breathing is observed and pulsatile blood flow is absent, followed by a no-touch period to confirm irreversibility of the condition [*Vävnadsrådet,* 2020]. The DCD process is similar to DBD, with a few key differences, as shown in Figure 2.1. If donation is found to be possible, withdrawal of life-sustaining therapy (WLST) occurs following the decision point and investigation of the patient's will and suitability to donate. WLST includes stopping mechanical ventilation, the administration of drugs, or any other treatments used to sustain a patient in critical condition. After WLST, *ante mortem* interventions to support or-

[2] A non-beating state induced by infusion of an electrolyte solution, resulting in lowered metabolic activity.

gan donation may begin, in a manner similar to the DBD case though more restrictive, as discussed further in the next section. As the donor's circulatory system comes to a stop, blood pressure and oxygen saturation fall, leaving the organs in a warm ischemic state. Warm ischemia causes organ damage more quickly than cold ischemia, due to ongoing metabolic activity. The period of warm ischemia continues as circulatory arrest is observed, the no-touch period of 5 minutes[3] elapses, and death is declared. The warm ischemia time ends only once the heart is cooled (as with SCS preservation, starting cold ischemia) or machine perfusion is applied to stop ischemia, as discussed in Section 2.2. The resulting ischemic damage to the organs is a critical difference between DCD and DBD. In the absence of organ perfusion, procurement and preservation must occur as soon as possible following the declaration of death to maintain organ viability[4].

Compared to DBD, DCD introduces additional clinical challenges, while also presenting more opportunities to respect a patient's will to donate organs after death by broadening the circumstances under which a patient can become a donor. The increased risk of warm ischemic damage results in greater organ quality uncertainty at the time of recovery and less margin for further ischemia following the declaration of death. In order to increase the safe use of DCD hearts, a number of strategies are being investigated to improve the assessment of DCD organs and limit ischemic damage during the transplantation process. Some of these strategies are illustrated in Figure 2.2, and discussed in the following sections.

2.2 Heart preservation

2.2.1 *Ante mortem* interventions

In DCD, organ preservation measures taken after WLST but prior to the declaration of death, so called *ante mortem* interventions, aim to minimize the deleterious effects of warm ischemia. *Ante mortem* interventions include the use of drugs such as heparin, steroids, or vasodilators, as well as cannulation or marking of vessels in preparation for *post mortem* perfusion. These interventions are part of standard clinical practice in several european countries, while others are still undergoing preclinical or clinical trials [Lomero et al., 2020; *EDQM,* 2022]. One such example is automated stabilization of patient blood pressure following WLST. Our group showed the prevention of

[3] Most european countries have a no-touch period of 5 minutes, with 10 minutes in a few exceptions, and 20 minutes in Italy [Lomero et al., 2020].

[4] The current Swedish protocol for DCD [*Vävnadsrådet,* 2020] specifies that the time between cardiac arrest and organ preservation (i. e., machine perfusion)must be less than 30 minutes for DCD lung donation to be possible. Shorter times could be expected in a similar protocol for hearts due to their higher sensitivity to ischemic damage.

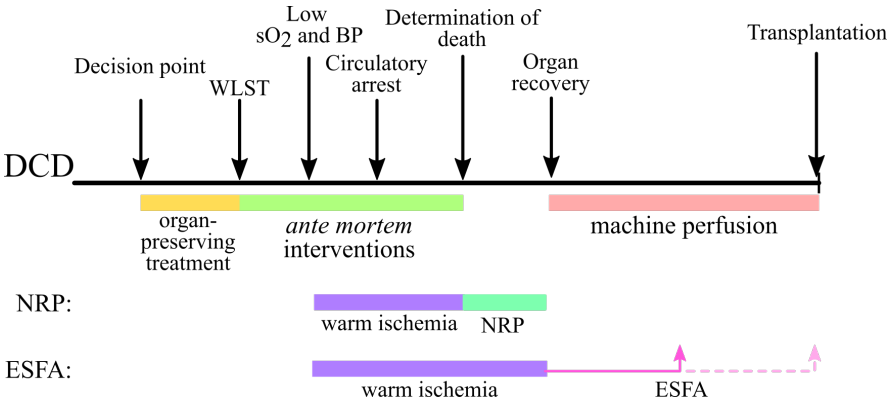

Figure 2.2 Timeline illustrating strategies for assessment and organ preservation in donation after circulatory determination of death (DCD). Following standard organ-preserving treatment prior to WLST, such as those used in DBD, *ante mortem* interventions (e. g., heparin) may be administered prior to the declaration of death to improve conditions for organ donation. Machine perfusion strategies such as non-ischemic heart preservation (NIHP) can be used to allow DCD hearts to be transported to remote centers without extending ischemia time. Normothermic regional perfusion (NRP) can help shorten warm ischemia time (WIT) by providing organ perfusion *in situ* prior to recovery. NRP also allows for basic functional assessment before organ recovery. *Ex situ* functional assessment (ESFA), using a working mode system, enables functional assessment between recovery and transplantation, e. g., at a centralized assessment facility, or at the recipient hospital. Although these strategies are illustrated for DCD, they could also be used to facilitate safe procurement from other non-standard risk donors (e. g., older DBD donors, or those requiring longer transport times). WLST: withdrawal of life-sustaining therapy. sO_2: oxygen saturation. BP: blood pressure.

ischemic myocardial contracture—a sign of ischemic damage—by automating vasodilator and vasoconstrictor drug dosing to control blood pressure in a porcine DCD donor model [Wahlquist et al., 2021]. Recent revisions to Swedish transplant law provides legal grounds for *ante mortem* interventions (§3 and §4 following change SFS 2022:582), supporting clinical adoption of DCD [*Riksdagen* 2022].

2.2.2 *In situ* machine perfusion

Machine perfusion (MP) of the heart can be used to preserve organs after declaration of donor death. Rather than slowing the onset of ischemic damage by reducing the metabolic activity as in SCS, MP aims to prevent ischemia by actively perfusing the organs with an oxygenated solution.

Normothermic regional perfusion (NRP) is an *in situ* MP strategy using extracorporeal circulation with membrane oxygenation (ECMO) or a similar perfusion setup to supply oxygenated blood to the abdominal and thoracic organs[5] while excluding cerebral circulation to mitigate the risk autoresuscitation. The technique is a relatively simple and inexpensive means of keeping the organs perfused until they are recovered.

2.2.3 *Ex situ* machine perfusion

Organ preservation using MP can also be performed *ex situ*, after the organ has been recovered from the donor. A key advantage of *ex situ* MP over NRP is that it enables organ preservation during transportation, using a portable perfusion device. [Qin et al., 2022] provides a comprehensive overview of current MP strategies for heart preservation, and [Hatami et al., 2023] considers the topic in the context of enabling transplantation of DCD organs. By eliminating cold ischemia time during transport, *ex situ* MP can enable organ transport beyond the typical 4 hour time constraint and facilitate functional heart assessment at facilities other than the donor hospital.

Today, the only commercially available, clinically approved *ex situ* heart perfusion device for transplantation is the TransMedics Organ Care System (OCS). The OCS keeps the heart in a normothermic, empty-beating state[6]. One multicenter heart transplant study has been done with the OCS, using DBD donors for both the OCS and SCS groups. The study showed no significant difference in patient outcomes between the two groups [Ardehali et al., 2015]. Other studies have since shown comparable DBD outcomes to SCS using the OCS, despite longer extracorporeal times in the OCS device. Initial studies have also shown promising results with DCD hearts, achieving similar results to DBD hearts preserved with SCS [Messer et al., 2020; Chew et al., 2019]. An analysis of results at a single center in the United Kingdom ($n = 66$) showed that, although extracorporeal times could be extended with the OCS, time in the machine was strongly correlated with primary graft disfunction [Avtaar Singh et al., 2019].

An alternative *ex situ* MP strategy is to keep the heart in a hypothermic, non-beating state to limit metabolic activity while still providing oxygen to the heart. This approach, referred as non-ischemic heart preservation (NIHP)[7], perfuses the heart continuously with a nutrient-hormone solution at 8 °C including clean red blood cells. The method demonstrated safe transplantation after 24 hours of preservation in a porcine model [Steen et al.,

[5] When NRP is used to perfuse not only the abdominal organs but also the thoracic organs, the abbreviation TA-NRP is commonly used. Here, I use NRP to refer to TA-NRP.

[6] Otherwise known as Langendorff perfusion.

[7] Also referred to as hypothermic MP (HMP), hypothermic oxygenated perfusion (HOPE), or hypothermic *ex situ* heart perfusion (H-ESHP).

2016], as well as promising initial results in a single-center clinical trial [Nilsson et al., 2020]. A multicenter trial ($n = 24$) showed safe preservation times of 7 hours with no correlation between extracorporeal time and primary graft disfunction at 30 days post-transplant [McGiffin et al., 2023], with corroborating results in a pre-clinical sheep heart study following 8 hours of NIHP [See Hoe et al., 2023]. Further multicenter and single center clinical trials are ongoing (NCT03991923 and NCT04066127) and the device used—the XVIVO Heart Preservation System—is projected to be commercially available for clinical use within the coming year.

2.3 Heart assessment

There are a number of reasons to reject hearts for use in transplantation, including poor heart function, structural deformities, coronary artery disease, long-term diabetes, old age, substance use disorders, expectation of long ischemic time, and poor donor-recipient matching (e. g., sex, size, immunology). Some of these risks can be addressed by *in vivo* assessments done before organ recovery. However, in order to address the risks associated with DCD and other non-standard risk donors[8], it is desireable to assess the heart after declaration of death or transport to ensure that ischemic damage does not invalidate the organ for safe transplant use.

2.3.1 *In situ* assessment

NRP provides an opportunity for functional heart assessment *in situ*, after the declaration of death and prior to organ recovery. By weaning the heart from machine-supported perfusion during NRP, echocardiogram and pulmonary artery flotation catheters have successfully been used to measure ejection fraction, cardiac output, and atrial pressures [Messer et al., 2017; Tchana-Sato et al., 2019]. A disadvantage with *in situ* functional assessment is that the loading condition of the heart is constrained to that posed by the donor's vasculature. NRP does not enable functional assessment under a variety of cardiac outputs or afterload conditions representing a range of potential recipients. Furthermore, NRP is constrained to the donor hospital where clinical expertise and equipment for functional assessment may be limited. Due to the risk of organ deterioration during trasport, it may be desireable to instead perform functional assessment along the route to the recipient, or at the recipient hospital.

2.3.2 *Ex situ* assessment – a new way forward?

Using hearts from DCD donors or other non-standard risk donors motivates the use of assessment techniques that can elucidate hemodynamic function

[8] I. e., older donors (> 60 years) or donors with preexisting conditions.

immediately before, during, or after *ex situ* preservation. Although the heart is kept metabolically active in the OCS, functional assessment is limited by the heart not pumping fluid. Key hemodynamic metrics, such as ventricular and arterial pressures during contraction and relaxation, as well as the flow generated by the heart, cannot be assessed using the OCS. The initial OCS study presented metabolic measurements during perfusion as a possible indicator of organ suitability for transplantation. This approach has been called into question and subsequent studies have shown that functional assessment provides more reliable metrics for predicting heart transplant outcomes [Freed and White, 2015; White et al., 2015; Ribeiro et al., 2020].

The use of an *ex situ* working heart model for functional heart assessment enables hearts to be tested under a variety of conditions representative of potential organ recipients, while simultaneously preserving organ function via perfusion with an oxygenated, nutrient-hormone solution, as described in Paper I.

3

Author contributions

Here I outline my contributions (solid black text) according to the Contributor Roles Taxonomy [*ANSI/NISO Z39.104* 2022], an attributions standard employed by major publishers including, among others, Elsevier, Springer, and Wiley. The roles are defined in Table 3.1.

Paper I

H. Pigot, K. Soltesz, S. Steen (in press, 2024). "Ex vivo working porcine heart model". In: *Experimental Models of Cardiovascular Diseases*. 2nd ed. Methods in Molecular Biology. Humana Press, New York, NY

Writing - original draft	Writing - review & editing	Conceptualization
Data curation	Formal analysis	Investigation
Methodology	Resources	Software
Supervision	Validation	Visualization

Paper II

H. Pigot, J. Hansson, A. Paskevicius, Q. Liao, T. Sjöberg, S. Steen, K. Soltesz (Jan. 2021). "Identification of cardiac afterload dynamics from data". *IFAC-PapersOnLine*. 11th IFAC Symposium on Biological and Medical Systems BMS 2021 **54**:15, pp. 508–513. DOI: 10.1016/j.ifacol.2021.10.307

Writing - original draft	Writing - review & editing	Conceptualization
Data curation	Formal analysis	Investigation
Methodology	Resources	Software
Supervision	Validation	Visualization

Paper III

H. Pigot and K. Soltesz (June 2022). "The differential-algebraic Windkessel model with power as input". In: *2022 American Control Conference (ACC)*, pp. 3006–3011. DOI: 10.23919/ACC53348.2022.9867889

Writing - original draft	Writing - review & editing	Conceptualization
Data curation	Formal analysis	Investigation
Methodology	Resources	Software
Supervision	Validation	Visualization

Paper IV

H. Pigot, K. Soltesz, A. Paskevicius, Q. Liao, T. Sjöberg, S. Steen (Sept. 2022). "A novel nonlinear afterload for ex vivo heart evaluation: Porcine experimental results". *Artificial Organs* **46**:9, pp. 1794–1803. DOI: 10.1111/aor.14307

Writing - original draft	Writing - review & editing	Conceptualization
Data curation	Formal analysis	Investigation
Methodology	Resources	Software
Supervision	Validation	Visualization

Paper V

H. Pigot, Y. Wahlquist, K. Soltesz (Jan. 2023). "Actively controlled cardiac afterload". *IFAC-PapersOnLine*. 22nd IFAC World Congress **56**:2, pp. 6484–6489. DOI: 10.1016/j.ifacol.2023.10.863

Writing - original draft	Writing - review & editing	Conceptualization
Data curation	Formal analysis	Investigation
Methodology	Resources	Software
Supervision	Validation	Visualization

Patent

H. Pigot, T. Norlander, K. Soltesz (filed 2023-05-17). "Afterload for heart evaluation". (Sveriges patent och registreringsverket)

Writing - original draft	Writing - review & editing	Conceptualization
Data curation	Formal analysis	Investigation
Methodology	Resources	Software
Supervision	Validation	Visualization

Publications not included in the thesis

K. Soltesz, A. Paskevicius, H. Pigot, Q. Liao, T. Sjöberg, S. Steen (May 2019). "Phase-controlled intermittent intratracheal insufflation of oxygen during chest compression-active decompression mCPR improves coronary perfusion pressure over continuous insufflation". *Resuscitation* **138**, pp. 215–221. DOI: 10.1016/j.resuscitation.2019.02.045

Writing - original draft	Writing - review & editing	Conceptualization
Data curation	Formal analysis	Investigation
Methodology	Resources	Software
Supervision	Validation	Visualization

H. Pigot, C. B. Sancho, A. Paskevicius, S. Steen, K. Soltesz (July 2020). "Advantage of new ventilation method for cardiopulmonary resuscitation qualitatively captured by simple respiratory mechanics models". In: *2020 American Control Conference (ACC)*, pp. 1317–1322. DOI: 10.23919/ACC45564.2020.9147868

Writing - original draft	Writing - review & editing	Conceptualization
Data curation	Formal analysis	Investigation
Methodology	Resources	Software
Supervision	Validation	Visualization

Y. Wahlquist, K. Soltesz, Q. Liao, X. Liu, H. Pigot, T. Sjöberg, S. Steen (Apr. 2021). "Prevention of Ischemic Myocardial Contracture Through Hemodynamically Controlled DCD". *Cardiovasc Eng Tech.* DOI: 10.1007/s13239-021-00537-8

Writing - original draft	Writing - review & editing	Conceptualization
Data curation	Formal analysis	Investigation
Methodology	Resources	Software
Supervision	Validation	Visualization

Table 3.1 Contributor Roles Taxonomy

Role	Definition
Writing – original draft	Preparation, creation and/or presentation of the published work, specifically writing the initial draft (including substantive translation).
Writing – review & editing	Preparation, creation and/or presentation of the published work by those from the original research group, specifically critical review, commentary or revision – including pre- or post-publication stages.
Conceptualization	Ideas; formulation or evolution of overarching research goals and aims.
Data curation	Management activities to annotate (produce metadata), scrub data and maintain research data (including software code, where it is necessary for interpreting the data itself) for initial use and later re-use.
Formal analysis	Application of statistical, mathematical, computational, or other formal techniques to analyze or synthesize study data.
Funding acquisition	Acquisition of the financial support for the project leading to this publication.
Investigation	Conducting a research and investigation process, specifically performing the experiments, or data/evidence collection.
Methodology	Development or design of methodology; creation of models.
Project administration	Management and coordination responsibility for the research activity planning and execution.
Resources	Provision of study materials, reagents, materials, patients, laboratory samples, animals, instrumentation, computing resources, or other analysis tools.
Software	Programming, software development; designing computer programs; implementation of the computer code and supporting algorithms; testing of existing code components.
Supervision	Oversight and leadership responsibility for the research activity planning and execution, including mentorship external to the core team.
Validation	Verification, whether as a part of the activity or separate, of the overall replication/reproducibility of results/experiments and other research outputs.
Visualization	Preparation, creation and/or presentation of the published work, specifically visualization/data presentation.

Bibliography

ANSI/NISO Z39.104 (2022). *ANSI/NISO Z39.104-2022, CRediT, Contributor Roles Taxonomy*. Baltimore, Maryland, U.S.A. DOI: 10.3789/ansi.niso.z39.104-2022.

Ardehali, A., F. Esmailian, M. Deng, E. Soltesz, E. Hsich, Y. Naka, D. Mancini, M. Camacho, M. Zucker, P. Leprince, R. Padera, and J. Kobashigawa (2015). "Ex-vivo perfusion of donor hearts for human heart transplantation (PROCEED II): a prospective, open-label, multicentre, randomised non-inferiority trial". *The Lancet* **385**:9987, pp. 2577–2584. DOI: 10.1016/S0140-6736(15)60261-6.

Avtaar Singh, S. S., N. R. Banner, S. Rushton, A. R. Simon, C. Berry, and N. Al-Attar (2019). "ISHLT Primary Graft Dysfunction Incidence, Risk Factors, and Outcome: A UK National Study". *Transplantation* **103**:2, p. 336. DOI: 10.1097/TP.0000000000002220.

Chew, H. C., A. Iyer, M. Connellan, S. Scheuer, J. Villanueva, L. Gao, M. Hicks, M. Harkness, C. Soto, A. Dinale, P. Nair, A. Watson, E. Granger, P. Jansz, K. Muthiah, A. Jabbour, E. Kotlyar, A. Keogh, C. Hayward, R. Graham, P. Spratt, P. Macdonald, and K. Dhital (2019). "Outcomes of Donation After Circulatory Death Heart Transplantation in Australia". *Journal of the American College of Cardiology* **73**:12, pp. 1447–1459. DOI: 10.1016/j.jacc.2018.12.067.

Domínguez-Gil, B. (2022). "International figures on donation and transplantation 2021". *EDQM - Council of Europe*. Newsletter Transplant **27**. ISSN: 2171-4118.

Freed, D. H. and C. W. White (2015). "Donor heart preservation: straight up, or on the rocks?" *The Lancet* **385**:9987, pp. 2552–2554. DOI: 10.1016/S0140-6736(15)60614-6.

EDQM, (2022). *Guide to the Quality and Safety of Organs for Transplantation*. 8th ed. European Directorate for the Quality of Medicines & HealthCare. ISBN: 978-92-871-9240-0. (Visited on 2023-08-10).

Guyton, A. C. and J. E. Hall (2006). *Textbook of Medical Physiology*. 11th ed. Elsevier Saunders. ISBN: 978-0-7216-0240-0.

Hatami, S., J. Conway, D. H. Freed, and S. Urschel (2023). "Thoracic organ donation after circulatory determination of death". *Transplantation Reports* **8**:1, p. 100125. DOI: 10.1016/j.tpr.2022.100125.

John, M. M., W. Shih, D. Estevez, T. P. Martens, L. L. Bailey, A. J. Razzouk, and D. G. Rabkin (2019). "Interaction Between Ischemic Time and Donor Age on Adult Heart Transplant Outcomes in the Modern Era". *Ann Thorac Surg* **108**:3, pp. 744–748. DOI: 10.1016/j.athoracsur.2019.03.042.

Riksdagen (2022). *Lag (1995:831) om transplantation m.m.* https://www.riksdagen.se/sv/dokument-och-lagar/dokument/svensk-forfattningssamling/lag-1995831-om-transplantation-m.m_sfs-1995-831/. (Visited on 2023-11-15).

Lomero, M., D. Gardiner, E. Coll, B. Haase-Kromwijk, F. Procaccio, F. Immer, L. Gabbasova, C. Antoine, J. Jushinskis, N. Lynch, S. Foss, C. Bolotinha, T. Ashkenazi, L. Colenbie, A. Zuckermann, M. Adamec, J. Czerwiński, S. Karčiauskaitė, H. Ström, M. López-Fraga, B. Dominguez-Gil, and t. E. C. o. O. T. o. t. C. of Europe (CD-P-TO) (2020). "Donation after circulatory death today: an updated overview of the European landscape". *Transplant International* **33**:1, pp. 76–88. DOI: 10.1111/tri.13506.

McGiffin, D. C., C. E. Kure, P. S. Macdonald, P. C. Jansz, S. Emmanuel, S. F. Marasco, A. Doi, C. Merry, R. Larbalestier, A. Shah, A. Geldenhuys, A. K. Sibal, C. A. Wasywich, J. Mathew, E. Paul, C. Cheshire, A. Leet, J. L. Hare, S. Graham, J. F. Fraser, and D. M. Kaye (2023). "Hypothermic oxygenated perfusion (HOPE) safely and effectively extends acceptable donor heart preservation times: Results of the Australian and New Zealand trial". *The Journal of Heart and Lung Transplantation*. DOI: 10.1016/j.healun.2023.10.020.

Messer, S., S. Cernic, A. Page, M. Berman, P. Kaul, S. Colah, J. Ali, E. Pavlushkov, J. Baxter, R. Quigley, M. Osman, E. Nachum, J. Parameshwar, Y. Abu-Omar, J. Dunning, M. Goddard, S. Bhagra, S. Pettit, C. Cheshire, C. Lewis, A. Kydd, A. Ali, C. Sudarshan, D. Jenkins, S. Tsui, R. Hall, P. Catarino, and S. R. Large (2020). "A 5-year single-center early experience of heart transplantation from donation after circulatory-determined death donors". *The Journal of Heart and Lung Transplantation* **39**:12, pp. 1463–1475. DOI: 10.1016/j.healun.2020.10.001.

Messer, S., A. Page, R. Axell, M. Berman, J. Hernández-Sánchez, S. Colah, B. Parizkova, K. Valchanov, J. Dunning, E. Pavlushkov, S. K. Balasubramanian, J. Parameshwar, Y. A. Omar, M. Goddard, S. Pettit, C. Lewis, A. Kydd, D. Jenkins, C. J. Watson, C. Sudarshan, P. Catarino, M. Find-

lay, A. Ali, S. Tsui, and S. R. Large (2017). "Outcome after heart transplantation from donation after circulatory-determined death donors". *The Journal of Heart and Lung Transplantation* **36**:12, pp. 1311–1318. DOI: 10.1016/j.healun.2017.10.021.

Nilsson, J., V. Jernryd, G. Qin, A. Paskevicius, C. Metzsch, T. Sjöberg, and S. Steen (2020). "A nonrandomized open-label phase 2 trial of nonischemic heart preservation for human heart transplantation". *Nat Commun* **11**:1, p. 2976. DOI: 10.1038/s41467-020-16782-9.

GODT, (2023). *Organ Donation and Transplantation Activities 2022 Report*. Tech. rep. Global Observatory on Donation and Transplantation (GODT). (Visited on 2023-11-24).

Pigot, H., J. Hansson, A. Paskevicius, Q. Liao, T. Sjöberg, S. Steen, and K. Soltesz (2021). "Identification of cardiac afterload dynamics from data". *IFAC-PapersOnLine*. 11th IFAC Symposium on Biological and Medical Systems BMS 2021 **54**:15, pp. 508–513. DOI: 10.1016/j.ifacol.2021.10.307.

Pigot, H., T. Norlander, and K. Soltesz (filed 2023-05-17). "Afterload for heart evaluation". (Sveriges patent och registreringsverket).

Pigot, H., C. B. Sancho, A. Paskevicius, S. Steen, and K. Soltesz (2020). "Advantage of new ventilation method for cardiopulmonary resuscitation qualitatively captured by simple respiratory mechanics models". In: *2020 American Control Conference (ACC)*, pp. 1317–1322. DOI: 10.23919/ACC45564.2020.9147868.

Pigot, H. and K. Soltesz (2022). "The differential-algebraic Windkessel model with power as input". In: *2022 American Control Conference (ACC)*, pp. 3006–3011. DOI: 10.23919/ACC53348.2022.9867889.

Pigot, H., K. Soltesz, A. Paskevicius, Q. Liao, T. Sjöberg, and S. Steen (2022). "A novel nonlinear afterload for ex vivo heart evaluation: Porcine experimental results". *Artificial Organs* **46**:9, pp. 1794–1803. DOI: 10.1111/aor.14307.

Pigot, H., K. Soltesz, and S. Steen (in press, 2024). "Ex vivo working porcine heart model". In: *Experimental Models of Cardiovascular Diseases*. 2nd ed. Methods in Molecular Biology. Humana Press, New York, NY.

Pigot, H., Y. Wahlquist, and K. Soltesz (2023). "Actively controlled cardiac afterload". *IFAC-PapersOnLine*. 22nd IFAC World Congress **56**:2, pp. 6484–6489. DOI: 10.1016/j.ifacol.2023.10.863.

Vävnadsrådet, (2020). *Protokoll För Donation Efter Cirkulationsstillestånd – DCD Version 2:0*. Tech. rep. Vävnadsrådet.

Qin, G., V. Jernryd, T. Sjöberg, S. Steen, and J. Nilsson (2022). "Machine Perfusion for Human Heart Preservation: A Systematic Review". *Transpl Int* **35**, p. 10258. DOI: 10.3389/ti.2022.10258.

Ribeiro, R. V. P., J. S. Alvarez, F. Yu, M. B. Adamson, E. Paradiso, A. R. M. Hondjeu, L. Xin, B. Gellner, M. Degen, V. Bissoondath, M. Meineri, V. Rao, and M. V. Badiwala (2020). "Comparing Donor Heart Assessment Strategies During Ex Situ Heart Perfusion to Better Estimate Posttransplant Cardiac Function". *Transplantation* **104**:9, pp. 1890–1898. DOI: 10.1097/TP.0000000000003374.

See Hoe, L. E., G. Li Bassi, K. Wildi, M. R. Passmore, M. Bouquet, K. Sato, S. Heinsar, C. Ainola, N. Bartnikowski, E. S. Wilson, K. Hyslop, K. Skeggs, N. G. Obonyo, T. Shuker, L. Bradbury, C. Palmieri, S. Engkilde-Pedersen, C. McDonald, S. M. Colombo, M. A. Wells, J. D. Reid, H. O'Neill, S. Livingstone, G. Abbate, A. Haymet, J.-S. Jung, N. Sato, L. James, T. He, N. White, M. A. Redd, J. E. Millar, M. V. Malfertheiner, P. Molenaar, D. Platts, J. Chan, J. Y. Suen, D. C. McGiffin, and J. F. Fraser (2023). "Donor heart ischemic time can be extended beyond 9 hours using hypothermic machine perfusion in sheep". *The Journal of Heart and Lung Transplantation* **42**:8, pp. 1015–1029. DOI: 10.1016/j.healun.2023.03.020.

Soltesz, K., A. Paskevicius, H. Pigot, Q. Liao, T. Sjöberg, and S. Steen (2019). "Phase-controlled intermittent intratracheal insufflation of oxygen during chest compression-active decompression mCPR improves coronary perfusion pressure over continuous insufflation". *Resuscitation* **138**, pp. 215–221. DOI: 10.1016/j.resuscitation.2019.02.045.

SOSFS (2022). *SOSFS 2005:10 Socialstyrelsens föreskrifter om kriterier för bestämmande av människans död*. https://www.socialstyrelsen.se/kunskapsstod-och-regler/regler-och-riktlinjer/foreskrifter-och-allmanna-rad/konsoliderade-foreskrifter/200510-om-kriterier-for-bestammande-av-manniskans-dod/. (Visited on 2023-11-27).

Steen, S., A. Paskevicius, Q. Liao, and T. Sjöberg (2016). "Safe orthotopic transplantation of hearts harvested 24 hours after brain death and preserved for 24 hours". *Scandinavian Cardiovascular Journal* **50**:3, pp. 193–200. DOI: 10.3109/14017431.2016.1154598.

Tchana-Sato, V., D. Ledoux, O. Detry, G. Hans, A. Ancion, V. D'Orio, P. B. Massion, P. Amabili, S. Bruls, J. P. Lavigne, J. Monard, M.-H. Delbouille, N. Sakalihasan, and J. O. Defraigne (2019). "Successful clinical transplantation of hearts donated after circulatory death using normothermic regional perfusion". *The Journal of Heart and Lung Transplantation* **38**:6, pp. 593–598. DOI: 10.1016/j.healun.2019.02.015.

Socialstyrelsen (2022). *Vägledning för hälso- och sjukvården om donation*.

Wahlquist, Y., K. Soltesz, Q. Liao, X. Liu, H. Pigot, T. Sjöberg, and S. Steen (2021). "Prevention of Ischemic Myocardial Contracture Through Hemodynamically Controlled DCD". *Cardiovasc Eng Tech*. DOI: 10.1007/s13239-021-00537-8.

White, C. W., E. Ambrose, A. Müller, Y. Li, H. Le, B. Hiebert, R. Arora, T. W. Lee, I. Dixon, G. Tian, J. Nagendran, L. Hryshko, and D. Freed (2015). "Assessment of donor heart viability during ex vivo heart perfusion". *Can. J. Physiol. Pharmacol.* **93**:10, pp. 893–901. DOI: 10.1139/cjpp-2014-0474.

Paper I

Ex vivo working porcine heart model

Henry Pigot Kristian Soltesz Stig Steen

Abstract

Ex vivo working porcine heart models allow for the study of a heart's function and physiology outside the living organism. These models are particularly useful due to the anatomical and physiological similarities between porcine and human hearts, providing an experimental platform to investigate cardiac disease or assess donor heart viability for transplantation. This chapter presents an in-depth discussion of the model's components, including the perfusate, preload, and afterload. We explore the challenges of emulating cardiac afterload and present a historical perspective on afterload modeling, discussing various methodologies and their respective limitations. An actively controlled afterload device is introduced to enhance the model's ability to rapidly adjust pressure in the large arteries, thereby providing a more accurate and dynamic experimental model. Finally, we provide a comprehensive experimental protocol for the *Ex vivo* working porcine heart model.

In press as a book chapter for Experimental Models of Cardiovascular Diseases, 2nd edition (2024). Reprinted with permission.

1. Introduction

An *Ex vivo* working heart model is an experimental setup that aims to mimic the *in vivo* hemodynamic conditions of the heart outside of the body. Porcine hearts in particular are used due to their anatomical and physiological similarities to the human heart [Lelovas et al., 2014]. In the working heart model, the organ is perfused with a blood-like solution, whereby the solution is fed to the atrium and—by the work of the heart—follows the natural direction of blood flow from the atria to the ventricles and out through the large arteries. The model enables the study of heart physiology and function in a controlled environment, isolated from other bodily systems. It is used to investigate the heart under various physiological, pharmacological, and pathological conditions, leading to a better understanding of cardiovascular diseases and potential treatments.

In the context of heart transplantation, an *Ex vivo* working heart model could provide clinicians with functional metrics to assess the viability of a donor heart. The model enables testing different loading conditions by varying preload and afterload, which are crucial factors in determining the heart's ability to pump blood efficiently. This follows from the Frank-Starling mechanism [Knowlton and Starling, 1912] which describes the relationship between myocardial stretch in the ventricle and the subsequent force of contraction. Initial studies suggest that functional metrics of heart performance are better predictors of transplantation outcomes than the metabolic metrics available in non-working heart perfusion models such as the commercially available Transmedics Organ Care System [White et al., 2015; Ribeiro et al., 2020].

The ability to evaluate candidate heart organ function is particularly important for enabling the use of marginal donor hearts. Marginal donors are those who would not typically be considered for use in transplantation due to their age or medical history, or who have undergone circulatory death (so called DCD donors). Motivated by organ shortages, some countries have started transplanting organs from DCD donors, and research groups are investigating a variety of strategies to increase their safe use [Messer et al., 2023; Joshi et al., 2023; Madan et al., 2022; Soltesz et al., 2018; Wahlquist et al., 2021; Messer et al., 2016]. Such organs present both an opportunity and an additional risk. Working heart models offer a platform for evaluating each marginal organ to ensure its function and evaluate its suitability for a particular recipient.

Heart transplantation is a highly time-sensitive procedure, and functional organ evaluation requires time between organ removal and transplantation. The ischemic time—the period during which the organ lacks perfusion with a blood-like fluid—has been an important factor in determining the success of heart transplants. The ischemic time is dominated by the transport of the organ, and is generally restricted to 4 hours to limit ischemia and reper-

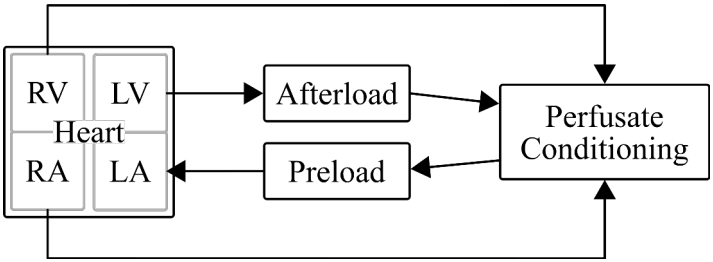

Figure 1. Ex vivo working heart system overview. Arrows indicate the movement of perfusate through the system. Perfusate is conditioned and sent to the preload device, where it enters the left atrium. The perfusate is then ejected from the left atrium, with perfusate flowing through the afterload device back to the perfusate conditioning reservoir. Some perfusate flows through the coronary arteries and out from the right heart to the reservoir.

fusion damage when using static cold storage (SCS). SCS involves flushing the heart with a cold cardioplegic solution and transporting it on ice. Non-ischemic heart preservation (NIHP) is a potential alternative to static cold storage (SCS), whereby the heart is perfused in a portable machine using an oxygenated cardioplegic blood-like solution. Preclinical porcine studies have shown that hearts can be preserved safely with NIHP for 24 h, and its feasibility for clinical use has been shown in an initial study [Steen et al., 2016; Nilsson et al., 2020]. Machine perfusion strategies like NIHP would enable the transition of an organ from the donor, to a working heart model for functional evaluation, and from the evaluation to the recipient with minimal total ischemic time.

1.1 Working heart model overview

A typical working heart model is illustrated as a block diagram in Figure 1, wherein the left side of the heart is working. The key components are the heart, perfusate, perfusate conditioning, preload device, and afterload device. The perfusate is a blood-like fluid for transporting oxygen, nutrients, and hormones to the heart. Perfusate conditioning includes oxygenation, temperature control (typically together via an oxygenator connected to a heater-cooler), arterial filtration, and the addition of drugs or other additives for the maintenance of heart function or experimental intervention. In particular, the ex vivo heart has no contact with the pituitary gland and brain stem, necessitating pharmacological support via the perfusate to regulate heart rate, contractility, and vascular tonus as described in [Steen et al., 2012].

The preload device is used to set the degree of stretch experienced by the ventricle at the end of diastole, which affects cardiac output according

to the Frank-Starling mechanism. This is typically done by setting the mean atrial pressure, for example by controlling the height of a perfusate column that feeds the atrium. The perfusate is then pumped by the heart from the ventricle through the afterload device, which controls the impedance that the ventricle must overcome to eject blood during systole (analogous to vascular impedance in vivo). From the afterload device, the perfusate returns to the perfusate conditioning system, before arriving back to the heart via the preload device.

When testing only the left-side of the heart, the right atrium and ventricle should be vented to prevent pressure build-up. The preload and afterload setup can be mirrored to the right side of the heart with reduced pressures, making a biventricular working heart model. Although less common, right-heart-only working mode can be done, provided that coronary perfusion is accounted for, e. g., by Langendorff perfusion of the aortic root [Langendorff, 1895].

In addition to the basic functional blocks, measurement transducers and data acquisition can be used to monitor parameters such as pressure, volume, flow, temperature, and electrical activity. Pacing may also be used to up-regulate the heart rhythm during experiments.

1.2 Working heart model objectives

To test a variety of working conditions, the ex vivo working heart model should allow independent adjustment of the following parameters, to within the limits defined by the ability of the heart under test: cardiac output, and systolic and diastolic pressures in the large artery. These adjustments are also reflected in the observed ventricular pressure.

The heart adjusts stroke volume based on venous return, leading to changes in cardiac output. As such, it is desirable that the preload in the working heart model can be manipulated to study the heart's response to changes in venous return and test different cardiac outputs.

Systolic and diastolic pressures vary between individuals and within a given individual depending on factors such as exertion, stress, and medical conditions. Controlling the two, independent of each other and cardiac output, is therefore necessary to emulate the range of physiological and pathological scenarios that a heart may encounter in vivo, from a healthy resting state to disease states such as hypertension.

Beyond adjusting cardiac output, systolic pressure, and diastolic pressure, maintaining an upper systolic limit and a lower diastolic limit in real-time, despite changes in cardiac inotropy, is a desirable safety feature. An afterload that can maintain pressure between these limits on a beat-to-beat basis can help ensure adequate coronary perfusion, while also avoiding ventricular hyperextension.

Between the set systolic and diastolic pressures, a working heart model should aim for reasonable pressure-flow dynamics to accurately reproduce in vivo hemodynamic conditions. An example of such dynamics is the well-established Windkessel model of cardiac afterload which uses a simple lumped parameter model to represent the resistance, compliance, and inertance of the systemic (or pulmonary) vasculature [Westerhof et al., 2009].

1.3 Establishing cardiac afterload

Cardiac afterload is the force the ventricle must exert to propel fluid into the large artery. In an ex vivo working heart model, we aim to emulate cardiac afterload using a mechanical device. In constructing such a device, it is helpful to be familiar with previous attempts to model cardiac afterload in the literature. Afterload has traditionally been modeled as the relationship between flow and pressure in the large arteries. The classic model, introduced by Frank at the end of the 19th century, combines discrete resistive and compliant elements in a lumped parameter circuit model [Frank, 1899]. In these so-called Windkessel models, the elements account for the resistance and compliance of the systemic vasculature, as shown in Figure 2. Windkessel models employ a circuit analogy where volumetric flow is represented as current, and pressure as voltage. During the 20th century, Frank's two element Windkessel model with one resistor and one capacitor was expanded to include up to 4 discrete elements [Westerhof et al., 2009; Westerhof et al., 1971; Burattini and Gnudi, 1982], improving its ability to model the pressure-flow relationship observed in the aorta [Segers et al., 2008].

The first isolated mammalian heart preparation, performed by Martin in 1881 [Martin, 1881; Fye, 1986], used a simple clamp resistor placed on the return line from the aorta to the perfusate reservoir. Starling went on to refine Martin's simple facsimile of peripheral vascular resistance using an adjustable resistor in 1912 [Knowlton and Starling, 1912]. The ability to adjust the heart load helped lead to his publication of the Frank-Starling law in 1918. Today, working heart models still make use of resistive afterloads, though improved to better fulfill the aforementioned objectives.

Mechanical implementations of Windkessel models are one such method, as shown in Figure 3. The compliant element, a sealed chamber containing a volume of gas, dampens pressure peaks during systole and provides coronary perfusion back to the heart during diastole. Resistive elements are generally constructed using a simple clamp on a tube, or a collection of small lumens in a tube. Detailed construction and benchtop analysis of one such afterload is provided by [Kung and Taylor, 2011], with [Abicht et al., 2018] illustrating its application in a biventricular porcine working heart model. A left-side only device has also been shown in a porcine working heart model, though it relied on a separate coronary perfusion circuit [de Hart et al., 2011]. An

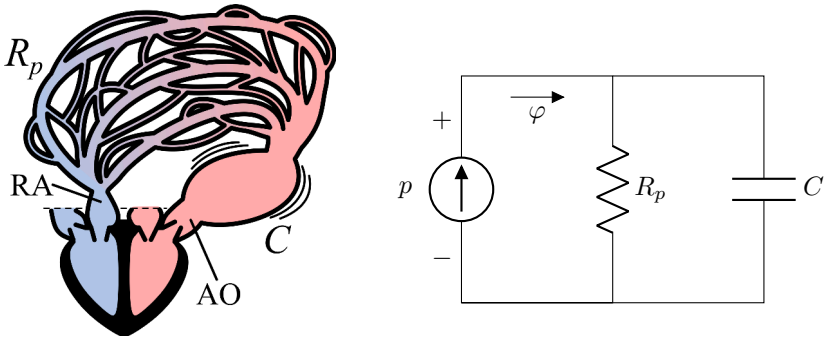

Figure 2. Functional sketch of physiological cardiac afterload (a), and corresponding electric circuit diagram (b). In the body, arterial compliance (C) comes primarily from the larger arteries e. g., the aorta (AO), and resistance (R_p) from the peripheral vasculature. In the circuit model, the heart is a current source, generating aortic blood flow φ resulting in aortic pressure p given C and R_p.

advantage of these Windkessel afterloads is that, with correctly adjusted elements, they can produce near-physiological pressure waveforms in the large arteries [Segers et al., 2008]. However, identifying valid parameter values and adjusting the elements accordingly is non-trivial [Pigot et al., 2021]. Since the mid-80s, the ability of these models to adjust aortic pressure in working heart models has been explored. Fisher demonstrated the use of a computer controlled slide to set mean aortic pressure by varying the peripheral resistance [Fisher et al., 1984], and included a manually adjustable compliance. More recently, Gellner published results of a working porcine heart using a manually adjustable Windkessel afterload, though the study did not reproduce physiological diastolic pressures or cardiac outputs [Gellner et al., 2020]. Adjusting the Windkessel model parameter values (resistance and compliance) has a coupled effect on systolic and diastolic pressure; adjusting a single element impacts both the systolic and diastolic pressures, complicating independent adjustment of the two. This coupling and the mechanical difficulty of rapidly changing the parameter values make the Windkessel afterload unsuited for maintaining upper and lower limits on aortic pressure beat-to-beat during the experiment. Furthermore, diastolic pressure support is limited by the volume of fluid stored in the compliant element, i. e., if the heart is weak or stops, the afterload is unable to maintain coronary perfusion for extended periods. Such support is important to recover performance as the heart is perfused and reconditioned at the start of the experiment, giving it the opportunity to safely stabilize to its full working potential. To overcome the

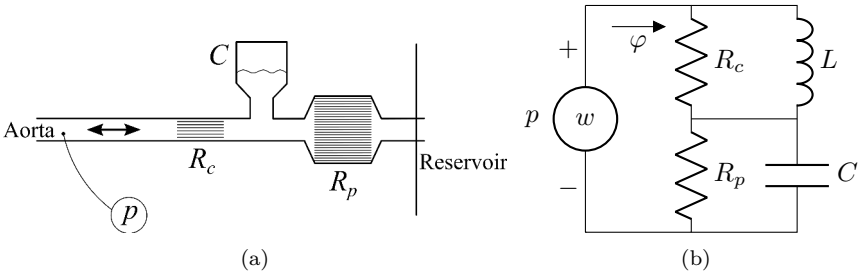

Figure 3. Physical implementation of a 4-element Windkessel afterload model (a) and its equivalent circuit model with the heart represented as power source w (b). Blood is pumped from the heart through the afterload made up of a resistive characteristic aortic impedance (R_c), inertance of the ejected blood (inductance) L, vascular compliance (capacitance) C, and peripheral vascular resistance R_p. This results in aortic pressure p and flow φ. In the physical implementation, L is captured by the inherent inertance of the perfusate fluid. Circuit (b) modified from [Pigot and Soltesz, 2022] with permission from the American Automatic Control Council.

latter limitation, a pump to facilitate Langendorff perfusion can be added to the aortic root.

Another afterload implementation uses a pump to force perfusate towards the aortic root during working mode, generally in combination with a resistive element and sometimes a compliant chamber. The resistor shunts excess flow away from the aortic root. In systole, perfusate flows from both the ventricle and pump through the resistor. In diastole, with the aortic valve closed, perfusate flows from the pump through both the resistor and coronary arteries. The afterload resistance, being much lower than the coronary artery resistance, defines the resulting diastolic pressure according to Poiseuille's law. As in the Windkessel model, a compliant element may be added to dampen pressure spikes during systole, and support diastolic pressure levels. In contrast to the passive Windkessel model approach, the pump is able to support diastolic pressure regardless of heart performance, helping to secure coronary perfusion throughout the ex vivo procedure.

Two examples of such pump-supported afterload methods are shown in Figure 4 with a centrifugal pump (a) or roller pump (b). The centrifugal pump differs from the roller pump in two key ways: it has a smooth flow profile and a lower internal resistance, allowing for negative flow through the pump. Furthermore, the internal resistance of the centrifugal pump is proportional to its rotational velocity. As such, afterload on the large arteries can be adjusted using the speed of the pump, and the shunt resistor can be small or eliminated entirely. This is the approach taken by Freed's group, where pump speed is manually adjusted to set diastolic pressure [White et

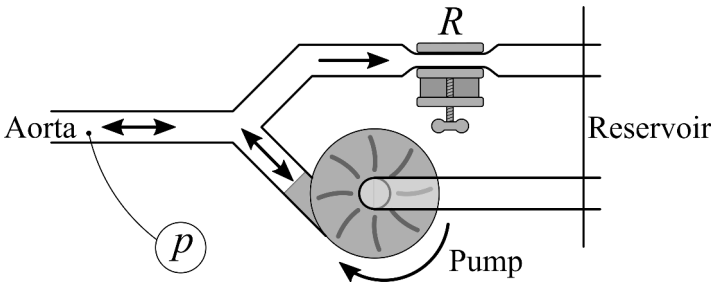

(a) centrifugal pump supported afterload

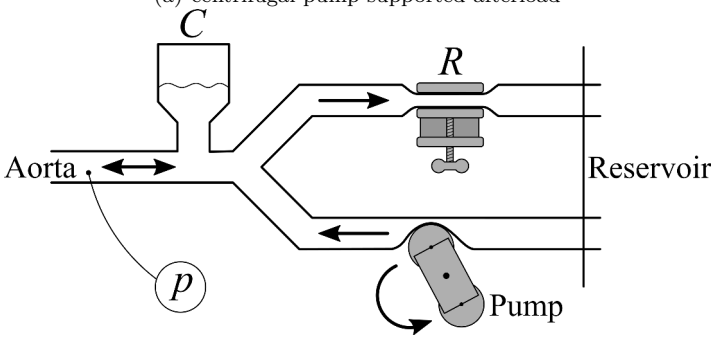

(b) roller pump supported afterload

Figure 4. Simplified drawings of afterload techniques (a) centrifugal pump supported, and (b) roller pump supported, with aortic pressure p and shunt resistor R, and compliance chamber C. Arrows indicate the direction of perfusate flow. The internal resistance of the centrifugal pump in (a) is proportional to the square of pump velocity.

al., 2015; Hatami et al., 2019]. A similar approach has been demonstrated by [Schechter et al., 2014] as well as Badiwala's group who included a manually adjustable shunt resistor [Hondjeu et al., 2020; Xin et al., 2018].

It is common to see the addition of a compliance chamber as part of the afterload, which also helps smooth the pulsatile flow coming from the roller pump [Kobayashi et al., 2020; Snoeckx et al., 1986]. The internal impedance of the roller pump is high relative to the shunt resistor, so flow only travels towards the attached larger artery and additional load elements (resistor and compliance). Pump-based afterload methods face the same challenges as Windkessel-based approaches. The afterload parameters are coupled, i. e., a change in one of pump speed or shunt resistance will impact both systolic and diastolic pressure. Although the pumps ensure a lower bound on diastolic pressure, unlike the Windkessel based approach, they do not address the issue of safely limiting systolic pressure on a beat-to-beat basis. Without the use of an additional compliance chamber (creating a 2-element

Windkessel model in combination with the pump) and careful tuning of both the shunt resistance and compliance for each hemodynamic condition, pump-based methods do not produce the physiological pressure waveforms that can be accomplished with a Windkessel afterload. Our group has investigated an alternative afterload approach using an adjustable pneumatic system based on Starling's original design wherein the pressure surrounding a flexible tube through which the perfusate flows is modulated to control afterload [Pigot et al., 2022]. The afterload demonstrated physiological loading conditions in multiple porcine working heart experiments. By enforcing pressure limits on the gas around the flexible tube, beat-to-beat pressure limiting may be possible. A disadvantage of the pneumatic system is its elaborate mechanical design requiring complex geometries and multiple pressure control systems.

1.4 Actively controlled afterload

In order to overcome the aforementioned shortcomings of existing afterload devices and fulfill the objectives of the working heart model, an actively controlled afterload device can be used. A simple construction using a variable flow conductance and pump is combined with feedback control principles to allow the user to program the desired pressure-flow dynamics. A drawing of such a device is shown in Figure 5, and described in detail in [Pigot et al., 2023]. The basic operating principle is akin to the previously mentioned pump-based afterloads, with the key difference that pressure in the large arteries can be rapidly adjusted. Measurements of the pressure in the artery and state of the afterload device are used to continuously adjust the afterload such that it mimics the desired afterload dynamics [Åström and Murray, 2021]. For example, the physiological waveforms offered by Windkessel dynamics can be combined with hard upper and lower limits on arterial pressure to ensure safe conditions for the heart throughout the experiment, or Windkessel model parameters can be programmed to change throughout the experiment to represent different disease states or the load presented by multiple potential transplant recipients [Pigot and Soltesz, 2022; Pigot et al., 2023].

A more detailed view of an actively controlled afterload device is shown in Figure 6. Adjusting the position of the plunger u changes the resistance to fluid flow through the device, with maximum resistance in the fully closed position $u = 0$. In systole, flow from both the heart (φ) and the pump (ϕ) travels through the variable flow conductance. During diastole the flow from the pump is divided between flow through the aorta to the coronary arteries and flow through the conductance. This auxiliary flow provided by the pump is important for enabling positive arterial pressures even when arterial flow is zero or negative, as in diastole. As such, the purely resistive plunger device is capable of delivering volume back towards the heart, as arterial compliance

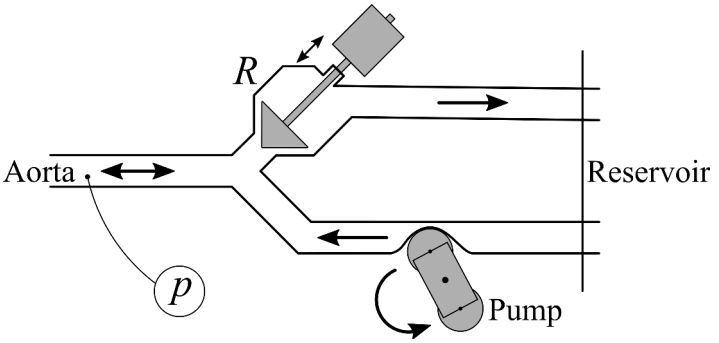

Figure 5. Simplified drawing of actively controlled afterload, with aortic pressure p. Variable flow conductance R is adjusted to achieve the desired aortic pressure-flow dynamics. A pump provides auxiliary flow to the aortic root, which is shunted through R together with flow from the aorta. The flow returns from the afterload device to the perfusate reservoir.

does in the body. A roller pump is used for this application due to its high internal resistance, ensuring that flow cannot travel back through the pump during periods of high afterload pressure.

A diagram of the control system is shown in Figure 7. An embedded controller is used to adjust the afterload resistance in real time at a frequency much higher than typical hemodynamics, which are generally below 20 Hz for a heart rate of 80 bpm [Westerhof et al., 2019]. The controller takes measurements of arterial pressure, plunger position, and motor current, as well as control parameters from an attached computer such as the desired pressure limits or Windkessel model parameters. Based on these inputs, the embedded controller calculates the desired plunger position and the corresponding motor voltage applied to manipulate the plunger position to achieve the corresponding aortic pressure and flow.

A prototype of the actively controlled afterload device is shown in Figure 8. A detachable cannula is used to cannulate the large artery on the heart during excision, which is then attached to the main afterload device body. A similar cannula is used for the atrium and preload device. A barbed connector is used to attach the auxiliary roller pump flow source. The auxiliary flow is directed orthogonal to the direction of flow from the large artery to limit the impact of auxiliary flow linear momentum on the pressure-flow dynamics. After passing the plunger body, perfusate exits the afterload through a large opening and returns to the perfusate reservoir.

Figure 9 shows a simplified overview of the complete ex vivo working heart model setup for the left side of the heart. A description of the setup and operating procedure is provided below in the Method section. A heater-cooler

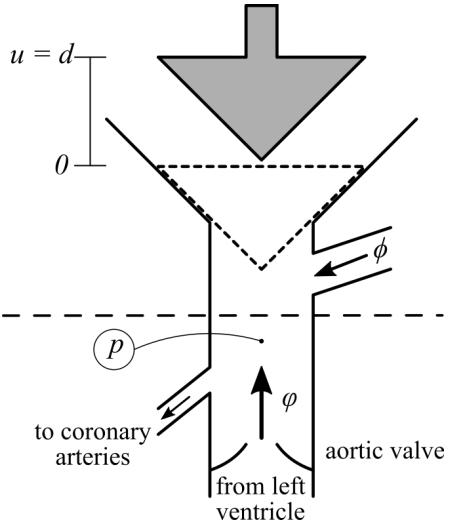

Figure 6. Schematic of an actively controlled afterload device (above dashed line) connected to the heart (below). The afterload consists of a plunger actively controlled to position $0 < u < d$. The flow through the device consists of the aortic flow φ, and an auxiliary contribution ϕ, chosen to ensure $\varphi + \phi > 0$. Plunger position control is based on measurements of aortic pressure p. Reproduced from [Pigot et al., 2023] with permission from the International Federation of Automatic Control.

and oxygenator condition the perfusate, with a roller pump ensuring adequate circulation through the oxygenator. The heart is suspended in a reservoir such that it is partially submerged and supported by the perfusate. The valves of the heart's right side are kept open to allow accumulated perfusate from the coronary arteries to move freely back into the reservoir. Perfusate is pumped to a preload device on the left atrium made up of a vortex with a compliant chamber above. The vortex limits the linear momentum of the pump flow to prevent forced atrial filling, while the compliant chamber fills to establish preload according to the balance between the incoming flow and the heart's movement of perfusate through the atrium to the ventricle as described in [Pigot et al., 2022; Steen et al., 2019]. Perfusate is pumped from the ventricle through the afterload device, where it returns to the reservoir. Both the preload and afterload feature deairing ports at their highest points to help prevent the accumulation of harmful air bubbles in the perfusion circuit.

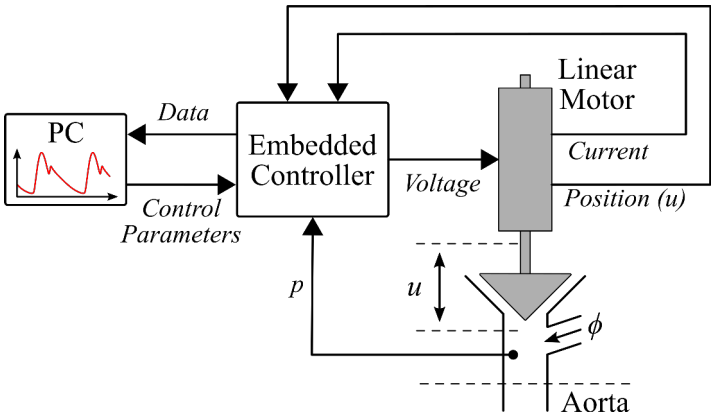

Figure 7. Sketch of the actively controlled afterload system connected to the aortic root, with constant auxiliary flow (ϕ). Control parameters such as the desired systolic and diastolic pressures are sent from the computer to the embedded controller. The embedded controller uses aortic pressure measurements (p), plunger position (u) measurements, and motor current measurements to rapidly control the motor voltage such that the resulting position yields the desired afterload dynamics.

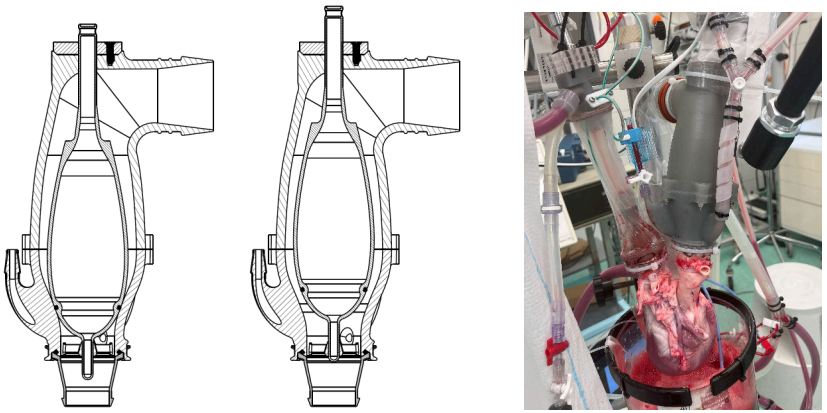

(a) (b)

Figure 8. (a) shows a plane view of the actively controlled afterload in the closed (left) and open (right) position. (b) shows a photo of the afterload in an ex vivo working porcine heart model (left side of the heart) with the preload on the left hand side of the photo, and the afterload on the right hand side. The linear motor controlling the plunger position are outside of the photo, above the device.

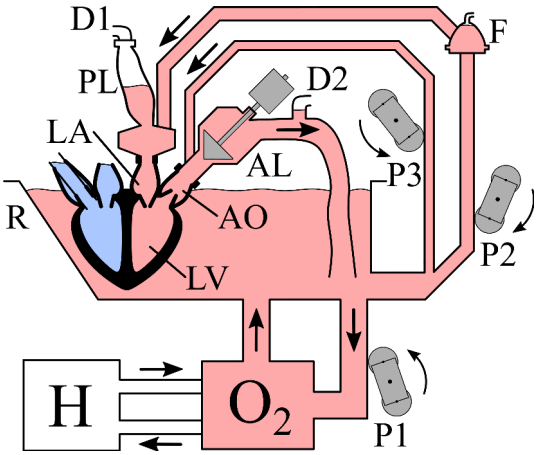

Figure 9. The left-side working mode experimental setup. Recirculation pump (P1) moves perfusate from the reservoir (R) through the oxygenator (O_2) connected to the heater-cooler (H). The preload pump (P2) provides perfusate through an arterial filter (F) to the preload device (PL) during working mode, which is connected to the left atrium (LA). Perfusate is pumped by the left ventricle (LV) out through the aorta (AO) to the afterload device (AL) where it returns to the reservoir. Auxiliary flow pump (P3) provides flow to the aortic root during Langendorff perfusion and working mode. Deairing pumps (not pictured) are connected to PL and AL at D1 and D2, respectively. Additional passive deairing may be done at F. All deairing drains back into R. Arrows indicate pump rotation and fluid flow direction during working mode.

2. Materials

The active afterload device has been evaluated in pilot porcine experiments using the left-ventricular working mode setup described above and illustrated in Fig. 8 and 9, following ethics approval 5.8.18-15906/2020 issued by "Malmö/Lunds Djurförsöksetiska Nämnd". The Materials and Method here describe the experimental protocol used, though the principles are applicable to other preload and afterload devices.

2.1 Measurement

1. Three pressure transducers for measuring aortic pressure, central venous pressure, and left atrial pressure in vivo.
2. Three central venous catheters.
3. Three pressure transducers for measuring left atrial, aortic, and left ventricular pressure ex vivo.

4. Aortic flow probe (see **Note 1**).
5. Data acquisition system.
6. Blood-gas analyzer (see **Note 2**).

2.2 Sedation and anesthesia

The following are for a 70 kg Swedish domestic pig (*sus scrofa domesticus*) according to local guidelines; your ethical and legal requirements may vary (see **Note 3**). Each is prepared in solution form in a syringe.

1. Sedation bolus: 1 g ketamine, 140 mg xylazin, 750 µg atropine.
2. Anesthesia bolus: 100 µg fentanyl, 20 mg midazolam.
3. Pre-tracheotomy bolus: 40 mg rocuronium.
4. Anesthesia maintenance solution: 10 ml of 100 mg/ml ketamine, 6 ml of 5 mg/ml midazolam, 20 ml of 10 mg/ml rocuronium; and 14 ml of 0.9 % NaCl saline solution.
5. Heparin bolus of 400 U/kg.
6. Infusion pump for anesthesia maintenance.
7. Central venous catheter for anesthesia maintenance.
8. St. Thomas cardioplegic solution at 4 °C.
9. Mechanical ventilator.

2.3 *Ex vivo* working heart setup

1. Krebs-Ringer solution: 119 mM NaCl, 15 mM $NaHCO_3$, 4.6 mM KCl, 1.5 mM $CaCl_2$, 1.2 mM NaH_2PO_4, 1.2 mM $MgCl_2$, 11 mM glucose.
2. Perfusate: 1.5 L Krebs-Ringer solution with 5 % Dextran 40, 7 % albumin, 10 000 U heparin, and approximately 1.5 L whole blood to yield a hematocrit of approximately 20 % (see **Note 4**).
3. Pharmacological support solution: 1 mg adrenaline, 1 mg noradrenaline, 1 mg cocaine 300 mg cortisol, 0.3 mg triiodothyronine diluted in a 50 ml syringe with 0.9 % NaCl saline solution (see **Note 5**).
4. Infusion pump for pharmacological support.
5. Three perfusion roller pumps that can accommodate ½ inch tubing (see **Notes 6-8**).

6. Two deairing roller pumps that can accommodate flow rates of approximately 200 mL/min.
7. Perfusate reservoir.
8. Oxygenator with heater-cooler and 95 % O_2 and 5 % CO_2 gas supply.
9. Arterial filter to remove bubbles and large particulates.
10. Preload device with matching atrial cannula.
11. Afterload device with matching aortic cannula.
12. Zip-ties for fastening the cannulas to the great vessels.
13. A structure for positioning the preload and afterload devices relative to the perfusate reservoir (see **Note 9**).
14. 1 mmol/ml $NaHCO_3$
15. 50 mg/ml glucose
16. 0.45 mmol/ml $CaCl_2$
17. 2 mmol/ml KCl
18. 1 mg/ml adrenaline

3. Methods

3.1 Preparation of the *ex vivo* working heart setup

1. Assemble ex vivo working mode setup excluding the perfusate solution and heart (see Figure 9).
2. Prepare pressure transducers for the atrium and ventricle (see **Note 10**).
3. Prepare pressure transducer for the aorta (see **Note 11**).
4. Set the heater-cooler to 37℃.
5. Apply 100 ml/min gas flow to the oxygenator.
6. Mix the perfusate solution in the reservoir and set the recirculation pump at 0.5 L/min (see **Note 12**).

7. Check blood-gas measurements of perfusate solution and adjust to preferred (homeostatic) levels. In particular: pH to 7.2–7.6 using $NaHCO_3$, keeping base excess close to zero; glucose to 4–8 mmol/L; Ca^{2+} to above 1.0 mmol/L (1.30 mmol/L preferred) using $CaCl_2$; Na^+ to 130–160 mmol/L (140 mmol/L preferred) using $NaHCO_3$ (or NaCl if necessary due to pH); K^+ to 4–5 mmol/L using KCl; hematocrit to 15–25 % by adding whole blood as necessary. Similar adjustments should be made as necessary throughout the experiment.

8. Mount the pharmacological support syringe into the infusion pump and connect its outlet to the perfusion circuit.

9. Set the afterload device to its minimum resistance (i. e., fully open).

10. Deair the preload and afterload tubing by slowly pumping perfusate via the preload pump and auxiliary flow pump (e. g., 0.5 L/min, see **Note 13**).

3.2 Preparation of the pig heart

1. Induce sedation with intramuscular injection of sedation bolus.

2. Establish intravenous access (see **Note 14**).

3. Give intravenous anesthesia bolus and confirm sufficient sedation.

4. Give intravenous pre-tracheotomy bolus and heparin bolus.

5. Establish ventilation via tracheotomy (see **Note 15**).

6. Insert two central venous catheters into the right internal jugular vein and guide them towards the right atrium, one for central venous pressure and the other for anesthesia maintenance. The catheter tip positions can be verified after sternotomy in step 3.2.11.

7. Insert a central venous catheter into the right carotid artery for aortic pressure measurement. The catheter tip position can be verified after sternotomy in step 3.2.11.

8. Insert anesthesia maintenance solution syringe into a continuous infusion pump and connect the infusion pump to one of the central venous catheters in the right internal jugular vein. Set infusion rate to 12–15 ml/h.

9. Attach pressure transducers to the central venous catheters for pressure measurement and calibrate to ambient pressure at the height of the atria.

10. Take a baseline blood-gas measurement. Adjust to preferred (homeostatic) levels.

11. Perform median sternotomy and cut away the pericardium and other surrounding tissues.

12. Insert a central venous catheter into the left atrium and attach a pressure transducer. Calibrate the transducer to ambient pressure at the height of the atria.

13. Place flow probe around the aorta.

14. Once the pig has stabilized, perform baseline pressure and flow measurements. Make note of systolic aortic pressure, diastolic aortic pressure, left atrial pressure, and cardiac output for use as points of comparison during ex vivo working mode.

15. Withdraw the central venous catheters from the superior vena cava and clamp the inferior and superior vena cava.

16. Wait until the heart has emptied, then remove the aortic flow probe and clamp the distal ascending aorta.

17. Inject 1 L of 4 °C cardioplegic solution into the ascending aorta, between the clamp and the aortic valve to induce cardiac arrest.

18. Cut the superior and inferior vena cava below the clamps so the cardioplegic solution can drain freely through the coronary arteries and out through the vena cava.

19. When the heart has stopped beating, excise the heart with the great vessels (see **Note 16**). The ischemic time (to step 3.3.8) should be minimized, and is typically 10–15 min.

20. Place the heart in ice slush such that the ventricles are submerged and the great vessels are exposed for attaching the cannulas.

21. Insert and fasten cannulas for attaching the preload and afterload devices to the atrium and aorta, respectively, using zip-ties (see **Note 17**).

3.3 Ex vivo working heart

1. Stop the preload and auxiliary flow pumps.

2. Set the pharmacological support infusion pump to 0.1 ml/h (see **Note 18**).

3. Mount the heart into the working mode setup by connecting the atrial cannula to the preload device, and the aortic cannula to the afterload device.

4. Refine the position of the heart so it is partially submerged in the perfusate, up to the level of the atrial-ventricular valves. Ensure that the position of the preload and afterload devices create a natural hanging position for the heart (see **Note 19**).

5. Slowly apply flow to the preload by increasing the speed of the preload pump, allowing the perfusate to slowly flow through the atrium, ventricle, and afterload device to prime the circuit and remove air bubbles.

6. Flush and zero the pressure transducers (see **Note 20**).

7. Start the afterload auxiliary flow pump (e. g., 2 L/min).

8. Set the afterload for a mean aortic pressure of 40–50 mmHg to begin Langendorff perfusion and flush the cardioplegic solution from the heart (see **Note 21**).

9. Throughout the experiment, deair as necessary using the deairing pumps on the preload and afterload devices (see **Note 22**).

10. When the heart develops a stable sinus rhythm (see **Note 23**), begin to provide perfusate to the left atrium (e. g., 2 L/min) to establish preload and start working mode.

11. Allow the heart to stabilize under low load, e. g., with diastolic pressure set at 50 mmHg and systolic pressure set at 80 mmHg and 2 L/min preload flow (see **Note 24**).

12. Adjust the evaluation parameters according to the desired experimental protocol. Physiologically relevant hemodynamics can be maintained for several hours using this model, provided that the perfusate is reconditioned according to the results of regular blood gas measurements (see **Note 25**).

13. When finished, revert to Langendorf perfusion by lowering the preload pump flow to zero and providing a low flow to the aortic root (e. g., 0.5 L/min) via the auxiliary flow pump while maintaining a mean aortic pressure of 50 mmHg or greater.

14. Induce cardioplegia by injecting cardioplegic solution into the aortic root.

15. Turn off afterload pump once the heart has stopped beating.

4. Notes

1. We use a Transonic Systems 20PS ultrasonic time-of-flight flow probe. Additionally, a coronary flow probe may be used.

2. We use a Radiometer ABL 700 blood-gas analyzer.

3. Our group treats the pigs according to relevant European guidelines [The European Parliament, 2010] and using a specific ethics approval from our local authority (Malmö/Lunds Djurförsöksetiska Nämnd). Ensure that you fulfill all regional animal welfare and ethics requirements before conducting this procedure. Here we describe our procedure, but yours may vary according to the relevant regulations.

4. The inclusion of albumin is important to yield a hyperoncotic solution which helps prevent edema during longer evaluations, however it may be excluded for shorter evaluations having lower edema risk. The total volume of perfusate required will vary depending on the exact assembly of your system (dimensions of tubes, reservoir, etc.).

5. Beyond the mechanical structure of the ex vivo working mode setup, pharmacological support is essential for heart function in isolation from the body [Steen et al., 2012]. In particular, the heart relies on the brainstem and pituitary gland to regulate vascular tonus, heart rate, and heart contractility, which are accounted for in the pharmacological support solution. Cocaine is included to inhibit noradrenaline reuptake.

6. ½ inch silicone is used in the roller pumps to minimize hemolysis that smaller tubing diameters (and therefore higher pump speeds) can cause. The use of smaller pump tubing may be possible if pump speeds and the resulting hemolysis risk are accounted for. Tubing of smaller diameter and other material can be used elsewhere in the circuit. Be wary of the high-pressure side of the circuit and secure tubing to barb connectors using zip-ties to help prevent leaks. Tubing lengths should be minimized where possible to lower the total perfusate volume needed in the circuit.

7. It is possible to rearrange the circuit to use only two roller pumps, by removing the recirculation pump and instead relying on one of the other pumps to circulate the perfusate through the oxygenator (e. g., the auxiliary flow pump), however sufficient flow for perfusate conditioning must be ensured to maintain temperature and gas exchange throughout the experiment.

8. It may be desirable to add a compliance chamber followed by a resistance (e. g., tube clamp) after the auxiliary flow pump to help smooth

the auxiliary flow arriving at the aortic root. High resistance is necessary to prevent backflow towards the compliant chamber during systole. Be wary of additional hemolysis that the resistance may introduce.

9. We use articulated arms with locking joints mounted above the reservoir to enable position adjustment of the preload and afterload device from which the heart hangs.

10. To measure atrial pressure we use a fluid-filled baby-feeding tube fed through the preload with its open tip extending just past the atrial cannula into the atrium itself. The other end of the tube protrudes from the top of the preload device and is attached via luer-lock to a pressure transducer. Another baby-feeding tube is similarly positioned such that it passes through the atrial cannula and the atrial-ventricular valve into the ventricle once the heart is mounted to the preload. Alternatively, transducer tips could be sown directly into the atrium and ventricle of the heart prior to mounting.

11. A luer-lock attachment at the aortic cannula facilitates the connection of a pressure transducer. Alternatively, a transducer tip could be sown directly into the aorta prior to mounting.

12. To prevent the accumulation of bubbles in the perfusate solution, mix slowly using the recirculation pump that feeds into the oxygenator (e. g., 0.5 L/min).

13. Minimize dripping or splashing of the fluid by submerging the lower opening of the preload and afterload devices below the perfusate surface.

14. We establish intravenous access on the pig ear, as the veins are clearly visible and relatively easy to access.

15. Using the mechanical ventilator, set $PaCO_2$ to approximately 5 kPa (e. g., with 8 ml/kg body weight tidal volume, 20 breaths/min, positive end-expiratory pressure 5 cmH_2O).

16. Enough tissue must remain on the heart to facilitate the connection of atrial and large-artery cannulas for connecting the preload and afterload devices. However, excessive tissue on the large arteries may introduce undesirable parasitic compliance and inertance, so a conservative amount of tissue is recommended (i. e., just enough to allow cannula attachment).

17. The atrial cannula is inserted via the pulmonary vein cut close to the atrial wall, forming a circle in the atrial wall. The cannula tip is inserted flush with the atrial wall, using just enough tissue to fasten the

cannula. Any other holes in the vessels should be closed with sutures. The valves of the right side of the heart should be propped open to prevent pressure-build up during perfusion, e. g., with pieces of silicone tubing. The atrial and aortic cannulas have the same opening diameter, which should be large so as not to restrict flow, e. g., 20–25 mm. The cannulas should also be as short as possible to minimize parasitic compliance and inertance.

18. The infusion rate of the pharmacological support solution should be adjusted throughout the experiment between 0.1 ml/h and 4 ml/h according to the desired heart rate in working mode. We typically aim for 100–110 bpm. Raising the infusion rate should raise the heart rate, though an excess can lead to tachycardia. If a higher heart rate is desirable during a shorter period, a 40 µg adrenaline bolus can be used.

19. Ensure that the heart tissue, especially the aorta, is not twisted or kinked such that flow to or from the heart is occluded. To achieve this, the angle and rotation of the preload and afterload devices may need to be adjusted.

20. Air bubbles in the pressure measurement lines should be eliminated to prevent artificial smoothing of the measured pressures. Prime the lines with perfusate. To zero all pressure transducers to the same reference value, set the tips of all pressure measurement lines level with the right atrium. When manipulating the experimental setup, changes in transducer or measurement line tip height may necessitate re-zeroing.

21. The successful resumption of coronary flow will be indicated by dark deoxygenated perfusate coming from the right side of the heart.

22. Active deairing pumps on the preload and afterload devices can be used to help remove accumulated air. They should be used only as necessary to avoid unnecessary hemolysis. If preload pump flow is used as a proxy for cardiac output, the flow removed by the deairing pumps must be accounted for.

23. Once Langendorff perfusion begins, sinus rhythm should begin within a few minutes. Provide 20–50 Joule defibrillation directly on the heart as required if ventricular tachycardia occurs. Note that the pharmacological support solution helps the heart to develop a steady sinus rhythm.

24. The diastolic and systolic pressure setpoints (afterload) and the flow provided to the atrium (i. e., preload and resulting cardiac output of the working heart) should be adjusted according to the observed performance of the heart in working mode. The in vivo measurements can

serve as a reference point for what performance can be expected. If the heart is unable to manage the set cardiac output and afterload, the preload pressure will rise as fluid accumulates in the preload device. If this occurs, preload pump flow should be reduced, and afterload settings reevaluated.

25. The hours-long experiments we typically run using this model are far longer than necessary in a transplantation context where the technology could serve as decision support. For physiological and pharmacological studies it may be relevant to maintain the working heart model for longer. This is yet to be explored, but we see no reason why times in the range of days could not be attainable as long as the perfusate is correctly conditioned and the heart is kept humid. During such longer experiments, the risks of edema (and therefore the inclusion of oncotically active albumin in the perfusate) and hemolysis deserve particular attention when constructing the system and conditioning the perfusate.

Acknowledgement

This work was supported by the Hans-Gabriel and Alice Trolle-Wachtmeister Foundation for Medical Research, the LMK Foundation, and the Swedish Foundation for Strategic Research (Grant: SM21-0037). The authors from the Department of Automatic Control are members of the ELLIIT Strategic Research Area at Lund University.

References

Abicht, J.-M., T. Mayr, J. Jauch, S. Guethoff, S. Buchholz, B. Reichart, and A. Bauer (2018). "Large-Animal Biventricular Working Heart Perfusion System with Low Priming Volume—Comparison between in vivo and ex vivo Cardiac Function". *Thorac cardiovasc Surg* **66**:01, pp. 071–082. DOI: 10.1055/s-0036-1580604.

Åström, K. J. and R. M. Murray (2021). *Feedback Systems: An Introduction for Scientists and Engineers, Second Edition*. Princeton University Press. ISBN: 978-0-691-19398-4.

Burattini, R. and G. Gnudi (1982). "Computer identification of models for the arterial tree input impedance: Comparison between two new simple models and first experimental results". *Med. Biol. Eng. Comput.* **20**:2, pp. 134–144. DOI: 10.1007/BF02441348.

de Hart, J., A. de Weger, S. van Tuijl, J. M. A. Stijnen, C. N. van den Broek, M. C. M. Rutten, and B. A. de Mol (2011). "An ex vivo platform to simulate cardiac physiology: a new dimension for therapy development and assessment". *Int J Artif Organs* **34**:6, pp. 495–505. DOI: 10.5301/IJAO.2011.8456.

Fisher, A., R. E. Challis, and P. Swann (1984). "A controllable artificial afterload for isolated heart studies". *J Biomed Eng* **6**:4, pp. 305–310. DOI: 10.1016/0141-5425(84)90080-3.

Frank, O. (1899). "Die Grundform des arteriellen pulses. Erste Abhandlung. Erste Abhandlung." *Zeitschrift für Biologie* 37, pp. 485–526.

Fye, W. B. (1986). "H. Newell Martin and the isolated heart preparation: the link between the frog and open heart surgery." *Circulation* **73**:5, pp. 857–864. DOI: 10.1161/01.CIR.73.5.857.

Gellner, B., L. Xin, R. V. P. Ribeiro, V. Bissoondath, P. Lu, M. B. Adamson, F. Yu, E. Paradiso, J. Zu, C. A. Simmons, and M. V. Badiwala (2020). "The Implementation of an Adjustable Afterload Module for Ex Situ Heart Perfusion". *Cardiovasc Eng Tech* **11**:1, pp. 96–110. DOI: 10.1007/s13239-019-00447-w.

Hatami, S., C. W. White, M. Ondrus, X. Qi, M. Buchko, S. Himmat, L. Lin, K. Cameron, D. Nobes, H.-J. Chung, J. Nagendran, and D. H. Freed (2019). "Normothermic Ex Situ Heart Perfusion in Working Mode: Assessment of Cardiac Function and Metabolism". *JoVE (Journal of Visualized Experiments)* 143, e58430. DOI: 10.3791/58430.

Hondjeu, A. R. M., A. Mashari, R. Ramos, G. M. Ruggeri, J. Q. Hiansen, B. Gellner, R. V. P. Ribeiro, F. Yu, L. Xin, M. B. Adamson, M. V. Badiwala, and M. Meineri (2020). *Echocardiographic Assessment of Left Ventricular Function in Ex Situ Heart Perfusion Using Pump Supported and Passive Afterload Working Mode, a Pilot Study.* Preprint. Preprints. DOI: 10.22541/au.160133257.75178254.

Joshi, Y., S. Scheuer, H. Chew, M. Ru Qiu, C. Soto, J. Villanueva, L. Gao, A. Doyle, S. Takahara, C. Jenkinson, N. Vaidhya, Y. Matsumoto, B. Hwang, C. Zhao, A. Iyer, M. Connellan, A. Watson, E. Granger, K. Muthiah, A. Jabbour, E. Kotlyar, A. Keogh, N. K. Bart, C. Hayward, K. Dhital, P. Jansz, and P. S. Macdonald (2023). "Heart Transplantation From DCD Donors in Australia: Lessons Learned From the First 74 Cases". *Transplantation* **107**:2, p. 361. DOI: 10.1097/TP.0000000000004294.

Knowlton, F. P. and E. H. Starling (1912). "The influence of variations in temperature and blood-pressure on the performance of the isolated mammalian heart". *J Physiol* **44**:3, pp. 206–219. ISSN: 0022-3751. (Visited on 2023-02-03).

Kobayashi, Y., Y. Kotani, N. Sakoda, S. Kadowaki, and S. Kasahara (2020). "Ex Vivo Evaluation of the Biventricular Cardiac Function for Donation After Circulatory Death Model: An Experimental Study". *Artificial Organs*. DOI: 10.1111/aor.13834.

Kung, E. O. and C. A. Taylor (2011). "Development of a Physical Windkessel Module to Re-Create In Vivo Vascular Flow Impedance for In Vitro Experiments". *Cardiovasc Eng Tech* **2**:1, pp. 2–14. DOI: 10.1007/s13239-010-0030-6.

Langendorff, O. (1895). "Untersuchungen am überlebenden Säugethierherzen". *Pflügers Arch.* **61**:6, pp. 291–332. DOI: 10.1007/BF01812150.

Lelovas, P. P., N. G. Kostomitsopoulos, and T. T. Xanthos (2014). "A Comparative Anatomic and Physiologic Overview of the Porcine Heart". *J Am Assoc Lab Anim Sci* **53**:5, pp. 432–438. ISSN: 1559-6109. (Visited on 2023-06-13).

Madan, S., O. Saeed, S. J. Forest, D. J. Goldstein, U. P. Jorde, and S. R. Patel (2022). "Feasibility and Potential Impact of Heart Transplantation From Adult Donors After Circulatory Death". *Journal of the American College of Cardiology* **79**:2, pp. 148–162. DOI: 10.1016/j.jacc.2021.10.042.

Martin, H. N. (1881). "On a Method of Isolating the Mammalian Heart". *Science* **os-2**:46, pp. 228–228. DOI: 10.1126/science.os-2.46.228.a.

Messer, S., S. Rushton, L. Simmonds, D. Macklam, M. Husain, A. Jothidasan, S. Large, S. Tsui, P. Kaul, J. Baxter, M. Osman, V. Mehta, D. Russell, U. Stock, J. Dunning, D. G. Saez, R. Venkateswaran, P. Curry, L. Ayton, M. Mukadam, J. Mascaro, J. Simmonds, G. Macgowan, S. Clark, J. Jungschleger, Z. Reinhardt, R. Quigley, J. Speed, J. Parameshwar, D. Jenkins, S. Watson, F. Marley, A. Ali, D. Gardiner, A. Rubino, J. Whitney, S. Beale, C. Slater, I. Currie, L. Armstrong, J. Foley, M. Ryan, S. Gibson, K. Quinn, A.-M. Macleod, S. Spence, C. J. E. Watson, P. Catarino, A. Clarkson, J. Forsythe, D. Manas, and M. Berman (2023). "A national pilot of donation after circulatory death (DCD) heart transplantation within the United Kingdom". *The Journal of Heart and Lung Transplantation* **0**:0. DOI: 10.1016/j.healun.2023.03.006.

Messer, S. J., R. G. Axell, S. Colah, P. A. White, M. Ryan, A. A. Page, B. Parizkova, K. Valchanov, C. W. White, D. H. Freed, E. Ashley, J. Dunning, M. Goddard, J. Parameshwar, C. J. Watson, T. Krieg, A. Ali, S. Tsui, and S. R. Large (2016). "Functional assessment and transplantation of the donor heart after circulatory death". *The Journal of Heart and Lung Transplantation* **35**:12, pp. 1443–1452. DOI: 10.1016/j.healun.2016.07.004.

Nilsson, J., V. Jernryd, G. Qin, A. Paskevicius, C. Metzsch, T. Sjöberg, and S. Steen (2020). "A nonrandomized open-label phase 2 trial of nonischemic

heart preservation for human heart transplantation". *Nat Commun* **11**:1, p. 2976. DOI: 10.1038/s41467-020-16782-9.

Pigot, H., J. Hansson, A. Paskevicius, Q. Liao, T. Sjöberg, S. Steen, and K. Soltesz (2021). "Identification of cardiac afterload dynamics from data". *IFAC-PapersOnLine*. 11th IFAC Symposium on Biological and Medical Systems BMS 2021 **54**:15, pp. 508–513. DOI: 10.1016/j.ifacol.2021.10.307.

Pigot, H. and K. Soltesz (2022). "The differential-algebraic Windkessel model with power as input". In: *2022 American Control Conference (ACC)*, pp. 3006–3011. DOI: 10.23919/ACC53348.2022.9867889.

Pigot, H., K. Soltesz, A. Paskevicius, Q. Liao, T. Sjöberg, and S. Steen (2022). "A novel nonlinear afterload for ex vivo heart evaluation: Porcine experimental results". *Artificial Organs* **46**:9, pp. 1794–1803. DOI: 10.1111/aor.14307.

Pigot, H., Y. Wahlquist, and K. Soltesz (2023). "Actively controlled cardiac afterload". *IFAC-PapersOnLine*. 22nd IFAC World Congress **56**:2, pp. 6484–6489. DOI: 10.1016/j.ifacol.2023.10.863.

Ribeiro, R. V. P., J. S. Alvarez, F. Yu, M. B. Adamson, E. Paradiso, A. R. M. Hondjeu, L. Xin, B. Gellner, M. Degen, V. Bissoondath, M. Meineri, V. Rao, and M. V. Badiwala (2020). "Comparing Donor Heart Assessment Strategies During Ex Situ Heart Perfusion to Better Estimate Posttransplant Cardiac Function". *Transplantation* **104**:9, pp. 1890–1898. DOI: 10.1097/TP.0000000000003374.

Schechter, M. A., K. W. Southerland, B. J. Feger, D. L. Jr, A. A. Ali, L. Njoroge, C. A. Milano, and D. E. Bowles (2014). "An Isolated Working Heart System for Large Animal Models". *JoVE (Journal of Visualized Experiments)* 88, e51671. DOI: 10.3791/51671.

Segers, P., E. Rietzschel, M. De Buyzere, N. Stergiopulos, N. Westerhof, L. Bortel, T. Gillebert, and P. Verdonck (2008). "Three-and-four-element Windkessel models: Assessment of their fitting performance in a large cohort of healthy middle-aged individuals". *Proceedings of the Institution of Mechanical Engineers. Part H, Journal of engineering in medicine* **222**, pp. 417–28. DOI: 10.1243/09544119JEIM287.

Snoeckx, L. H. E. H., G. J. V. D. Vusse, W. A. Coumans, P. H. M. Willemsen, T. V. D. Nagel, and R. S. Reneman (1986). "Myocardial function in normal and spontaneously hypertensive rats during reperfusion after a period of global ischaemia". *Cardiovascular Research* **20**:1, pp. 67–75. DOI: 10.1093/cvr/20.1.67.

Soltesz, K., T. Sjöberg, T. Jansson, R. Johansson, A. Robertsson, A. Paskevicius, Q. Liao, G. Qin, and S. Steen (2018). "Closed-loop regulation of

arterial pressure after acute brain death". *J Clin Monit Comput* **32**:3, pp. 429–437. DOI: 10.1007/s10877-017-0033-z.

Steen, S., T. Sjöberg, Q. Liao, G. Bozovic, and B. Wohlfart (2012). "Pharmacological normalization of circulation after acute brain death". *Acta Anaesthesiol Scand* **56**:8, pp. 1006–1012. DOI: 10.1111/j.1399-6576.2012.02721.x.

Steen, S., A. Paskevicius, and B. King (2019). "Afterload device for a beating heart during examination thereof". US10405756B2. (Visited on 2020-07-14).

Steen, S., A. Paskevicius, Q. Liao, and T. Sjöberg (2016). "Safe orthotopic transplantation of hearts harvested 24 hours after brain death and preserved for 24 hours". *Scandinavian Cardiovascular Journal* **50**:3, pp. 193–200. DOI: 10.3109/14017431.2016.1154598.

The European Parliament (2010). *On the Protection of Animals Used for Scientific Purpose*. Tech. rep. Council of Europe.

Wahlquist, Y., K. Soltesz, Q. Liao, X. Liu, H. Pigot, T. Sjöberg, and S. Steen (2021). "Prevention of Ischemic Myocardial Contracture Through Hemodynamically Controlled DCD". *Cardiovasc Eng Tech*. DOI: 10.1007/s13239-021-00537-8.

Westerhof, N., G. Elzinga, and P. Sipkema (1971). "An artificial arterial system for pumping hearts." *Journal of Applied Physiology* **31**:5, pp. 776–781. DOI: 10.1152/jappl.1971.31.5.776.

Westerhof, N., J.-W. Lankhaar, and B. E. Westerhof (2009). "The arterial Windkessel". *Med Biol Eng Comput* **47**:2, pp. 131–141. DOI: 10.1007/s11517-008-0359-2.

Westerhof, N., N. Stergiopulos, M. I. Noble, and B. E. Westerhof (2019). "Appendix 1 Times & Sines: Fourier Analysis". In: *Snapshots of Hemodynamics: An Aid for Clinical Research and Graduate Education*. Springer International Publishing, Cham, pp. 283–287. DOI: 10.1007/978-3-319-91932-4.

White, C. W., E. Ambrose, A. Müller, Y. Li, H. Le, B. Hiebert, R. Arora, T. W. Lee, I. Dixon, G. Tian, J. Nagendran, L. Hryshko, and D. Freed (2015). "Assessment of donor heart viability during ex vivo heart perfusion". *Can. J. Physiol. Pharmacol.* **93**:10, pp. 893–901. DOI: 10.1139/cjpp-2014-0474.

Xin, L., B. Gellner, R. V. P. Ribeiro, G. M. Ruggeri, D. Banner, M. Meineri, V. Rao, J. Zu, and M. V. Badiwala (2018). "A New Multi-Mode Perfusion System for Ex Vivo Heart Perfusion Study". *J Med Syst* **42**:2, p. 25. DOI: 10.1007/s10916-017-0882-5.

Paper II

Identification of cardiac afterload dynamics from data

Henry Pigot Jonas Hansson Audrius Paskevicius
Qiuming Liao Trygve Sjöberg Stig Steen
Kristian Soltesz

Abstract

The prospect of *ex vivo* functional evaluation of donor hearts is considered. Particularly, the dynamics of a synthetic cardiac afterload model are compared to those of normal physiology. A method for identification of continuous-time transfer functions from sampled data is developed and verified against results from the literature. The method relies on exact gradients and Hessians obtained through automatic differentiation. This also enables straightforward sensitivity analyses. Such analyses reveal that the 4-element Windkessel model is not practically identifiable from representative data while the 3-element model underfits the data. Direct comparison of aortic pressure–flow relations, without relying on matching of fitted Windkessel model parameters, is therefore suggested as an alternative for comparing afterload dynamics.

Originally published in IFAC-PapersOnLine, 11th IFAC Symposium on Biological and Medical Systems BMS (2021). Reprinted with permission.

1. Introduction

1.1 Ex vivo heart evaluation

Today, donor hearts are routinely discarded due to uncertainty about their function. A method of functional evaluation of donor hearts therefore has the potential to increase the availability of heart transplantation.

Such *ex vivo* (outside of the body) functional evaluation requires a system that mimics vascular dynamics—the afterload—and can be controlled to emulate a broad range of recipient physiology and working conditions.

The afterload can be decoupled from heart dynamics by simultaneously measuring aortic flow and pressure, and relating them through an impedance model. Here, we delimit our focus to Windkessel models, being a class of linear time-invariant (LTI) arterial impedance models introduced by Otto Frank in the late 19^{th} century and commonly employed both academically and clinically.

We propose a method for identifying the Windkessel models from data, and perform sensitivity analyses to quantify uncertainty of the identified models. Three data sources are considered: previously published *in vivo* human data; porcine heart beating *in vivo*; porcine heart beating *ex vivo* against a synthetic afterload. The data and code used to generate the results are available on GitHub, see [Pigot, 2021].

The novelty resides in performing a standard local identifiability analysis, whereas other publications on the topic generally focus on model fit in the output-error sense. In general, over-flexible models produce better fits, but can do so for a variety of parameter values as a consequence of being highly sensitive. This does not mean that such models are without utility, but they should not be compared in terms of their parameter values.

This work focuses on technical aspects related to identifiability and parameter identification; details on the device and data generating experiments will be presented elsewhere.

1.2 The arterial Windkessel

Several variants of the Windkessel model have been proposed in the literature, see for instance [Westerhof et al., 2009]. Here we have employed the parallel 4-element Windkessel model, being one of the more general formulations. It can be expressed in terms of the circuit analogy shown in Figure 1, that relates pressure (potential) y_c to antegrade flow (current) u_c through a dynamic impedance G_c, where we use subscript c to denote continuous time. The passive component parameters are described in Table 1.

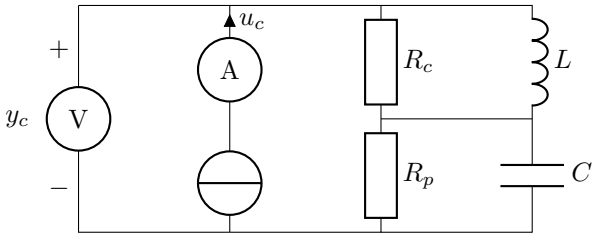

Figure 1. Circuit analogy of the parallel 4-element Windkessel model with driving current (flow) u_c, corresponding voltage (pressure) y_c, and parameters R_p, C, R_c, L.

Table 1. Parameters of the Windkessel model shown in Figure 1. Note that subscript c here denotes characteristic resistance (impedance) [Westerhof et al., 2009], not to be confused with our use of subscript c to indicate continuous time.

Parameter	Unit	Name
R_p	mmHg/(L/min)	Peripheral resistance
C	L/mmHg	Compliance
R_c	mmHg/(L/min)	Characteristic resistance
L	mmHg min/(L/min)	Inertance

Using the circuit analogy of Figure 1 we next derive the expression for the transfer function $G_c(s)$. In the Laplace domain the pressure (voltage) U across resistance R, inertance (inductance) L and compliance (capacitance) C relate to the flow (current) I flowing though each element through $RI = U$, $sLI = U$, and $I = sCU$, respectively. Denoting by p_c the (pressure) potential between the resistances according to Figure 1, Kirchhoff's current law yields

$$u_c = \frac{1}{R_c}(y_c - p_c) + \frac{1}{sL}(y_c - p_c) = \frac{1}{R_p}p_c + sCp_c. \tag{1}$$

From (1) we can eliminate $p_c = R_p/(1 + sCR_p)u_c$ to obtain the transfer function

$$G_c(s|\theta) = R_c + \frac{R_P}{1 + sCR_p} - \frac{R_c}{1 + sL/R_c} \tag{2}$$

from u_c to y_c, parameterized in $\theta = [R_p\ C\ R_c\ L]^\top \succ 0$.

The Windkessel model (2) is hence a parallel interconnection between R_c and two first-order systems. Note that the characteristic resistance R_c

only impedes accelerating flows, since for steady flows, the impedance of the inertance L is 0. This explains why the static gain of (2) is $G(0) = R_p$ (and not, as some might assume $R_c + R_p$). The 4-element Windkessel also comes in a less widespread series form, used in for example [Gellner et al., 2020]. In the series form, the inductance is connected in series with R_c, and its transfer function is obtained by replacing the last term in (2) by sL. The static gain is $R_c + R_p$, but the transfer function is improper, as the term sL corresponds to an unfiltered differentiation of the input.

Introducing the state $x_c = [x_{c1}\ x_{c2}]^\top$, defined through

$$y_c = R_c u_c + \underbrace{\frac{R_p}{1 + sCR_p} u_c}_{\frac{1}{C} x_{c1}} - \underbrace{\frac{R_c}{1 + sL/R_c} u_c}_{\frac{R_c}{L} x_{c2}}, \tag{3}$$

results in the state space form $\mathcal{S}_{c4}$ with matrices defined through

$$\begin{aligned} \dot{x}_c &= \underbrace{\begin{bmatrix} -\frac{1}{CR_p} & 0 \\ 0 & -\frac{R_c}{L} \end{bmatrix}}_{A_c} x_c + \underbrace{\begin{bmatrix} 1 \\ R_c \end{bmatrix}}_{B_c} u_c, \\ y_c &= \underbrace{\begin{bmatrix} \frac{1}{C} & -\frac{R_c}{L} \end{bmatrix}}_{C_c} x_c + \underbrace{\begin{bmatrix} R_c \end{bmatrix}}_{D_c} u_c, \end{aligned} \tag{4}$$

with x_{c1} being the volume (charge) in C. From (4) it is directly visible that the system has two poles corresponding to time constants $T_1 = CR_p$ and $T_2 = L/R_c$.

The 3-element and 2-element Windkessel models—$\mathcal{S}_{c3}$ and $\mathcal{S}_{c2}$—are commonly employed special cases of the 4-element version (4). In anticipation of Section 3, we note that $L/\|\theta\| \to 1$ results in $\mathcal{S}_{c4} \to \mathcal{S}_{c3}$, while either $L \to 0$, $R_c \to 0$, or $R_c/\|\theta\| \to 1$ result in $\mathcal{S}_{c4} \to \mathcal{S}_{c2}$.

2. Method

2.1 Experiments

The porcine data used in this work were recorded from two 65 kg Swedish pigs (*sus scrofa domesticus*). Large-animal experiments were needed to obtain a reliable characterization of the synthetic afterload module under consideration. All institutional and national guidelines for the care and use of laboratory animals were followed and approved by the appropriate institutional committees. The animals were treated in compliance with Directive

2010/63/EU, [The European Parliament, 2010]. The study ran under ethics permission M174-15, issued by "Malmö/Lunds Djurförsöksetiska Nämnd" (local REB).

In both the *in vivo* and *ex vivo* experiments, a CardioMed CM4000 ultrasonic transit time flow meter (Medistim ASA, Oslo, Norway) was secured to the ascending aorta. Aortic pressure was measured using a Meritrans DTXPlus pressure transducer (Merit Medical, Singapore). In-house developed data acquisition hardware and software were used to log the signals at 200 Hz.

Different hearts were used for the *in vivo* and *ex vivo* data. The *in vivo* data reflects normal sinus rhythm at rest. The *ex vivo* data was recorded after 24 hours of cold non-ischemic perfusion, as described in [Steen et al., 2016], beating against an actively controlled synthetic afterload akin to the device described by [Gellner et al., 2020].

2.2 Model formulation

We relate the continuous-time flow $u_c(t)$ to the aortic pressure $y_c(t)$ through $y_c = g_c * u_c + \epsilon_c$, where g_c is the impulse response of an LTI system model with transfer function G_c, and ϵ_c is the output error signal of the model, also referred to as the residual.

We do not have access to u_c and y_c directly, but only to corresponding measurement time series u, y, each of n elements. The time series will here be considered equi-temporarily sampled at a period of h, although the proposed methodology is readily applicable also under irregular sampling schemes.

Applying the zero-order-hold operator Ш_h we thus obtain $[u, y, \epsilon', G] = \text{Ш}_h[u_c, y_c, \epsilon_c, G_c]$ that relate through $y = g * u + \epsilon$ and discrete time state space realization $\mathcal{S} : \{A, B, C, D\} = \text{Ш}_h\mathcal{S}_c$

In order to evaluate the residual, ϵ, we simulate $\mathcal{S}$ with u as input.The residual can be decomposed into one model-mismatch term and one noise term. The former typically arises from a candidate g under-modelling the data u, y. The latter arises if y cannot be fully explained by u. This is for instance the case if u and y have been subjected to measurement noise. In this work we do not discern between the two contributors to ϵ.

To determine the initial state vector for this simulation, we could choose an arbitrary value, e.g. $x_0 = 0$ and drive $\mathcal{S}$ with a repeated stack $[u^\top \dots u^\top]^\top$ with sufficiently many repetitions of u for the transient caused by x_0 to fade, and then discard all but the last n simulated output samples. An efficient and approximation-free alternative is to directly enforce the corresponding "periodic stationarity" condition $x_0 = x_n$. Simulating the system forward in time over one cardiac cycle then gives

$$
\begin{aligned}
x_1 &= Ax_n + Bu_n \\
x_2 &= A^2x_n + ABu_n + Bu_1 \\
&\vdots \\
x_n &= A^n x_n + \underbrace{A^{n-1}Bu_n + \sum_{k=1}^{n-1} A^{n-k-1}Bu_k}_{M}\,.
\end{aligned} \tag{5}
$$

Using that $x_n = x_0$ we solve (5) for

$$x_0 = (I - A^n) \setminus M, \tag{6}$$

where, for numeric robustness, the sum in (5) is preferably computed as a convolution, rather than term-by-term.

2.3 Parameter identification

As stated in Section 2.2 we do not explicitly consider observation model (or other noise source) stochastics in this work, and therefore proceed with output error identification. The objective is hence to minimize the residual cost

$$J(\theta) = \frac{1}{2n}\epsilon(\theta)^\top \epsilon(\theta) \tag{7}$$

to identify

$$\theta^o = \arg\min_{\theta \succ 0} J(\theta). \tag{8}$$

For a candidate θ we can evaluate $\mathcal{S}(\theta) = \text{Ш}_h \mathcal{S}_c(\theta)$, and obtain x_0 using (5). Driving $\mathcal{S}$ with u, we then obtain the output $\hat{y}(\theta)$ and residual $\epsilon(\theta) = y - \hat{y}(\theta)$.

The solution θ^o of (8) will also minimize $J_c = \frac{1}{2hn}\|\epsilon_c\|_2^2$, under the assumption that u_c is piece-wise constant between the samples in u, and that the signals u_c and y_c have been subjected to analog filtering effectively removing spectral power above the Nyquist frequency $(2h)^{-1}$. The latter holds true for the data considered here. The former constitutes a valid approximation as long as $1/h$ is large compared to the magnitudes of the poles of G. Validity of this approximation has been ensured through sampling at a high frequency compared to the cardiac cycle dynamics.

The optimization problem (8) is generally non-convex in θ. We therefore employ a multiple initialization procedure. Being the static gain of the system, R_p is initialized with the mean output (pressure) divided by mean input (flow). The initial values of the remaining parameters are drawn from

a multivariate uniform distribution, and we retrospectively verify that this distribution covers the identified parameters θ^o.

For each initialization point, Newton's method is then used to obtain a cost minimizer candidate, and the one of them that minimizes J gets denoted θ^o.

A dual number implementation (see [Revels et al., 2016]) of the zero-order-hold operator Ш_h enabled *exact* (down to machine precision) forward-mode automatic differentiation and thus evaluation of the gradient $\nabla J(\theta)$ and Hessian $\nabla^2 J(\theta)$ required in each Newton iteration. This enables us to identify the continuous-time model parameter θ directly, without the need of finite difference, or other, approximations. It also means that we can obtain an *exact* evaluation of the Hessian $H = \nabla^2 J(\theta^o)$ of the cost J with respect to the parameter θ, evaluated at the optimum θ^o.

2.4 Persistence of excitation

A classical result for identification of LTI systems is that the order of persistence of excitation (PE) of an input sequence u determines whether u is sufficiently informative to distinguish parameter candidates θ and θ' given some model class, or structure, G. Particularly, PE of order at least m is required for u to be sufficiently informative to distinguish any pair of transfer functions of m parameters. See for example [Mareels et al., 1987] for further detail.

The PE degree can be determined in several (equivalent) ways, one being through a rank condition on the expectation of the auto-correlation matrix of u:

$$\Phi_{u,m} = \begin{bmatrix} r(0) & \dots & r(m-1) \\ \vdots & \ddots & \vdots \\ r(m-1) & \dots & r(0) \end{bmatrix}, \tag{9}$$

where $r(\tau)$ is expectation of the auto-correlation of u, with respect to some stochastic observation model relating u_c to u. In absence of stationary (additive) noise model, it is customary to assume that the observation $u_c(kh)$ is an unbiased and consistent estimate of $u(k)$ and use the observed auto-correlation, defined through (9) with

$$r(\tau) = \frac{1}{n} \sum_{k=0}^{n} \tilde{u}(k)\tilde{u}(k+\tau), \tag{10}$$

where $\tilde{u}(k)$ is typically defined as $u(k)$ for $1 \leq k \leq n$, and 0 otherwise. Since we are dealing with signals of periodic nature here, we will instead use the periodic expansion $\tilde{u}(k) = u((k \mod n)+1)$. We can efficiently evaluate the corresponding circular sample auto-correlation sequence

$$r = [r(0) \dots r(n-1)]^\top = \frac{1}{n}\overline{D}(Du \odot \overline{Du}), \tag{11}$$

where D is the $n \times n$ DFT matrix, $\overline{D}$ its conjugate, and $\odot$ denotes element-wise matrix-matrix multiplication.

The rank condition states that in order for u to be PE of order at least m, the corresponding Φ_u needs to be positive definite. A major concern here is that any u can be turned into a signal of arbitrarily high PE order by adding a signal of independent samples $\sim \mathcal{N}(0, \sigma^2)$, even with arbitrarily small $\sigma > 0$. From a practical perspective it is therefore more relevant to consider the spectrum of Φ_u.

2.5 Sensitivity analysis

Next, we investigate how much model fit, expressed in terms of the cost J, deteriorates if the optimal parameter θ^o is subject to an additive perturbation with magnitude $\|\delta\|_2$. The Taylor series expansion of the perturbed cost is

$$J(\theta^o + \delta) = J(\theta^o) + \underbrace{\nabla J(\theta^o)^\top}_{0} \delta + \frac{1}{2}\delta^\top \nabla^2 J(\theta^o)\delta + r(\delta), \tag{12}$$

where the residual $r(\delta)$ is a linear combination of monomials in the components of δ, each with degree at least 3. If $\|\delta\|_2$ is small, then the contribution of $r(\delta)$ to J is small. In that case the cost increment is well approximated by

$$J(\theta^o + \delta) - J(\theta^o) \approx Q(\delta) = \frac{1}{2}\delta^\top H \delta = \frac{1}{2}\delta^\top V \Sigma V^\top \delta, \tag{13}$$

where the Hessian $H = \nabla^2 J(\theta^o)$ is a symmetric real matrix and therefore has a singular value decomposition according to (13). The singular vectors make up the columns of the unitary matrix $V = [v_1 \dots v_m]$ and we can write the quadratic form as

$$Q(\delta) = \frac{1}{2}(\sigma_1(\delta^\top v_1)^2 + \dots + \sigma_m(\delta^\top v_m)^2). \tag{14}$$

For a fixed $\|\delta\|_2$, (14) is minimized (maximized) when δ is parallel to the singular vector v_k corresponding to the smallest (largest) singular value σ_k. This reveals in what direction a small move away from θ^o contributes least (most) to increase J. Further, the fraction between the largest and smallest singular value, being the condition number of H, reveals the relative change in cost when moving a small (infinitesimal) distance $\|\delta\|_2$ in the least and most sensitive directions, respectively. A large condition number is therefore an indicator of over-parametrization with respect to the experimental data.

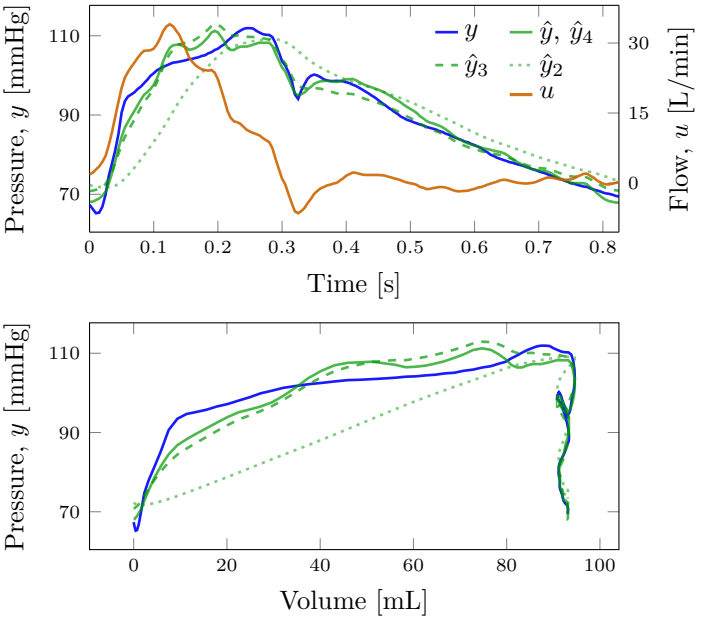

Figure 2. Data set u, y and reported 4-element Windkessel model output $\hat{y}$ digitized from Fig. 4 of [Stergiopulos et al., 1999]; model output $\hat{y}_k$ of the herein identified k-element Windkessel models. Top pane shows time domain model fit; bottom pane shows aortic PV loop.

3. Results

3.1 Identified models

The identification method was first validated against a previously published human data set—henceforth referred to as the *human* data—by digitizing the waveforms in Fig. 4 of [Stergiopulos et al., 1999]. Numerical values are reported in Table 2; time domain model outputs and corresponding pressure–volume (PV) loops in Figure 2; output error residuals in Figure 3. As seen in Figure 2, the parameter values identified using the method of Section 2 reproduce the appearance of the results in [Stergiopulos et al., 1999]. We also identified 2- and 3-element Windkessel models to see how they compare in terms of output error and sensitivity.

Moving on to the experimental data, identified parameter values, mean squared error (MSE) of the time domain model fit, being directly proportional to $J(\theta^o)$, and the condition number of the Hessian $H = \nabla^2 J(\theta^o)$ are listed in Table 2. Time domain model outputs and PV loops are shown in Figure 4 and Figure 5; output error residuals are shown in Figure 3.

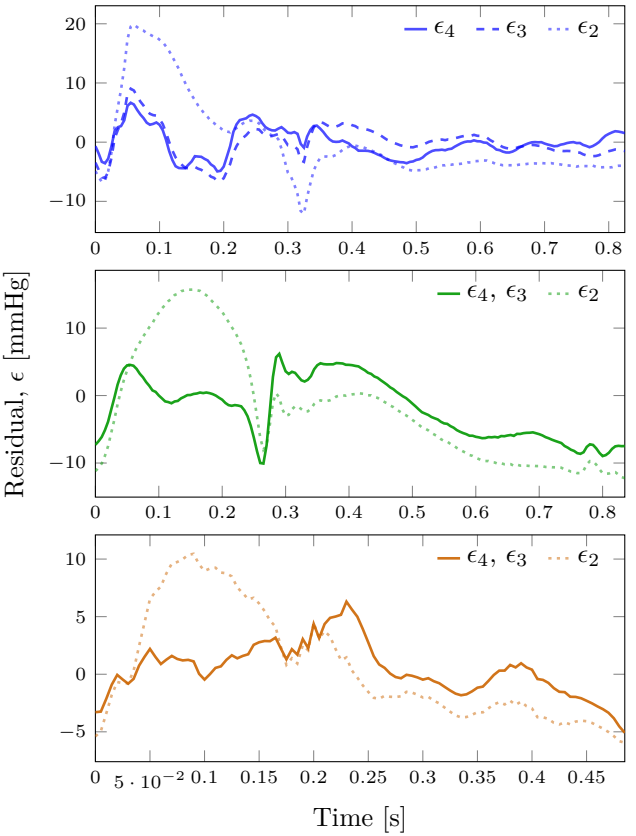

Figure 3. Output error residuals ϵ_k, of k-element Windkessel models identified from the human data (top), and porcine *in vivo* (middle) and *ex vivo* data (bottom).

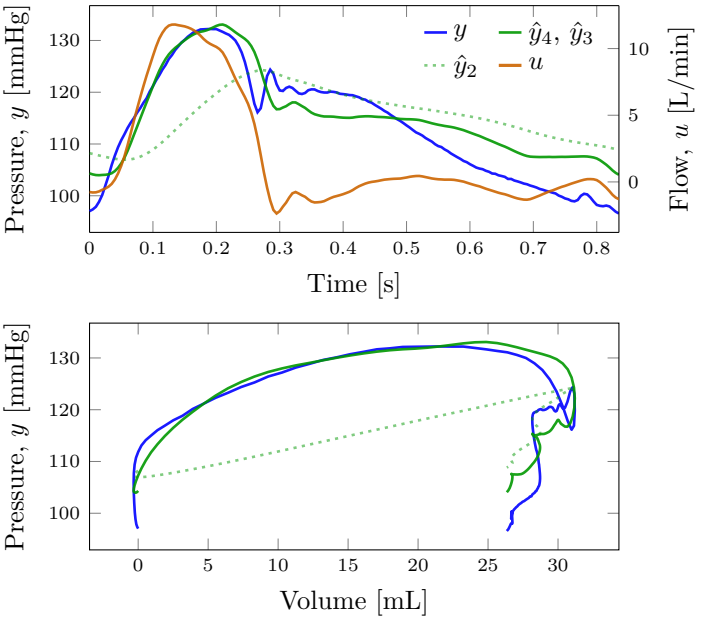

Figure 4. *In vivo* porcine data set u, y together with outputs $\hat{y}_k$ of identified k-element Windkessel models.

Table 2. Identified parameters of 4-, 3-, and 2-element Windkessel models together with mean squared error (MSE) [mmHg], directly proportional to $J(\theta^o)$ of (7). The last column shows the conditioning of $H = \nabla^2 J(\theta)$ at $\theta = \theta^o$.

	R_p	C	Rc	L	MSE	cond(H)
Human	13.6	0.0743	0.952	0.0952	5.88	3.18e3
	13.0	0.108	0.582		8.48	3.65e2
	13.6	0.0996			48.2	3.07e2
in vivo	62.9	0.0855	1.58	8.52	30.9	1.20e7
	61.3	0.0877	1.58		30.9	1.57e3
	62.9	0.0853			77.1	1.37e3
ex vivo	148	0.345	0.615	31.3	7.16	2.76e9
	148	0.346	0.615		7.16	1.00e2
	147	0.353			23.3	5.56e1

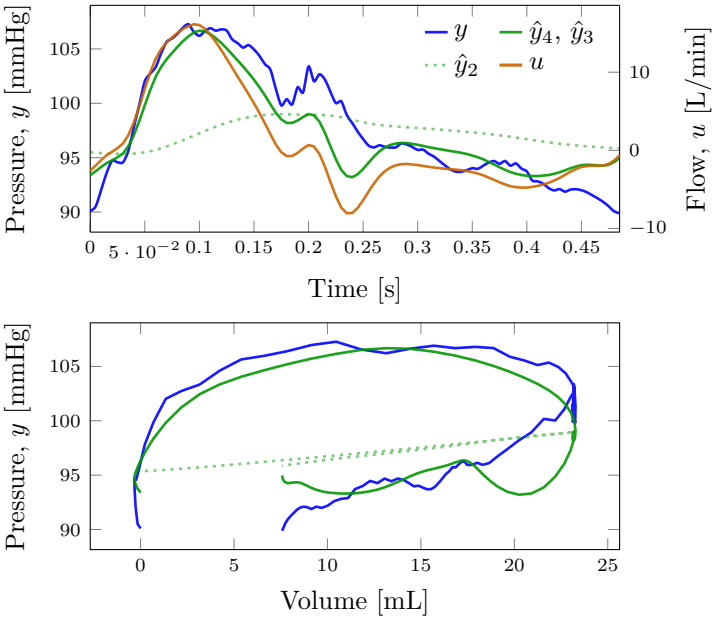

Figure 5. *Ex vivo* porcine data set u, y together with outputs $\hat{y}_k$ of identified k-element Windkessel models.

Bode plots of the identified models are shown in Figure 6. These indicate that for the experimental data an almost perfect pole-zero cancellation takes place in the 4-element models, as can be verified by inserting the parameter values of Table 2 into (2). This also explains why corresponding time-domain plots are visually indistinguishable.

3.2 Persistence of excitation

The 10 largest singular values of the auto-correlation matrices Φ_u for the inputs of the human, *in vivo*, and *ex vivo* data sets are shown in Figure 7. According to Section 2.4, the figure indicates that identification of 2 to 4 parameters may be feasible, which prompts further consideration of parameter sensitivity in the fitted models. Since the input is generated by the heart, it cannot be arbitrarily changed to increase excitation and elucidate more parameters.

One can note that two parameters (degrees of freedom) are necessary to reproduce arbitrary diastolic and systolic pressure levels. For the 4-element Windkessel model $\mathcal{S}_{c4}$, this leaves two parameters to influence the shape of the model output; one "shape" parameter for $\mathcal{S}_{c3}$; none for $\mathcal{S}_{c2}$.

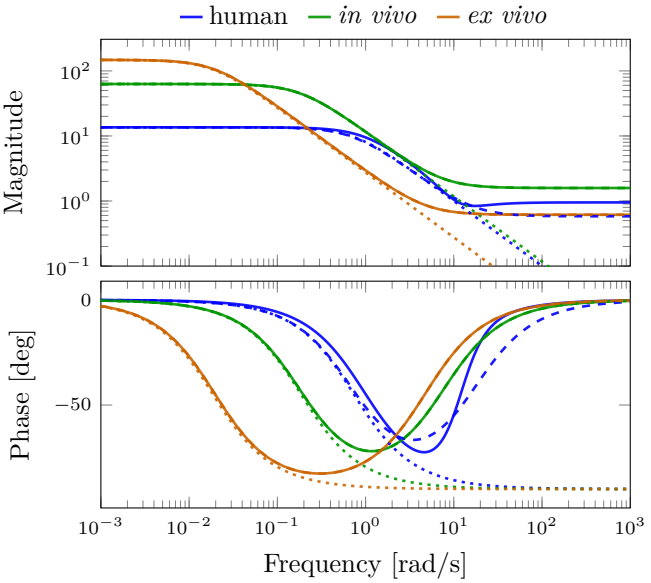

Figure 6. Bode plots of the identified 4-element (solid), 3-element (dashed), and 2-element (dotted) Windkessel models from the human (blue), *in vivo* porcine (green) and *ex vivo* porcine (bronze) data sets.

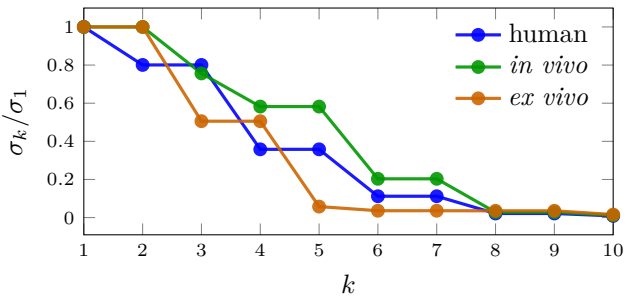

Figure 7. The 10 largest singular values $\sigma_1 \geq \ldots \geq \sigma_{10}$ of Φ_u, normalized by σ_1. The spectral densities Φ_u were computed using u from human (blue); *in vivo* data set (green); *ex vivo* data set (bronze).

Table 3. Singular value decomposition $H = V\Sigma V^\top$ of the Hessian $H = \nabla^2 J(\theta^o)$.

	V	$\mathrm{diag}(\Sigma)$
Human	$\begin{bmatrix} -0.00 & -0.00 & -1.00 & 0.01 \\ 1.00 & 0.02 & 0.00 & 0.02 \\ 0.02 & 0.03 & -0.01 & -1.00 \\ -0.02 & 1.00 & -0.00 & 0.03 \end{bmatrix}$	3.12e8 $\begin{bmatrix} 1.0000 \\ 0.0477 \\ 0.0009 \\ 0.0003 \end{bmatrix}$
In vivo	$\begin{bmatrix} 0.00 & 0.00 & 1.00 & 0.00 \\ 1.00 & 0.00 & 0.00 & 0.00 \\ 0.00 & -1.00 & 0.00 & 0.00 \\ 0.00 & 0.00 & 0.00 & 1.00 \end{bmatrix}$	3.36e7 $\begin{bmatrix} 1.0000 \\ 0.0038 \\ 0.0007 \\ 0.0000 \end{bmatrix}$
Ex vivo	$\begin{bmatrix} 0.00 & 0.00 & 1.00 & 0.00 \\ -0.07 & -1.00 & 0.00 & 0.00 \\ -1.00 & 0.07 & 0.00 & 0.00 \\ 0.00 & 0.00 & 0.00 & 1.00 \end{bmatrix}$	1.65e5 $\begin{bmatrix} 1.0000 \\ 0.6976 \\ 0.0102 \\ 0.0000 \end{bmatrix}$

3.3 Parameter sensitivities

The singular value decompositions $H = V\Sigma V^\top$ of the Hessian $H = \nabla^2 J(\theta)$, evaluated at the identified parameter $\theta = \theta^o$ are shown in Table 3. The last column of the V matrices indicate that the least certain direction in parameter space coincides with R_c for the human data. The *in vivo* and *ex vivo* data instead result in uncertain estimates of L. Recalling from Section 1.2 how limit cases of L and R_c correspond to the 2- and 3-element Windkessel structures, it is not surprising—given the indicated sensitivities—that the 3-element models explain the experimental data almost identically well, while the 2-element counterparts fail to do so based on lacking degrees of freedom, as mentioned in Section 3.2. Furthermore, the parameters dominating the least certain direction for the 3-element models were found to be C for the human data and R_p for the porcine data.

4. Discussion

A method for identification of continuous time dynamics from time series data has been proposed with the objective of comparing the dynamics of a synthetic afterload with those of normal physiology.

Upon validation against previously published results from [Stergiopulos et al., 1999], the method was therefore applied to two porcine data sets: one collected *in vivo*, featuring normal physiology; one collected *ex vivo*, with the heart working against a synthetic afterload, as may be used in functional eval-

uation of donor hearts prior to possible implantation. The human-data model MSEs were comparable to the results of [Segers et al., 2008] who reported mean MSEs of 9.2 and 8.9 for the 3 and 4-element models, respectively, when fitting to measured data from 2404 humans. We can note that our human-data model fit is slightly better than for our experimental data. This is presumably caused by how our measurement setup was devised, and we are planing to conduct similar but refined measurements to investigate this. Nonetheless, the non-whiteness of output error residuals from all three data sets, shown in Figure 3, suggest that the Windkessel structure under-models representative pressure–flow data. At the same time, the persistence of excitation analysis of Section 2.4 and local sensitivity analysis of Section 2.5 suggest that the inputs u do not support identification of substantially more complex LTI model structures than the 3-element Windkessel.

5. Conclusion

The well-established 4-element parallel Windkessel model is not reliably identifiable from our sets of experimentally collected porcine and previously published human aortic pressure–flow time series data. Particularly, the inertance parameter L is practically unidentifiable. For the sake of comparing afterload impedance dynamics, it is therefore advisable to look directly at the relation between aortic pressure and flow, rather than comparing Windkessel model parameters.

Acknowledgements

This work was partially funded by the Swedish Research Council (grant 2017-04989) and the Wallenberg AI, Autonomous Systems and Software Program (WASP) funded by the Knut and Alice Wallenberg Foundation. The authors from the Department of Automatic Control are members of the ELLIIT Strategic Research Area at Lund University.

References

Gellner, B., L. Xin, R. Ribeiro, V. Bissoondath, P. Lu, M. Adamson, F. Yu, E. Paradiso, J. Zu, C. Simmons, and M. Badiwala (2020). "The implementation of an adjustable afterload module for ex situ heart perfusion". *Cardiovascular Engineering and Technology* **11**:1, pp. 96–110. DOI: 10.1007/s13239-019-00447-w.

Mareels, I., R. Bitmead, M. Gevers, C. Johnson, R. Kosut, and M. Poubelle (1987). "How exciting can a signal really be?" *systems & Control Letters* **8**:3, pp. 197–204. DOI: 10.1016/0167-6911(87)90027-2.

Pigot, H. (2021). *Windkessel-id*. Commit: d7cdc0f. URL: https://github.com/hpigot/windkessel-id (visited on 2021-07-12).

Revels, J., M. Lubin, and T. Papamarkou (2016). "Forward-mode automatic differentiation in Julia". *arXiv:1607.07892 [cs.MS]*. URL: https://arxiv.org/abs/1607.07892.

Segers, P., E. Rietzschel, M. De Buyzere, N. Stergiopulos, N. Westerhof, L. Bortel, T. Gillebert, and P. Verdonck (2008). "Three-and-four-element Windkessel models: Assessment of their fitting performance in a large cohort of healthy middle-aged individuals". *Proceedings of the Institution of Mechanical Engineers. Part H, Journal of engineering in medicine* **222**, pp. 417–28. DOI: 10.1243/09544119JEIM287.

Steen, S., A. Paskevicius, Q. Liao, and T. Sjöberg (2016). "Safe orthotopic transplantation of hearts harvested 24 hours after brain death and preserved for 24 hours". *Scandinavian Cardiovascular Journal* **50**:3, pp. 193–200. DOI: 10.3109/14017431.2016.1154598.

Stergiopulos, N., B. E. Westerhof, and N. Westerhof (1999). "Total arterial inertance as the fourth element of the windkessel model". *American Journal of Physiology-Heart and Circulatory Physiology* **276**:1, H81–H88. DOI: 10.1152/ajpheart.1999.276.1.H81.

The European Parliament (2010). *On the protection of animals used for scientific purpose.* Tech. rep. Directive 2010/63/EU. Council of Europe.

Westerhof, N., J.-W. Lankhaar, and B. E. Westerhof (2009). "The arterial Windkessel". *Medical & Biological Engineering & Computing* **47**:2, pp. 131–141. DOI: 10.1007/s11517-008-0359-2.

Paper III

The differential-algebraic Windkessel model with power as input

Henry Pigot **Kristian Soltesz**

Abstract

The lack of methods to evaluate mechanical function of donated hearts in the context of transplantation imposes large precautionary margins, translating into a low utilization rate of donor organs. This has spawned research into cyber-physical models constituting artificial afterloads (arterial trees), that can serve to evaluate the contractile capacity of the donor heart. The Windkessel model is an established linear time-invariant afterload model, that researchers committed to creating a cyber-physical afterload have used as a template. With aortic volumetric flow as input and aortic pressure as output, it is not directly obvious how a Windkessel model will respond to changes in heart contractility. We transform the classic Windkessel model to relate power, rather than flow, to pressure. This alters the model into a differential-algebraic equation, albeit one that is straightforward to simulate. We then propose a power signal model, that is based on pressure and flow measurements and optimal in a Bayesian sense within the class of C2 signals. Finally, we show how the proposed signal model can be used to create relevant simulation scenarios, and use this to illustrate why it is problematic to use the Windkessel model as a basis for designing a clinically relevant artificial afterload.

Originally published in the proceedings of the 2022 American Control Conference. Reprinted with permission.

1. Introduction

Heart evaluation in isolation from the body can help ensure that donor organs are safe prior to initiating transplantation, lowering costs and patient risk. At present, one heart preservation and evaluation system is clinically available, wherein the heart beats empty (unloaded) providing only metabolic indicators of heart function [Ardehali et al., 2015]. Such indicators have shown poor correlation to post-transplant outcomes compared to functional metrics[White et al., 2015; Ribeiro et al., 2020]. Functional evaluation of donor hearts enables direct observation of hemodynamic performance, giving clinicians insight into how well an organ will perform in a recipient.

Recent advances by our collaborators in nonischemic organ preservation extend the admissable *ex vivo* (out-of-body) time for heart organs from 4 h to 24 h [Steen et al., 2016; Qin et al., 2020]. This extended admissible time opens up for the use of extended-criteria donors [Soltesz et al., 2018; Wahlquist et al., 2021], and enables functional donor heart evaluation within the time constraints of the transplantation procedure.

Functional evaluation requires a supply of perfusate to the heart ventricles, as well as an artificial cardiac afterload for the heart to beat against. The afterload must maintain diastolic aortic pressure to ensure coronary flow and limit systolic pressure to a safe limit, while subjecting the heart to physiological loading conditions. Afterloads are commonly built as verbatim implementations of the common arterial Windkessel model, combining discrete resistive and compliant elements as an approximation of the arterial tree [Westerhof et al., 2009]. Some groups have implemented adjustable elements enabling computer control of mean aortic pressure, as in [Fisher et al., 1984], or manual adjustment of systolic and diastolic pressure, as in [Gellner et al., 2020].

In simulation of cardiac afterloads, changes in contractility (defining the forcefullness of heart beats) and arrhythmic conditions (irregular heart beats) are of foremost interest for evaluating heart function under a given loading condition. Here we investigate how an artificial afterload model, implemented as a Windkessel model, can be expected to behave when subjected to contractile changes and arrhythmia.

Julia code that can reproduce all results herein is available on GitHub [Pigot, 2022].

2. Differential-algebraic Windkessel model

2.1 Flow input Windkessel

The classic "lumped-parameter" Windkessel impedance is a low-order (at most two) LTI model that estimates aortic pressure $p(t)$ by $\hat{p}(t)$ based on

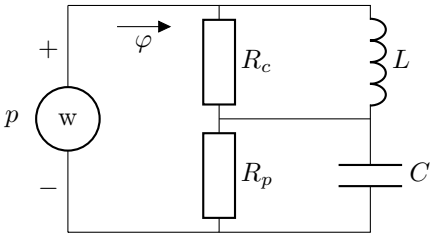

Figure 1. Circuit diagram equivalent of the 4-element parallel Windkessel model with parameters $\theta = [R_p\ C\ R_c\ L]^\top$, aortic flow (current) φ, and pressure (voltage) p. The heart is modeled as a power source w, as opposed to the flow (current) source utilized in the classic Windkessel formulation.

aortic volumetric flow $\varphi(t)$ [Westerhof et al., 2009]. Here we will consider the most general of these, the 4-element parallel Windkessel model [Stergiopulos et al., 1999]. The circuit diagram of its electric analogy, with electric current representing volumetric flow and electric potential (voltage) representing pressure, is shown in Figure 1. A state space realization of the system is provided by

$$\dot{x} = \underbrace{\begin{bmatrix} -\dfrac{1}{CR_p} & 0 \\ 0 & -\dfrac{R_c}{L} \end{bmatrix}}_{A} x + \underbrace{\begin{bmatrix} 1 \\ R_c \end{bmatrix}}_{B} \varphi, \tag{1a}$$

$$p = \underbrace{\begin{bmatrix} \dfrac{1}{C} & -\dfrac{R_c}{L} \end{bmatrix}}_{C} x + \underbrace{\begin{bmatrix} R_c \end{bmatrix}}_{D} \varphi. \tag{1b}$$

(Context will decide when C refers to the compliance parameter or state space output matrix.) In the physiology literature, the parameters

$$\theta = [R_p\ C\ R_c\ L]^\top \succ 0 \tag{2}$$

are ascribed mechanistic properties as per Table 1.

The parameters are typically identified from aortic volumetric flow samples $\varphi_1, \ldots, \varphi_n$ and corresponding aortic pressure samples $p_1, \ldots, p_n$ simultaneously sampled at $t_1 < \cdots < t_n$. The sampling instances are chosen so that consecutive samples are sufficiently close in time to resolve the dynamics to be modeled, and $t_n - t_1$ typically spans either an integer number of cardiac cycles, or one cardiac cycle that is periodically extended as in [Pigot et al., 2021]. Identification of θ is most commonly cast as an output-error minimization, with quadratic cost on $p_k - \hat{p}(t_k)$, see e. g., [Segers et al., 2008].

Table 1. Parameters of the Windkessel model of Figure 1 from [Stergiopulos et al., 1999].

Parameter	Value	Unit	Name
R_p	13.2	mmHg/(L/min)	Peripheral resistance
C	0.0732	L/mmHg	Compliance
R_c	0.933	mmHg/(L/min)	Characteristic resistance
L	0.085	mmHg $\cdot$ min/(L/min)	Inertance

2.2 Power input Windkessel

The Windkessel model provides a dynamic relation between aortic volumetric flow and aortic pressure, that matches observations well [Segers et al., 2008]. It is therefore not surprising that research prototypes of artificial dynamic afterloads (adjustable arterial tree models) to be used in functional *ex vivo* evaluation of donor hearts [Fisher et al., 1984; Seifen et al., 1987; Abicht et al., 2018; de Hart et al., 2011; Gellner et al., 2020], have been constructed to emulate the dynamics of the Windkessel model.

While the Windkessel model employs a volumetric flow source model of the heart, a power source model is much more relevant to our investigations of contractile function variations and arrhythmia. The work exerted by the left ventricle on the blood being ejected in one cardiac cycle is the area of a Carnot cycle, referred to in the literature as a pressure-volume loop, or just a PV-loop. The work w associated with transitioning from ventricular volume v_1 to v_2 along this cycle is

$$w(v_1, v_2) = -\int_{v_1}^{v_2} p(v)\ dv. \tag{3}$$

To be accurate, (3) provides an upper bound for this work, and that bound is tight for lossless systems. Letting t_1 and t_2 be the times corresponding to v_1 and v_2, such that $v(t_1) = v_1$), the work of (3) can be expressed as

$$w(t_1, t_2) = -\int_{t_1}^{t_2} p(t)\frac{dv}{dt}dt = -\int_{t_1}^{t_2} \varphi(t)p(t)\ dt. \tag{4}$$

In the PV-loop context, flow into the left ventricle (from the left atrium) is considered. Here, we are instead considering flow out of the left ventricle (through the aorta). We therefore employ (4) with a sign change of its right-hand-side, and conclude that the instantaneous power is

$$w = \varphi p. \tag{5}$$

Assuming for now that $\hat{p} = p$, i.e., that the Windkessel model captures the afterload dynamics perfectly, we can use (1b) together with (5) to algebraically relate the instantaneous power w to the flow φ through

$$w = (Cx + D\varphi)\varphi = Cx\varphi + D\varphi^2. \tag{6}$$

Combining (6) with (1) results in the nonlinear differential-algebraic equation (DAE)

$$\dot{x} = Ax + B\varphi \tag{7a}$$
$$w = Cx\varphi + D\varphi^2. \tag{7b}$$

The DAE (7) has index one (since there is no differentiation of its input, w), and is therefore readily solvable by numerical DAE integrators. The algebraic equation (7b) has solutions

$$\varphi = \frac{-Cx \pm \sqrt{(Cx)^2 + 4Dw}}{2D}, \tag{8}$$

meaning that any initial condition $x(t_0)$ fulfilling $(Cx(t_0))^2 + 4Dw(t_0) \geq 0$ is feasible (while others are not). In particular $x(t_0) = 0$ is feasible.

3. Power signal model

In this section we formulate a statistical signal estimation problem that is solved by employing cubic spline smoothing. To be notationally coherent and reproducible, we have chosen to explicitly include a small review of related topics.

3.1 Smoothing cubic splines

We consider modeling of the heart power input signal w from sampled flow φ and pressure p time series. The zero-order-hold (ZOH) interpolation is the default choice when sampled signals are considered in the context of control systems. Indeed it makes sense if the signal source is a digital controller, that maintains steady output levels between invocations. However, physiological signals seldom exhibit ZOH behavior. Instead, they are (with some exceptions such as neuronal signalling) smooth. We therefore assume that our samples are observations of some unknown $\mathcal{C}^2$ (twice differentiable, with continuous second derivative) signal, that we aim to estimate.

Based on observations $y = [y_1 \ \dots \ y_n]^\top$ of an unknown signal $x(t)$, sampled at times $\tau = [t_1 \ \dots, t_n]^\top$, we hence want to obtain a $\mathcal{C}^2$ signal model $\hat{x}$ of x on (t_1, t_n) with $\chi = [\hat{x}(t_1) \ \dots \ \hat{x}(t_n)]^\top$.Since we have no information about x between samples, we choose as objective to minimize the roughness

$$\rho(\hat{x}(t)) = \int_\tau \ddot{\hat{x}}(t) \, dt. \tag{9}$$

One can note that this is similar, but generally not identical to, minimizing total curvature, that is defined as the integral of $\ddot{\hat{x}}$ along the curve, integrating dl rather than dt.

If our observations have not been corrupted by noise, we are searching for the least rough $\mathcal{C}^2$ curve x that passes through the *knots* defined by τ and $\chi = y$. That curve is the natural cubic spline generated by (τ, χ) [De Boor, 2001]. It is a piece-wise cubic polynomial $\hat{x}(t) = \hat{x}_k(t)$, where

$$\begin{aligned} &\hat{x}_k(t) = \alpha_k + \beta_k(t - t_k) + \gamma_k(t - t_k)^2 + \delta_k(t - t_k)^3, \\ &t_k \leq t < t_{k+1},\ k = 1, \ldots, n-1, \end{aligned} \tag{10}$$

uniquely defined by the parameter $\theta = [\alpha^\top\ \beta^\top\ \gamma^\top\ \delta^\top]^\top$, with column vectors on the form $\alpha = [\alpha_1\ \ldots\ \alpha_{n-1}]^\top$. Particularly, the spline polynomials defined through (10) are linear in θ.

The spline is defined to pass through the knots, where its first and second derivatives are continuous. This corresponds to the constraints

$$\hat{x}_k(t_{k+1}) = \hat{x}_{k+1}(t_k) = \chi_k, \tag{11a}$$

$$\dot{\hat{x}}_k(t_{k+1}) = \dot{\hat{x}}_{k+1}(t_k), \tag{11b}$$

$$\ddot{\hat{x}}_k(t_{k+1}) = \ddot{\hat{x}}_{k+1}(t_k), \tag{11c}$$

holding for $k = 1, \ldots, n-1$. The constraints (11) uniquely define the always existing cubic spline down to boundary conditions. The two types of boundary conditions we will consider are *natural* (a.k.a. normal or ordinary) and *periodic*. The natural spline has zero second derivatives at its end-points

$$\ddot{\hat{x}}(t_1) = \ddot{\hat{x}}(t_n) = 0. \tag{12}$$

It is called natural because originally, when flexible rulers constrained by nails at the knot, were used to draw splines, leaving the ruler unconstrained beyond the end-points would correspond to the condition (12).

Many physiological signals, including cardiac cycles, are periodic to their nature, and it can therefore be desirable to extrapolate periodically using data covering (at least) one period.

The natural spline is not necessarily $\mathcal{C}^2$ across the period boundary. However, replacing (12) with explicit $\mathcal{C}^2$ constraints on the end-points

$$\hat{x}(t_1) = \hat{x}(t_n), \tag{13a}$$

$$\dot{\hat{x}}(t_1) = \dot{\hat{x}}(t_n), \tag{13b}$$

$$\ddot{\hat{x}}(t_1) = \ddot{\hat{x}}(t_n), \tag{13c}$$

equivalently results in an existing and uniquely defined spline.

It is reasonable to assume that our measurements y of x are corrupted by noise ϵ, so that $y = x + \epsilon$. In our formulation we will use the relevant case where ϵ is a realization of a zero-mean processes with covariance Σ. We note that it is sufficient to consider predictive performance at the instances defined by τ, since the cubic spline (normal or periodic) is uniquely defined by the knot abscissas χ at these ordinates. We could choose χ so the knots end up on a straight line. This results in a cubic spline of zero roughness. However, since $\mathbb{E}\epsilon = 0$, any choice but $\chi = y$ is associated with an estimation bias. In estimating x_k, this bias is simply $y_k - \chi_k$. On the other end of the scale we have $\chi = y$, which provides an unbiased estimator at the cost of higher variance.

As we will shortly see χ is linear in θ and minimizing the smoothing cubic spline cost

$$J(\theta;\lambda) = \lambda \underbrace{(y - \chi(\theta))^\top \hat{\Sigma}^{-1}(y - \chi(\theta))}_{J_1} + (1-\lambda)\underbrace{\rho(\chi(\theta))}_{J_2} \tag{14}$$

balances between reducing bias (second term) and variance (first term) through the parameter $\lambda \in (0,1)$. If $\epsilon \sim \mathcal{N}(0,\Sigma)$ and $\hat{\Sigma} = \Sigma$, the minimizer χ of J_1 is the maximum likelihood estimator (MLE) of y. By parametrizing J as convex combination of J_1 and J_2, we are left with determining λ within the closed interval $(0,1)$, as opposed to the interval $(0,\infty)$ associated with the common formulation $J = J_1 + \lambda J_2$ (where λ is now another parameter with the same role).

Returning to the spline fitting problem, the $\mathcal{C}^2$ conditions can be encoded into a linear equation system

$$S\gamma = 3V\alpha \tag{15}$$

in the knot values $\alpha_k = \chi_k$ and knot second derivatives $\ddot{\chi}_k = 2\gamma_k$, each defined for $k = 1,\ldots,n-1$ [De Boor, 2001]. The matrices S and V are constructed from t. Introducing $h_k = x_{k+1} - x_k$ and $q_k = 1/h_k$ where $k = 1,\ldots,n-1$, the matrices corresponding to the periodic case are

$$S = \begin{bmatrix} 2\Delta h_{n-1} & h_1 & & & & & & \\ h_1 & 2\Delta h_1 & h_2 & & & & & \\ \vdots & \vdots & \vdots & \vdots & \vdots & \vdots & \vdots & \\ & & & & h_{n-3} & 2\Delta h_{n-3} & h_{n-2} & \\ h_{n-1} & & & & & h_{n-2} & 2\Delta h_{n-2} & \end{bmatrix}, \tag{16a}$$

$$V = \begin{bmatrix} -\Delta q_{n-1} & q_1 & & & & & & q_{n-1} \\ q_1 & -\Delta q_1 & q_2 & & & & & \\ \vdots & \vdots & \vdots & \vdots & \vdots & \vdots & \vdots & \\ & & & & q_{n-3} & -\Delta q_{n-3} & q_{n-2} & \\ q_{n-1} & & & & & q_{n-2} & -\Delta q_{n-2} & \end{bmatrix}, \tag{16b}$$

where $\Delta(\cdot)_k = (\cdot)_k + (\cdot)_j$ with $j = (\max((k+1)\%n), 1)$.

The natural counterparts are obtained by setting

$$S_{1,n-1} = S_{n-1,1} = S_{1,2} = S_{n-1,n-2} = 0, \tag{17a}$$

$$V_{1,n-1} = V_{n-1,1} = V_{1,1} = V_{1,2} = 0, \tag{17b}$$

in (16a) and (16b), respectively. Using that $\alpha_k = \chi_k$ we can express the first term of (14) as

$$J_1 = (y-\alpha)^\top \hat{\Sigma}^{-1}(y-\alpha), \tag{18}$$

and as mentioned in e. g., [De Boor, 2001], the roughness of the cubic spline on (t_1, t_n) can be expressed

$$J_2 = \frac{2}{3}\gamma^\top S\gamma. \tag{19}$$

The objective (14) is therefore a quadratic form in α:

$$J = \lambda(y-\alpha)^\top(y-\alpha) + (1-\lambda)6\alpha^\top V^\top S^{-\top} V\alpha, \tag{20}$$

that can be written on the standard form

$$J = \frac{1}{2}a^\top U\alpha - v^\top\alpha + r, \tag{21}$$

with

$$U = 2\lambda\hat{\Sigma}^{-1} + 12(1-\lambda)V^\top S^{-\top}V, \tag{22a}$$

$$v = 2\lambda\hat{\Sigma}^{-1}y, \tag{22b}$$

$$r = \lambda y^\top\hat{\Sigma}^{-1}y. \tag{22c}$$

Minimizing (21) with respect to α (i.e. also with respect to θ) is an ordinary least squares problem, and the unique minimizer is the solution to $U\alpha = v$. Having obtained α, it is then possible to obtain the remaining parameters from the end-point constraints through the following equations that (after some manipulation) follow from the definition of the smoothing cubic spline:

$$\gamma = 3S^{-1}V\alpha, \tag{23a}$$

$$\delta = \frac{1}{3}H^{-1}D\gamma, \tag{23b}$$

$$\beta = H^{-1}D\alpha - H\gamma - H^2\delta, \tag{23c}$$

where $H = \operatorname{diag}(h)$ and

$$D = \begin{bmatrix} -1 & 1 & & & & & \\ & -1 & 1 & & & & \\ \vdots & \vdots & \vdots & \vdots & \vdots & \vdots & \\ 1 & & & & & -1 & \end{bmatrix} \tag{24}$$

3.2 Choice of smoothing parameter

The remaining question is how to choose the smoothing parameter $\lambda \in (0, 1)$, that constitutes a bias–variance trade-off. Using all available data for training, there is no way to determine whether one candidate is favorable to another (except for subjectively by looking at the resulting fit). A frequently used way to determine λ is therefor through leave-one-out cross validation. The predictive performance is measured as the mean square error over $k = 1, \ldots, n$ in predicting y_k with a predictor that has been trained on all data except (t_k, y_k):

$$J_\lambda = \frac{1}{n}\sum_{k=1}^{n}\left(y_k - \hat{x}^{(-k)}(t_k)\right)^2. \tag{25}$$

Here, $\hat{x}^{(-k)}$ denotes a cubic spline fitted to all data but (t_k, y_k), and since the spline is a function of the smoothing parameter λ, we can minimize J_λ over λ. A celebrated result [Silverman, 1984] enables cheap evaluation through

$$J_\lambda = \sum_{k=1}^{n-1}\left(\frac{y_k - \hat{x}(t_k)}{1 - W_{kk}}\right)^2, \tag{26}$$

where $\chi = Wy$ defines the smoothing matrix

$$W = \begin{bmatrix} w_1^\top \\ \vdots \\ w_n^\top \end{bmatrix} = \begin{bmatrix} 2\lambda U^{-1} \\ w_n^\top \end{bmatrix}. \tag{27}$$

The last row $w_n^\top$ of the right-hand-side of (27) corresponds to y_n. For the periodic case we therefore have $w_n = w_1$. For the natural case, w_n is instead obtained through (23). Alternatively, one could introduce γ_n as an explicit variable in the natural counterpart to (16), in which case the right-hand-side would be simply $2\lambda U^{-1}$.

It is also worth noting that the effective degree of freedom resulting from the regularization is $\operatorname{Tr} W$, making it monotonic in λ. That does not imply that J_λ lacks local minima, but for practical purposes it often suffices to determine λ through bisection search over $(0, 1)$, which is what we do in the upcoming examples.

3.3 Modeling heart power

We realistically assume that our φ and p measurement time series are time-aligned and corrupted by additive independent Gaussian noise drawn from $\mathcal{N}(0, \sigma_\varphi^2)$ and $\mathcal{N}(0, \sigma_p^2)$, respectively. Even if the time series are synchronized (which they do not need to be), we fit individual smoothing cubic splines $\hat{\varphi}$ and $\hat{p}$, and use $\hat{w} = \hat{\varphi}\hat{p}$ to model w in (7), to preserve the MLE property of the fitted curves.

For any time t where both splines $\hat{\varphi}$ and $\hat{p}$ are defined, their product $\hat{w}$ is the product of two third-order polynomials that we can explicitly compute. As a direct consequence, $\hat{w}$ will also be $\mathcal{C}^2$ and we can compute $\dot{\hat{w}}(t)$ and $\ddot{\hat{w}}(t)$ analytically from the underlying splines. Particularly, if $\hat{\varphi}$ and $\hat{p}$ have a coinciding end-point with a natural end-point condition, then $\hat{w}$ will have have a coinciding end-point with natural end-point condition.

It also follows directly from the definition that if $\hat{\varphi}$ is periodic with T_φ and $\hat{p}$ is periodic with T_p, then $\hat{w}$ will be periodic unless T_φ/T_p is irrational, with period at least $\max(T_\varphi, T_p)$ and at most $\operatorname{lcm}(T_\varphi, T_p)$. If $T = T_\varphi = T_p$, then $\hat{w}$ will be periodic with period (evenly dividing) T. The noise variance σ^2 just shifts the balance between J_1 and J_2 in (14), in a way that can be compensated for using λ. We therefore fix $\sigma_p^2 = \sigma_\varphi^2 = \sigma^2 = 1$ and leave it up to the cross validation to suggest a λ that minimizes its approximation of the expected prediction error.

4. Simulation examples

Implementing the DAE (7) within the `Julia DifferentialEquations.jl` suite and providing its right-hand-side with $w = \hat{w}$, modeled as described in Section 3, we simulate the Windkessel with power input using the `Sundials.jl` DAE integrator. Our simulations are based on digitized waveforms from [Stergiopulos et al., 1999], representing homeostatic human aortic volumetric flow and aortic pressure, respectively, as further explained in [Pigot et al., 2021].

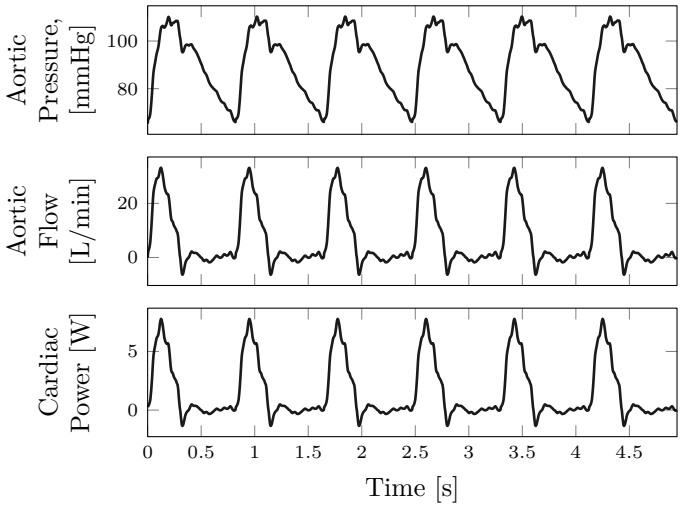

Figure 2. Windkessel DAE simulation with periodically extended power input w. Top panes show the resulting pressure p and flow φ.

4.1 Periodic input

As a first example, we simulate a train of cardiac cycles, by evaluating the periodic extension of the φ and p splines, and forming $w = \varphi p$ pointwise from these. Figure 2 shows w, and the resulting φ and p from simulating with the DAE Windkessel model. The initial state of the DAE has been selected for transient elimination by solving a two-point boundary value problem, enforcing the DAE states at the beginning and end of one cardiac cycle to match. Another possibility is to set $x(0) = 0$ (or other feasible value), simulate sufficiently long for any transient to fade, and then truncate. The system matrix A of (1) has eigenvalues $-1/(CR_p)$ and $-Rc/L$ corresponding to poles with time constants $T_1 = CR_p = 1\,\text{min}$ and $L/R_c = 5.5\,\text{s}$. If the cardiac cycle duration is T_c, each state component has therefore reached within $100e^{-t}$ % of its "transient free" value within $l\lceil t/T_c \rceil$ cardiac cycles.

Varying contractility Figure 3 illustrates the flow and pressure response to a beat with increased contractile strength. The input was generated by adding an offset spline to the w spline of Figure 2 to double the amplitude of the 3rd beat.

Arrhythmic event Figure 4 illustrates the response to an arrhythmic event. The input was generated by shifting the w spline abscissas of Figure 2 back 0.7 cycle periods after beat 3. (This does not exactly correspond

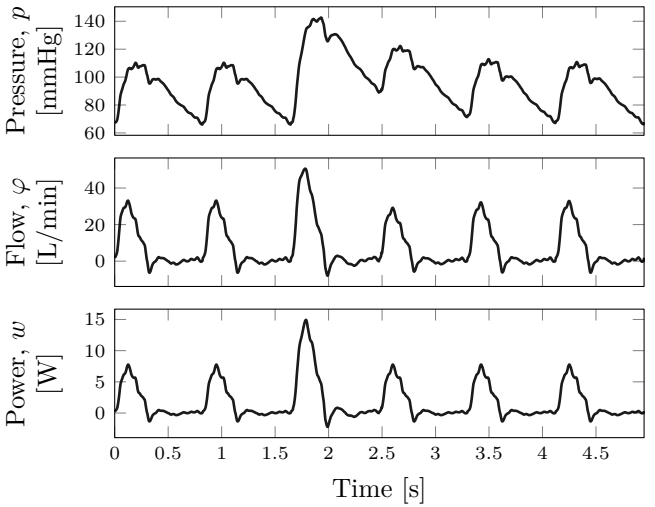

Figure 3. Windkessel DAE simulation with double contractile strength (power w) in beat 3. Top panes show the resulting pressure p and flow φ.

to a physiologically correct PVC, but serves to illustrate that we can alter a nominal power input by arbitrary offsets in magnitude and time.)

5. Discussion

We have proposed expressing the Windkessel model as a DAE, to use instantaneous power, rather than volumetric flow, as its input. This has enabled us to investigate how the dynamics react to changes in contractility and arrhythmia.

To handle flow and pressure measurements only being available at time-aligned, but not necessarily synchronized nor evenly spaced sampling instances, a continuous time signal model was employed. This signal model constitutes the MLE estimator under the assumption that the underlying singnals are $\mathcal{C}^2$ and corrupted with additive identically independently distributed Gaussian noise. Regularization was added to avoid possible overfitting, and its extent determined through cross validation.

Our simulation examples show how the considered Windkessel model responds to changes in heart contractility and double-beat arrhythmia. These events notably affect the resulting pressure profile. As a consequence of the Windkessel dynamics, there is no simple relation between the model parameters (2) and the resulting diastolic and systolic pressure. Compensating through feedback control of the Windkessel model parameters to maintain

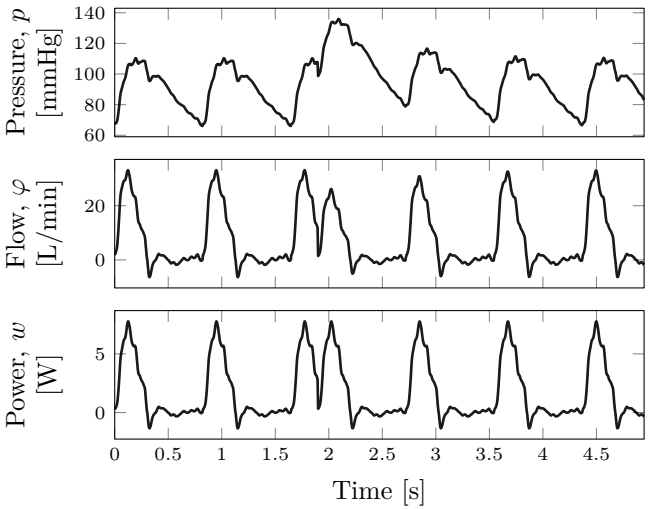

Figure 4. Windkessel DAE simulation with an early contraction in beat 4 of the input power w. Top panes show the resulting pressure p and flow φ.

prescribed safe upper systolic pressure and lower diastolic pressure bounds as proposed in [Gellner et al., 2020] is therefore non-trivial, and motivates investigation of artificial afterloads based on other principles than a verbatim implementation of Windkessel dynamics.

6. Conclusion

- Its volumetric flow input makes the classic lumped-parameter Windkessel model ill-suited for investigating how changes in contractility affect aortic pressure. For this purpose, a DAE representation with instantaneous power as input is more adequate.

- Smoothing cubic splines constitute a motivated class of functions for modeling aortic flow and pressure signal from sampled data. These models can readily be combined into a power signal model that maintains the smoothness properties of the cubic spline.

- It is desirable, but not straightforward, to independently control diastolic and systolic pressure within a Windkessel model with adjustable parameters.

Acknowledgment

This work was funded by the Swedish Research Council (grant 2017-04989) and the Swedish Foundation for Strategic Research (grant SM21-0037). We would like to acknowledge our collaborators with the Division of Thoracic Surgery at Lund University, and Jonas Hansson with the Department of Automatic Control, who inspired us to use smoothing splines for signal modeling.

References

Abicht, J.-M., T. Mayr, J. Jauch, S. Guethoff, S. Buchholz, B. Reichart, and A. Bauer (2018). "Large-Animal Biventricular Working Heart Perfusion System with Low Priming Volume—Comparison between in vivo and ex vivo Cardiac Function". *Thorac cardiovasc Surg* **66**:01, pp. 071–082. DOI: 10.1055/s-0036-1580604.

Ardehali, A., F. Esmailian, M. Deng, E. Soltesz, E. Hsich, Y. Naka, D. Mancini, M. Camacho, M. Zucker, P. Leprince, R. Padera, and J. Kobashigawa (2015). "Ex-vivo perfusion of donor hearts for human heart transplantation (PROCEED II): a prospective, open-label, multicentre, randomised non-inferiority trial". *The Lancet* **385**:9987, pp. 2577–2584. DOI: 10.1016/S0140-6736(15)60261-6.

De Boor, C. (2001). "A Practical Guide to Splines (Revised Edition)". In: Springer, pp. 207–214. ISBN: 978-0-387-90356-9.

de Hart, J., A. de Weger, S. van Tuijl, J. M. A. Stijnen, C. N. van den Broek, M. C. M. Rutten, and B. A. de Mol (2011). "An ex vivo platform to simulate cardiac physiology: a new dimension for therapy development and assessment". *Int J Artif Organs* **34**:6, pp. 495–505. DOI: 10.5301/IJAO.2011.8456.

Fisher, A., R. E. Challis, and P. Swann (1984). "A controllable artificial afterload for isolated heart studies". *J Biomed Eng* **6**:4, pp. 305–310. DOI: 10.1016/0141-5425(84)90080-3.

Gellner, B., L. Xin, R. V. P. Ribeiro, V. Bissoondath, P. Lu, M. B. Adamson, F. Yu, E. Paradiso, J. Zu, C. A. Simmons, and M. V. Badiwala (2020). "The Implementation of an Adjustable Afterload Module for Ex Situ Heart Perfusion". *Cardiovasc Eng Tech* **11**:1, pp. 96–110. DOI: 10.1007/s13239-019-00447-w.

Pigot, H. (2022). *Power-windkessel*. commit 8dac16a. URL: https://github.com/hpigot/power-windkessel/tree/v1.0.0 (visited on 2022-03-14).

Pigot, H., J. Hansson, A. Paskevicius, Q. Liao, T. Sjöberg, S. Steen, and K. Soltesz (2021). "Identification of cardiac afterload dynamics from data". In: *11th IFAC Symposium on Biological and Medical Systems BMS 2021*. IFAC-PapersOnLine, accepted (forthcoming).

Qin, G., B. Wohlfart, L. Zuo, J. Hu, T. Sjöberg, and S. Steen (2020). "Intact coronary and myocardial functions after 24 hours of non-ischemic heart preservation". *Scandinavian Cardiovascular Journal* **54**:1, pp. 59–65. DOI: 10.1080/14017431.2019.1684553.

Ribeiro, R. V. P., J. S. Alvarez, F. Yu, M. B. Adamson, E. Paradiso, A. R. M. Hondjeu, L. Xin, B. Gellner, M. Degen, V. Bissoondath, M. Meineri, V. Rao, and M. V. Badiwala (2020). "Comparing Donor Heart Assessment Strategies During Ex Situ Heart Perfusion to Better Estimate Posttransplant Cardiac Function". *Transplantation* **104**:9, pp. 1890–1898. DOI: 10.1097/TP.0000000000003374.

Segers, P., E. Rietzschel, M. De Buyzere, N. Stergiopulos, N. Westerhof, L. Bortel, T. Gillebert, and P. Verdonck (2008). "Three-and-four-element Windkessel models: Assessment of their fitting performance in a large cohort of healthy middle-aged individuals". *Proceedings of the Institution of Mechanical Engineers. Part H, Journal of engineering in medicine* **222**, pp. 417–28. DOI: 10.1243/09544119JEIM287.

Seifen, E., A. B. Seifen, R. H. Kennedy, G. A. Bushman, G. E. Loss, and T. G. Williams (1987). "Comparison of cardiac effects of enflurane, isoflurane, and halothane in the dog heart-lung preparation". eng. *Journal of Cardiothoracic Anesthesia* **1**:6, pp. 543–553. DOI: 10.1016/0888-6296(87)90041-x.

Silverman, B. W. (1984). "A Fast and Efficient Cross-Validation Method for Smoothing Parameter Choice in Spline Regression". *Journal of the American Statistical Association* **79**:387, pp. 584–589. DOI: 10.2307/2288404.

Soltesz, K., T. Sjöberg, T. Jansson, R. Johansson, A. Robertsson, A. Paskevicius, Q. Liao, G. Qin, and S. Steen (2018). "Closed-loop regulation of arterial pressure after acute brain death". *J Clin Monit Comput* **32**:3, pp. 429–437. DOI: 10.1007/s10877-017-0033-z.

Steen, S., A. Paskevicius, Q. Liao, and T. Sjöberg (2016). "Safe orthotopic transplantation of hearts harvested 24 hours after brain death and preserved for 24 hours". *Scandinavian Cardiovascular Journal* **50**:3, pp. 193–200. DOI: 10.3109/14017431.2016.1154598.

Stergiopulos, N., B. E. Westerhof, and N. Westerhof (1999). "Total arterial inertance as the fourth element of the windkessel model". en. *American Journal of Physiology-Heart and Circulatory Physiology* **276**:1, H81–H88. DOI: 10.1152/ajpheart.1999.276.1.H81.

Wahlquist, Y., K. Soltesz, Q. Liao, X. Liu, H. Pigot, T. Sjöberg, and S. Steen (2021). "Prevention of Ischemic Myocardial Contracture Through Hemodynamically Controlled DCD". *Cardiovasc Eng Tech.* DOI: 10.1007/s13239-021-00537-8.

Westerhof, N., J.-W. Lankhaar, and B. E. Westerhof (2009). "The arterial Windkessel". *Med Biol Eng Comput* **47**:2, pp. 131–141. DOI: 10.1007/s11517-008-0359-2.

White, C. W., E. Ambrose, A. Müller, Y. Li, H. Le, B. Hiebert, R. Arora, T. W. Lee, I. Dixon, G. Tian, J. Nagendran, L. Hryshko, and D. Freed (2015). "Assessment of donor heart viability during ex vivo heart perfusion". *Can. J. Physiol. Pharmacol.* **93**:10, pp. 893–901. DOI: 10.1139/cjpp-2014-0474.

Paper IV

A novel nonlinear afterload for *ex vivo* heart evaluation: porcine experimental results

Henry Pigot Kristian Soltesz Audrius Paskevicius
Qiuming Liao Trygve Sjöberg Stig Steen

Abstract

Background: Existing working heart models for *ex vivo* functional evaluation of donor hearts often use cardiac afterloads made up of discrete resistive and compliant elements. This approach limits the practicality of independently controlling systolic and diastolic aortic pressure to safely test the heart under multiple loading conditions. We present and investigate a novel afterload concept designed to enable such control.

Methods: Six ∼70 kg pig hearts were evaluated *in vivo*, then *ex vivo* in left-ventricular working mode using the presented afterload. Both *in vivo* and *ex vivo*, the hearts were evaluated at two exertion levels: at rest and following a 20 ug adrenaline bolus, while measuring aortic pressure and flow, left ventricular pressure and volume, and left atrial pressure.

Results: The afterload gave aortic pressure waveforms that matched the general shape of the *in vivo* measurements. A wide range of physiological systolic pressures (93–160 mmHg) and diastolic pressures (73–113 mmHg) were generated by the afterload. At each exertion level, the pair-wise mean difference in mean systolic pressure, diastolic pressure, pulse pressure, and cardiac power between each heart *in vivo* and *ex vivo* were not found to be significant ($P > 0.05$).

Conclusions: With the presented afterload concept, multiple physiological loading conditions could be tested *ex vivo*, and compared with the corresponding *in vivo* data. An additional control loop from the set pressure limits to the measured systolic and diastolic aortic pressure is proposed to address discrepancies observed between the set limits and the measured pressures.

Originally published in Artificial Organs (2022). Reprinted with permission.

1. Introduction

Ex vivo beating heart models enable the study of denervated heart physiology under varying conditions in physiological isolation. In an effort to meet growing demand for donor heart organs, such models have been investigated as a means to increase the safe use of extended criteria heart donors [White et al., 2018]. These donors typically include older individuals, those with previous conditions, and donors with circulatory (DCD), as opposed to brain (DBD), determined death [Beuth et al., 2019; Monteagudo Vela et al., 2018]. The potential risks of using such hearts has motivated the study of non-beating [Steen et al., 2016; Nilsson et al., 2020]; empty beating [Ardehali et al., 2015]; and working heart models [Abicht et al., 2018; Gellner et al., 2019; Messer et al., 2016; Hatami et al., 2019] to perfuse the cardiac muscles and provide indicators of heart performance prior to transplantation.

In contrast to non-beating and empty beating models, hearts in working mode actively pump perfusate through a flow impedance, referred to as the afterload. The hemodynamic function of the heart can then be observed directly, whereas non-working models only provide metabolic indicators of heart condition. Although popularized by the first clinically approved *ex vivo* heart perfusion device [Ardehali et al., 2015], studies have shown that metabolic metrics are unreliable predictors of post-transplant outcomes and point to functional metrics as a promising alternative [García Sáez et al., 2015; Stamp et al., 2015; White et al., 2015; Messer et al., 2016; Dhital et al., 2020; Ribeiro et al., 2020].

Here we consider left-ventricular working mode, where only the left side of the heart is loaded. An afterload must at least establish the minimum diastolic aortic pressure required for sufficient coronary flow. In order to test a wide range of hearts under a variety of loading conditions, an afterload would ideally enable control of diastolic aortic pressure and systolic aortic pressure, independently of cardiac output.

The systemic arterial tree—the left-heart afterload in the body—has long been represented using lumped-parameter linear models known as Windkessel models [Westerhof et al., 2009], illustrated in Figure 1, to describe the relationship between aortic flow and pressure. Mechanical afterloads have been constructed according to the Windkessel model, with discrete resistive and compliant elements, in an attempt to recreate physiological aortic pressure waveforms [Kung and Taylor, 2011; de Hart et al., 2011; Abicht et al., 2018; Gellner et al., 2020]. The peripheral resistance, R_p, determines the static gain from flow to pressure, while the compliance, C, affects both the systolic and diastolic pressure. Any systolic and diastolic pressure combination can be achieved for a given aortic flow by varying R_p and C. However, the parameters are coupled; to adjust only systolic or diastolic pressure, both

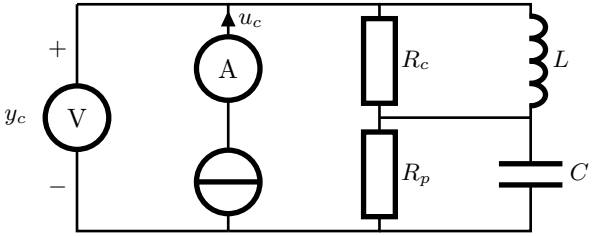

Figure 1. Circuit analogy of the parallel 4-element Windkessel model with signals: driving current (aortic flow) u_c, corresponding voltage (aortic pressure) y_c, and parameters: peripheral resistance, R_p, arterial compliance, C; characteristic aortic impedance, R_c; and perfusate inertance, L.

resistance and compliance must be manipulated. Doing so also changes the shape of the aortic pressure waveform.

Traditionally, *ex vivo* working heart models using Windkessel-based afterload designs are constructed with fixed or manually adjustable resistive and compliant elements. Due to the aforementioned coupled parameters, such afterloads are unable to practically emulate a variety of loading conditions and respond to hemodynamic changes in a time-constrained clinical setting. Two groups have published large-animal studies on adjustable Windkessel-based afterloads, though with the exception of [Xin et al., 2018] they only tested single loading conditions for each heart [de Hart et al., 2011; Gellner et al., 2020]. Notably, in [de Hart et al., 2011] coronary perfusion was controlled with a separate perfusion loop and in [Gellner et al., 2020] and [Xin et al., 2018] physiological diastolic pressures were not demonstrated. Matching the parameters of discrete Windkessel afterload elements to estimated parameters in a potential recipient has been suggested in [Gellner et al., 2020]. However, our sensitivity analysis of the Windkessel model with porcine and human data showed that simultaneous identifiability of its parameters from representative data is limited [Pigot et al., 2021]. This means that parameters identified *in vivo* under one working condition are not necessarily adequate for evaluation of the same heart *ex vivo* under another working condition.

As an alternative to Windkessel-based afterloads, some groups have pumped perfusate retrograde into the aorta with a centrifugal pump to control diastolic aortic pressure [White et al., 2015; Xin et al., 2018; Hatami et al., 2019]. These systems ensure diastolic aortic pressure regardless of cardiac output. However, systolic pressure is left uncontrolled and dependant on the geometry and position of the perfusate path and the rotational-velocity-dependent flow impedance of the centrifugal pump. Independent control of systolic and diastolic aortic pressures is not practical with this afterload method.

Here we present and investigate a novel afterload concept, designed to allow independent control of hemodynamic parameters critical to the safety and evaluation of the organ under test: diastolic pressure to ensure sufficient coronary flow and systolic pressure to facilitate physiological loading conditions while safely limiting peak aortic pressures. This paper is the first evaluation of technology patented in [Steen et al., 2019]. To the best of our knowledge, it is the first demonstration of heart evaluation using an adjustable cardiac afterload operating at physiological systolic and diastolic aortic pressures.

The afterload was tested with 6 hearts from ∼70 kg pigs, representative of adult human hearts, both at rest and in a state of exertion. The objective was to compare observations *in vivo* and *ex vivo* for each individual heart to investigate the feasibility of establishing and maintaining a range of physiological loading conditions by adjusting systolic and diastolic aortic pressures. Tight feedback control of the pressures has been left for future work, though a strategy to achieve such control is discussed.

2. Methods

Six ∼70 kg Swedish domestic pigs (*sus scrofa domesticus*) were used in the study. Each heart was evaluated *in vivo* with an open chest in two states of cardiac exertion: in resting state and in a high exertion state induced by a 20 µg adrenaline bolus.

In each state, aortic pressure and flow, ventricular pressure and volume, and atrial pressure were recorded. This was then repeated with each heart in an *ex vivo* left-ventricular working heart model using the considered nonlinear afterload, with cardiac output (flow provided to the left atrium), systolic aortic pressure, and diastolic aortic pressure controlled to physiological levels.

Conductance catheter ventricular pressure-volume signals were recorded at 200 Hz with LabChart 8 (AD Instruments, Boulder, CO). All pressures and aortic flow were sampled with a data acquisition system built in-house using AD7730 converters (Analog Devices, Norwood, MA) at 200 Hz and low pass filtered with a 50 Hz −3 dB cut-off frequency—twice the expected frequency of relevant physiological signals. Pulse pressure was calculated as the difference between systolic and diastolic pressure. Instantaneous cardiac power was calculated as the pointwise in time product of left ventricular pressure and aortic flow.

2.1 Nonlinear cardiac afterload

The *ex vivo* working heart model is illustrated in Figure 2. The heart is suspended in a perfusate reservoir, with the right atrium at the perfusate surface level. The perfusate is circulated by a roller pump through an oxygenator for heat and gas exchange. A second roller pump delivers perfusate

from the reservoir to the left atrium. Above the left atrium, the perfusate first passes through a vortex, pictured on the bottom left in Figure 3. This is not primarily designed to be physiological, but rather to lower perfusate linear momentum and limit forced atrial filling. A compliant sleeve above the vortex allows perfusate to accumulate, generating preload according to the balance between the input flow from the roller pump and the cardiac output. At steady state, roller pump flow to the left atrium is used as a measurement of cardiac output. The heart beats perfusate from the left ventricle through the adjustable afterload attached to the aorta, generating pulsatile aortic flow. A third roller pump connected to the aorta enables Langendorff perfusion of the coronaries arteries, e.g. when first attaching a cardioplegic heart to the system or as a safe fall-back in the event of heart fibrillation.

The afterload is a pressurized air-filled cuff through which the heart forces perfusate, as illustrated in Figure 4. The cuff is made of compliant polyisoprene, surrounded by a rigid plastic shell. The pressure limits of the air in the cuff are continuously controlled to a user-defined setpoint, corresponding to the diastolic and systolic aortic pressure limits. The minimum and maximum air pressure limits in the cuff are continuously controlled. The minimum (diastolic) pressure limit is enforced by a large pressure-controlled compliant chamber and a check valve. As the ventricle relaxes any perfusate flowing through the cuff is pressed back into the aorta or out into the reservoir by the pressurized cuff as its lumen closes. If the cuff pressure drops below the diastolic-limit chamber pressure air flows from the chamber through the check valve into the cuff. The cuff presses against the perfusate in the aorta at the air pressure set in the diastolic-limit chamber (see the left side of Figure 4), facilitating coronary perfusion.

The maximum (systolic) cuff air pressure limit is set by a pressure-regulated diaphragm valve. As the ventricle contracts, the perfusate exerts pressure against the cuff; the air in the cuff is compressed and its pressure rises, closing the check valve and opening a lumen through which perfusate flows back to the reservoir. If the air pressure in the cuff exceeds the systolic-limit setting, the diaphragm valve opens and air escapes back into the diastolic-limit chamber, widening the lumen to limit perfusate pressure in the aorta (see the right side of Figure 4). This nonlinear resistance in systole is designed to increase the safety and stability of operation *ex vivo*, where the heart lacks protection from over-distention that is provided by the pericardium *in vivo*.

2.2 *In vivo* evaluation

All animals were treated according to European guidelines [The European Parliament, 2010], under ethics approval 5.8.18-15906/2020 issued by "Malmö/Lunds Djurförsöksetiska Nämnd" (local REB). Porcine experiments

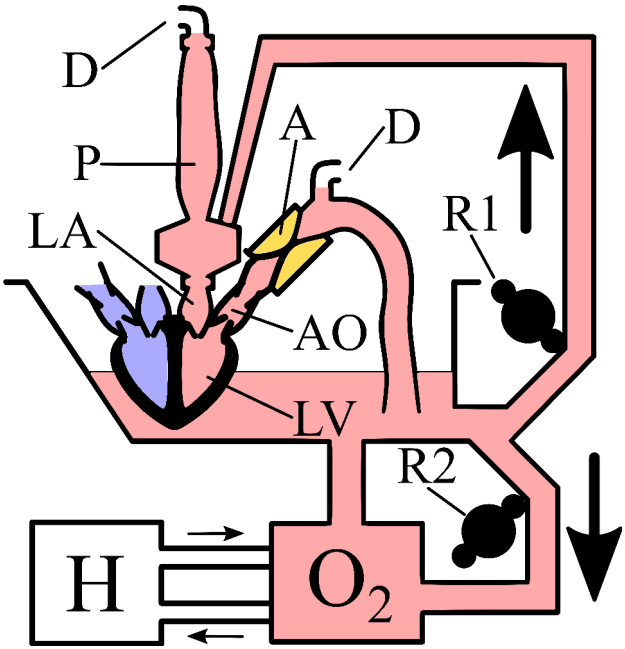

Figure 2. *Ex vivo* setup, with the afterload (A). Roller pump R1 delivers perfusate to the preload (P) at the left atrium (LA). At the preload, the perfusate goes through a vortex to lower its linear momentum to limit forced atrial filling. A compliant reservoir sits above the vortex, allowing a column of perfusate to accumulate, resulting in atrial preload pressure. Ports D, above the compliant reservoir and the highest point of the afterload, provide de-airing driven by small roller pumps. The heart pumps the perfusate from the left ventricle (LV) through the aorta (AO) and the afterload and back to the reservoir. The perfusate in the reservoir is circulated by roller pump R2 through an oxygenator (O2) that also provides heat exchange via a heater-cooler unit (H). An additional roller pump (not pictured) is used to provide Langendorff perfusion when the cardioplegic heart is first placed in the system.

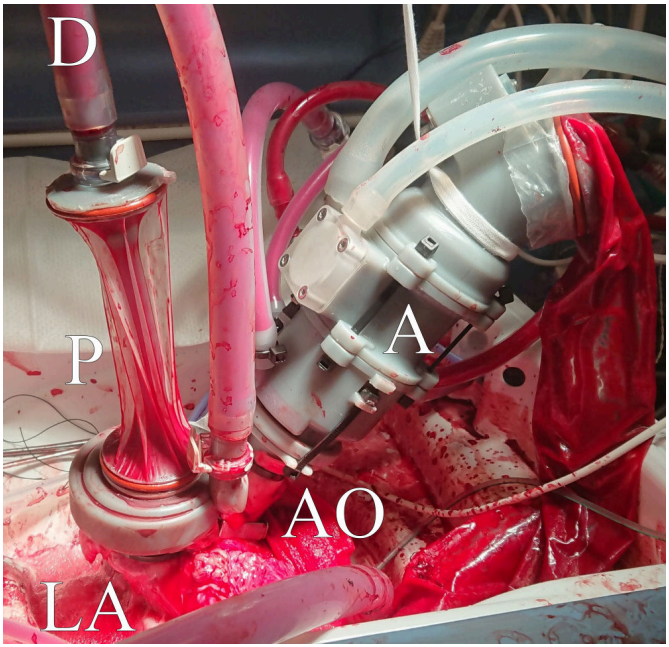

Figure 3. The *ex vivo* working heart model, with the afterload pictured on the left attached to the aorta, and preload on the right attached to the left atrium. The heart is partially submerged in perfusate.

were motivated by the physiological similarity between porcine and adult human hearts, and to accurately test the afterload in the absence of realistic mechanical heart models.

Sedation was induced with an intramuscular bolus of 1 g ketamine (Ketaminol vet, Intervet, Boxmeer, Netherlands), 140 mg xylazin (Rompun vet, Bayer AB, Solna, Sweden), and 750 µg atropine (Atropin, Mylan AB, Stockholm). Anesthesia was established with an intravenous bolus of 100 µg fentanyl (Fentanyl, B. Braun Melsungen AG, Danderyd, Sweden) and 20 mg midazolam (Midazolam accord, Accord healthcare Ltd. United Kingdom). An additional intravenous bolus of 40 mg rocuronium (Rocuronium, Fresenius Kabi, Graz, Austria) was given pre-tracheotomy. Anesthesia was maintained with 12–15 ml/h continuous intravenous infusion of the following drugs mixed into a 50 ml syringe: 10 ml of 100 mg/ml ketamine; 6 ml of 5 mg/ml midazolam; 20 ml of 10 mg/ml rocuronium; and 0.9% NaCl saline solution 14 ml. Normoventilation ($PaCO_2$ around 5 kPa), was obtained using a tidal volume of 8 ml/kg body weight at about 20 breaths/min, and a positive end-expiratory pressure of 5 cmH_2O.

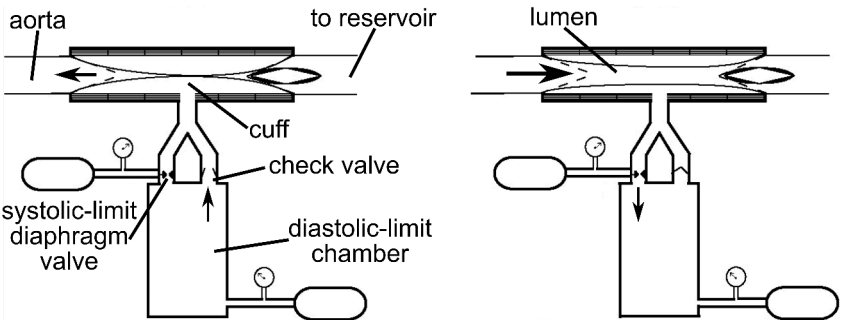

Figure 4. Schematic of the nonlinear adjustable afterload in diastole (left) and systole (right) adapted from [Steen et al., 2019]. Black arrows indicate the direction of fluid flow. Two pressures in the afterload are continuously controlled: the pressure in the diastolic-limit chamber, and the pressure at which the systolic-limit diaphragm valve opens. In diastole, air flows through a check valve from the diastolic-limit chamber into the cuff. The air pressure in the cuff is exerted on the perfusate in the aorta, facilitating coronary perfusion. In systole, the contracting ventricle causes the perfusate pressure in the aorta to rise, compressing the air in the cuff, opening a perfusate lumen through the cuff, and closing the check valve. If the air pressure in the cuff exceeds the set point of the systolic-limit diaphragm valve, air flows through the valve back into the diastolic-limit chamber, maintaining the systolic pressure set point in the cuff and widening the lumen through the cuff.

Separate catheters (Secalon-T ,Merit Medical, Singapore) were inserted into the right atrium via the right internal jugular vein for pressure measurement and anesthesia maintenance, as well into the aorta via the right carotid artery for pressure measurement and blood gas sampling. Heparin was administered (400 U/kg). Median sternotomy was performed. A pressure-volume catheter (VentriCath 510S, Millar Inc, Houston, TX) was inserted into the left ventricle via the ascending aorta and the left atrium was catheterized for pressure measurement. Non-ventricular pressures were measured with Meritrans DTXPlus transducers (Merit Medical, Singapore). Aortic flow was measured with an ultrasonic transit-time flow probe (20PS, Transonic Systems Inc, Ithica, NY). The probe was calibrated against the roller pump supplying perfusate to the left atrium *ex vivo*, using simultaneous probe and roller pump time-volume measurements collected prior to the start of experiments. This aortic flow was used as a measurement of *in vivo* cardiac output. Blood gas measurements (ABL 700, Radiometer, Copenhagen, Denmark) were taken prior to at-rest measurements to ensure normal blood chemistry. *in vivo* hemodynamic measurements were recorded at rest and following a 20 µg adrenaline bolus.

2.3 *Ex vivo* evaluation

The *ex vivo* system was primed with perfusate composed of 1.5 L Kreps solution with 5 % Dextran 40, and 7 % albumin, into which fresh whole blood from the donor pig was mixed to achieve a mean hematocrit of 22 % (2 % SE), making a total volume of ∼3 L. The oxygenator kept the perfusate at normothermia and facilitated gas exchange using 100 ml/min of 95 % oxygen and 5 % carbon dioxide. In addition to the heparin left in the whole blood, 5000 U were added to the perfusate. Pharmacological support for heart function in the absence of the pituitary gland and brain stem was provided via continuous infusion, as specified in [Steen et al., 2012]: 1 mg adrenaline and 1 mg noradrenaline for vascular tonus, heart rate, and heart contractility, 1 mg cocaine to prevent noradrenaline reuptake, 0.3 mg triiodothyronine, and 300 mg cortisol were all diluted with 0.9% NaCl saline solution into a 50 ml syringe. Infusion rates were initially set at 0.1 ml/h and adjusted up to 4 ml/h according to need.

After the *in vivo* testing, the heart was preserved with St. Thomas' cardioplegic solution at 4 °C. Custom-made cannulas were fastened to the aorta and left atrium. The pressure-volume-loop catheter was inserted into the left ventricle via the aorta, and the left atrium was cannulated for pressure measurement. The cardioplegic time was 30 min (4 min standard error, hereafter SE).

The heart was mounted into the system, connecting the preload and afterload to the atrium and aorta, respectively. To de-air the system, the aorta was positioned vertically, then the heart was slowly filled with perfusate via the left atrium, with the afterload set fully open (both pressure limits set to 0 mmHg). Flow to the atrium was then stopped, and the heart was flushed by pumping perfusate into the aorta at 900 ml/min and setting the afterload diastolic-limit-chamber pressure to achieve a mean aortic pressure of 50 mmHg, leaving the systolic-limit pressure set to 0 mmHg. This provided pressure-regulated coronary flow (Langendorff perfusion) to flush and warm the heart. Perfusate not flowing into the coronary arteries escaped through the afterload to the reservoir. Defibrillation was provided in the event of ventricular fibrillation. Once empty-beating sinus rhythm was established, the pump to the aorta was stopped and perfusate was provided to the left atrium via the preload, initiating working mode perfusion.

Cardiac output (roller pump flow to the left atrium), diastolic-limit-chamber pressure, and systolic-limit pressure were then slowly adjusted to physiological resting levels, aiming to match the heart's measured *in vivo* values. However, its observed performance *ex vivo* was considered when adjusting, so as not to damage the heart in an attempt to perfectly match

the *in vivo* loading. Measurements were taken after the heart reached a steady state. The system was similarly readjusted after administering the 20 µg adrenaline bolus.

3. Results

Hemodynamic waveforms from three cardiac cycles under each test condition representative of the group are shown in Figure 5. *In vivo* and *ex vivo* hemodynamics are shown for each heart at rest in Figure 6 and after a 20 µg adrenaline bolus in Figure 7. Aortic pressures are shown with the corresponding afterload limit settings, with mean (markers) and extrema (bars, representing systolic and diastolic pressures) averaged over five representative cardiac cycles. Similarly, the mean aortic flow, left atrial pressure, and heart rate are shown. Across all hearts *ex vivo*, these mean systolic and diastolic pressures had ranges 93–123 mmHg and 73–104 mmHg respectively at rest, and 103–160 mmHg and 73–113 mmHg respectively post-adrenaline. Grouped by exertion level, mean systolic, diastolic, and pulse pressures were slightly higher *in vivo* than *ex vivo* over five representative cardiac cycles: +14 (SE 6) mmHg, +6 (SE 4), and +7 (SE 4) mmHg respectively at rest ($n = 6$), and +26 (SE 10), +16 (SE 12), and +10 (SE 10) mmHg respectively post-adrenaline ($n = 5$).

In 4 out of 6 hearts, blood loss during *in vivo* cannulation led to hypovolymia, requiring saline infusion and, in the case of Heart 6, defibrillation and continuous adrenaline infusion (0.1 µg/kg/min). Heart 6 received excessive defibrillation energy *in vivo* due to a defibrillator error, after which it was frequently arrhythmic. As a result, the left atrium in Heart 6 was not catheterized for pressure measurement *in vivo*, and the heart showed little response to adrenaline *ex vivo* so the diastolic and systolic afterload limits were not raised from the resting level. Heart 2 had chronic pericarditis resulting in poor left ventricular performance and making it prone to arrhythmia. As such, an adrenaline bolus was not administered to this individual *ex vivo*. Despite the instability of these hearts, they were successfully perfused in working mode at physiological systolic and diastolic aortic pressures.

Figure 8 shows instantaneous cardiac powre (CP) for Heart 1 over five cardiac cycles, representative of the hearts tested. Across all individuals, there was no significant difference in mean CP *in vivo* and *ex vivo*, while peak cardiac powers were significantly higher *in vivo* in particular in the post-adrenaline case. The differences between *in vivo* and *ex vivo* mean CP were +26 (SE 19) mmHgL/min at rest ($n = 6$), and +125 (SE 83) mmHgL/min at post-adrenaline ($n = 5$), while the differences in peak CP were +384 (SE 109) mmHgL/min at rest ($n = 6$), and +1550 (SE 196) mmHgL/min at post-adrenaline ($n = 5$).

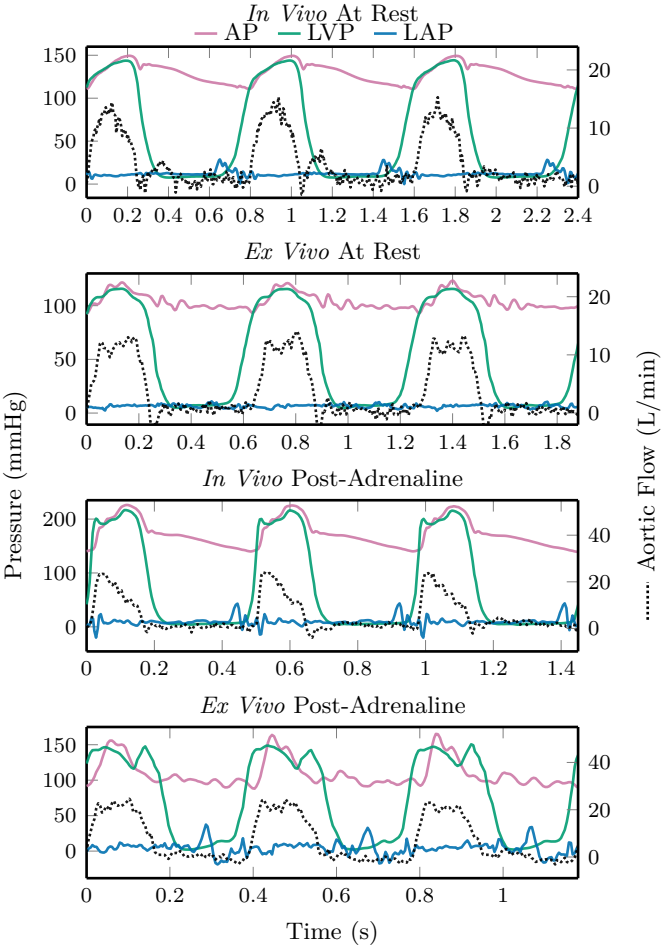

Figure 5. Comparison of aortic pressure (AP), left ventricular pressure (LVP), left atrial pressure (LAP), and aortic flow *in vivo* and *ex vivo*, at rest and after a 20 µg adrenaline bolus. Measurements are from Heart 1 and representative of the group.

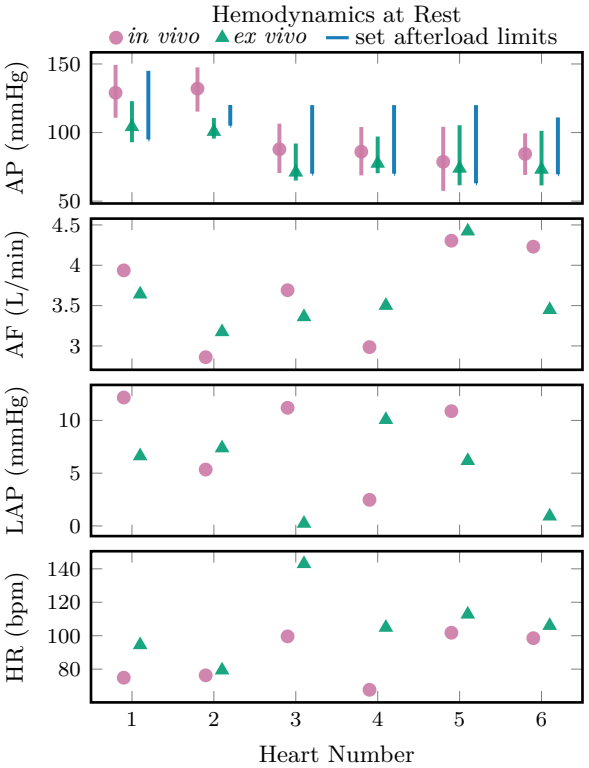

Figure 6. Aortic pressure (AP), aortic flow (AF), left atrial pressure (LAP), and heart rate (HR) *in vivo* (pink, circles) and *ex vivo* (measured values in green with triangle markers, interval between set afterload limits in blue) for each heart at rest. The pink and green bars show the total range and the markers show the mean of each value averaged over five cardiac cycles.

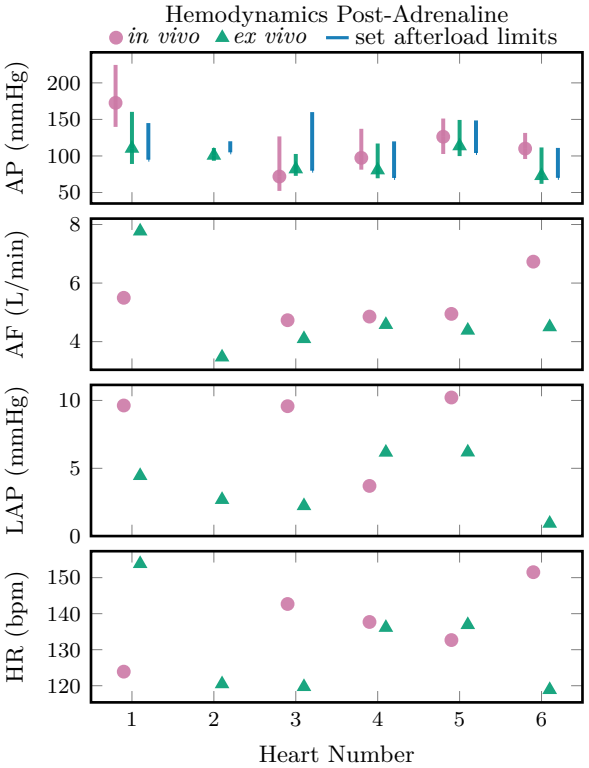

Figure 7. Aortic pressure (AP), aortic flow (AF), left atrial pressure (LAP), and heart rate (HR) *in vivo* (pink, circles) and *ex vivo* (measured values in greeb with triangle markers, interval between set afterload limits in blue) for each heart after a 20 µg adrenaline bolus. The pink and green bars show the total range and the markers show the mean of each value averaged over five cardiac cycles.

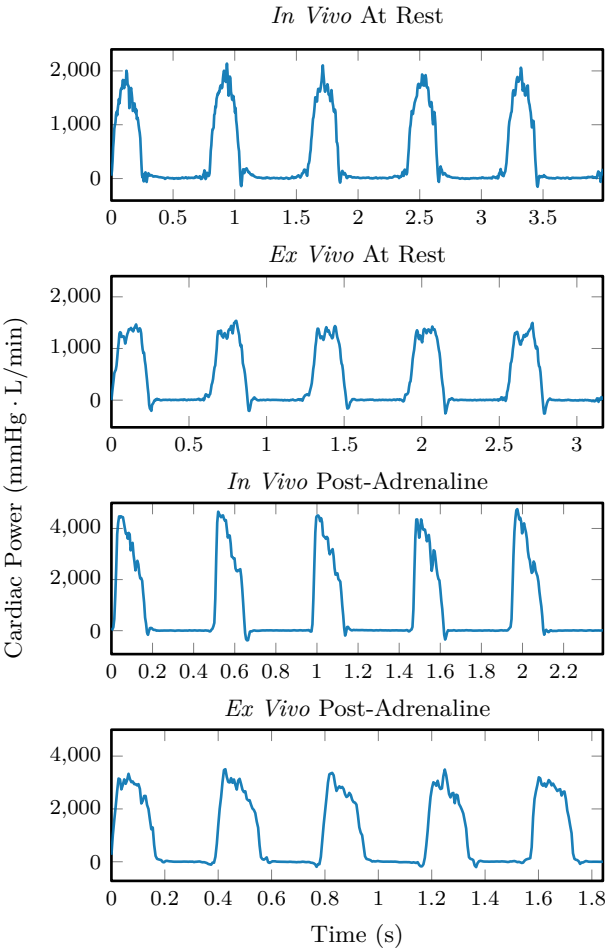

Figure 8. Instantaneous cardiac power of Heart 1, calculated as the pointwise product of left ventricular pressure and aortic flow, at rest and after a 20 µg adrenaline bolus, both *in vivo* and *ex vivo*.

The waveforms in both Figure 5 and Figure 8 are in systole for a larger portion of each cardiac cycle *ex vivo* compared to *in vivo*, as is expected due to the higher *ex vivo* heart rates. Shorter ventricular filling times at these *ex vivo* heart rates may account for lower peak CP.

Difficulties in the placement and orientation of the conductance catheter resulted in unreliable volume measurements. With the exception of 3 *in vivo* and 4 *ex vivo* treatments out of a total of 23, the volume measurements were

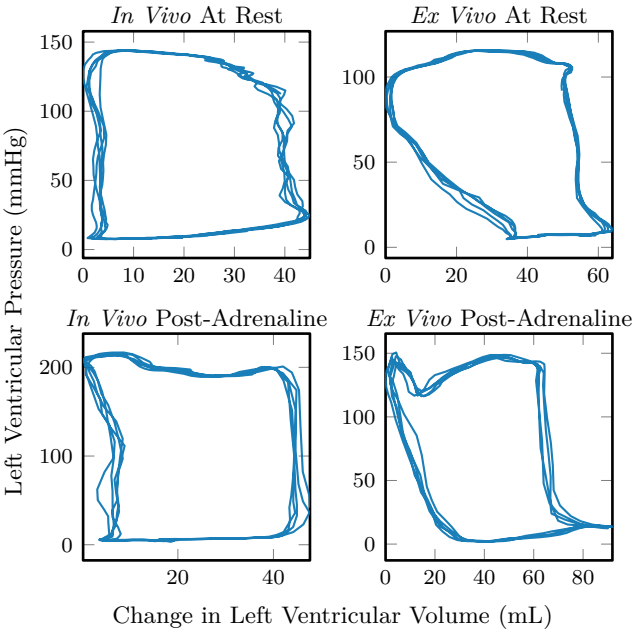

Figure 9. Left ventricular pressure-volume loop measurements over five cardiac cycles in Heart 1.

contrary to the physiological pressure and flow waveforms measured. Figure 9 shows the one heart where all four treatments gave representative pressure-volume loops. The *ex vivo* loops show early filling of the ventricle during diastole. The *ex vivo* heart is susceptible to aortic valve insufficiency; early filling is observed in previously published *ex vivo* working heart pressure-volume loops using various afterloads [White et al., 2015; Xin et al., 2018; Gellner et al., 2020]. The pressure peak at end-systole *ex vivo* post-adrenaline is suspected to be a measurement artifact caused by compression of the pressure transducer against the ventricle wall.

4. Discussion

In this paper we evaluated the design of a novel *ex vivo* cardiac afterload with independently adjustable systolic and diastolic pressure limits. The afterload was tested with 6 porcine hearts at rest and following an adrenaline bolus, with systolic and diastolic aortic pressure and cardiac output adjusted to near-physiological levels in both cases. The afterload generated multiple loading conditions in each heart representative of physiological values,

though yielding slightly lower *ex vivo* pressures as compared to *in vivo* pressures for the same heart. The general shape of *ex vivo* AP matches the *in vivo* measurements, as seen in Figure 5. As this study is an initial evaluation of the afterload concept, data was collected from only 6 hearts. Given this low number, statistical analysis beyond means and standard errors has been omitted.

A discrepancy between the afterload limit values and the observed systolic and diastolic aortic pressures is seen in Figure 6 and Figure 7. The column of perfusate between the afterload cuff and the aortic pressure transducer contributes a positive offset between the aortic pressures and their corresponding limits in the afterload. Although the afterload is designed to behave in an on-off fashion at the systolic and diastolic pressure limits, the physical construction of the afterload leads to some linear dynamics. The air volume in the cuff contributes compliance, and the lumen through the cuff contributes resistance to flow. As a result of this resistive property, increasing flows yield slightly higher systolic pressures even at the same the same afterload pressure limits, for example during the onset of increased heart rate and higher peak aortic flows post-adrenaline, so long as the pressures remain below the set limit. An exception is seen in Heart 1 post-adrenaline, where systolic aortic pressures exceed the set limit. Occasional sticking of the systolic limit diaphragm valve was observed, and in this case the valve may have not opened fully, limiting the displacement of volume from the cuff and preventing a widening of the afterload lumen.

When the afterload is operating in pressure ranges between the diastolic and systolic limits there are two possible mechanisms for volume displacement in the cuff, allowing the lumen through the afterload to widen. Cuff volume can be reduced by compression of the air in the cuff, or by leakage through the valves. An ideal systolic-limit diaphragm valve would not allow any airflow out of the cuff until the limit pressure is exceeded. Consequently, increases in the systolic-limit pressure would have no impact on the observed systolic aortic pressure while the heart is generating pressures below the set limit. However, this was not the behavior observed. At systolic aortic pressures below the limit, an increase in the systolic limit pressure resulted in increased systolic aortic pressure. Rather than behaving in an on-off fashion, the systolic-limit diaphragm valve acts as a variable resistance with the systolic limit controlling the resistance of air leakage from the cuff through the valve. As a result, the systolic aortic pressure is controllable via the systolic limit despite being below the set limit. Furthermore, when operating between the set limits, systolic aortic pressure depends on the diastolic pressure limit, since both air compression in the cuff and leakage through the systolic-limit diaphragm valve are proportional to the difference between cuff pressure and the diastolic-limit pressure. Managing this coupled behavior manually becomes impractical in a time-pressured clinical setting. Instead we propose

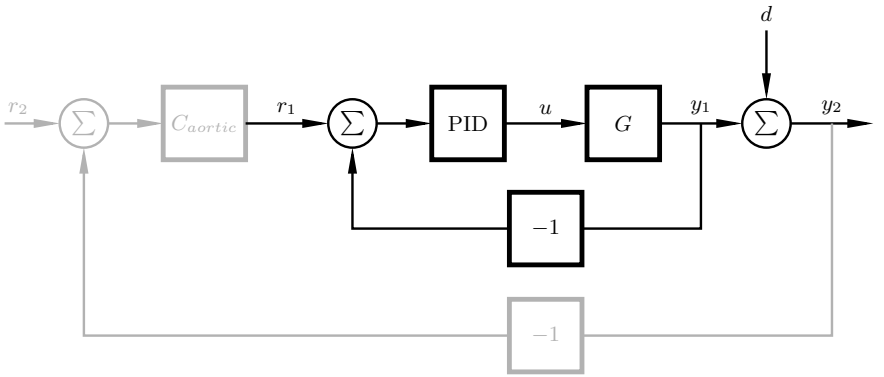

Figure 10. The control loop used for the diastolic- and systolic-limit pressures in the afterload, with C_{cuff} being a hand-tuned PID controller. In the diastolic case, the pressure of the diastolic-limit chamber is controlled (setpoint r_1 and measurement y_1), with a roller pump forcing air into the chamber (u). In the systolic case, a roller pump (u) pressurizes the membrane of a diaphragm valve; the pressure in the cuff must exceed the set pressure of the diaphragm valve (setpoint r_1 and measurement y_1) to escape from the cuff back into the diastolic-limit chamber. Disturbance d represents the offset between the measured diastolic or systolic aortic pressure and the corresponding afterload pressure. An outer loop (grey) may be added to compensate for d using aortic pressure feedback, with diastolic or systolic-limit set point r_2 and corresponding aortic measurement y_2.

an additional control loop to set the pressure limits in the afterload according to feedback of the measured systolic and diastolic aortic pressures, as illustrated in grey in Figure 10. This would enable more rapid and accurate control of the loading conditions while maintaining the safety limits offered by the nonlinear behavior of the adjustable afterload. To similarly maintain safe beat-to-beat systolic and diastolic aortic pressures would require impractically fast parameter adjustment in a Windkessel-style afterload. An example of manually implemented cascaded control was done with Heart 5, matching *ex vivo* aortic pressures to those measured *in vivo*, as shown in Figure 6 and Figure 7.

5. Conclusion

The afterload demonstrated the ability to recreate a variety of cardiac loading conditions *ex vivo*, under varying levels of exertion and across multiple hearts. The afterload concept enables control diastolic and systolic aortic pressure by means of the air cuff pressure limits. However, slight discrepancies between

the set pressure limits and resulting aortic pressures were observed. While possible to manually compensate for these, as done with Heart 5, doing so in a future clinical setting is impractical, and a cascaded automatic feedback control structure is therefore proposed.

Acknowledgements

This work was funded by the Swedish Research Council (grant 2017-04989), the Swedish Foundation for Strategic Research (grant SM21-0037), and the Hans-Gabriel and Alice Trolle-Wachtmeister Foundation for Medical Research. The authors from the Department of Automatic Control are members of the ELLIIT Strategic Research Area at Lund University. The funding sources have not influenced any aspect of the study or the manuscript.

Author contributions

Henry Pigot wrote the original manuscript draft. All other authors reviewed and edited the manuscript. Additionally,

- Henry Pigot: conceptualization, data curation, formal analysis, investigation, software, visualization;
- Kristian Soltesz: conceptualization, funding acquisition;
- Audrius Paskevicius: investigation, methodology, software;
- Qiuming Liao: investigation, resources;
- Trygve Sjöberg: project administration, resources;
- Stig Steen: conceptualization, funding acquisition, investigation, methodology, supervision.

References

Abicht, J.-M., T. Mayr, J. Jauch, S. Guethoff, S. Buchholz, B. Reichart, and A. Bauer (2018). "Large-Animal Biventricular Working Heart Perfusion System with Low Priming Volume—Comparison between in vivo and ex vivo Cardiac Function". *Thorac cardiovasc Surg* **66**:01, pp. 071–082. DOI: 10.1055/s-0036-1580604.

Ardehali, A., F. Esmailian, M. Deng, E. Soltesz, E. Hsich, Y. Naka, D. Mancini, M. Camacho, M. Zucker, P. Leprince, R. Padera, and J. Kobashigawa (2015). "Ex-vivo perfusion of donor hearts for human heart transplantation (PROCEED II): a prospective, open-label, multicentre, randomised non-inferiority trial". *The Lancet* **385**:9987, pp. 2577–2584. DOI: 10.1016/S0140-6736(15)60261-6.

Beuth, J., F. Falter, R. V. Pinto Ribeiro, M. Badiwala, and M. Meineri (2019). "New Strategies to Expand and Optimize Heart Donor Pool: Ex Vivo Heart Perfusion and Donation After Circulatory Death: A Review of Current Research and Future Trends". *Anesthesia & Analgesia* **128**:3, pp. 406–413. DOI: 10.1213/ANE.0000000000003919.

de Hart, J., A. de Weger, S. van Tuijl, J. M. A. Stijnen, C. N. van den Broek, M. C. M. Rutten, and B. A. de Mol (2011). "An ex vivo platform to simulate cardiac physiology: a new dimension for therapy development and assessment". *Int J Artif Organs* **34**:6, pp. 495–505. DOI: 10.5301/IJAO.2011.8456.

Dhital, K., P. Ludhani, S. Scheuer, M. Connellan, and P. Macdonald (2020). "DCD donations and outcomes of heart transplantation: the Australian experience". *Indian Journal of Thoracic and Cardiovascular Surgery*. DOI: 10.1007/s12055-020-00998-x.

García Sáez, D., A. Elbetanony, P. Lezberg, A. Hassanein, C. T. Bowles, A.-F. Popov, B. Zych, A. Sabashnikov, P. Mohite, and A. R. Simon (2015). "Ex vivo heart perfusion after cardiocirculatory death; a porcine model". *Journal of Surgical Research* **195**:1, pp. 311–314. DOI: 10.1016/j.jss.2014.12.039.

Gellner, B., L. Xin, R. V. Ribeiro, V. Bissoondath, M. B. Adamson, F. Yu, P. Lu, E. Paradiso, A. Mbadjeu, C. A. Simmons, and M. V. Badiwala (2019). "The Implementation of Physiological Afterload during Ex Situ Heart Perfusion Augments Prediction of Post-Transplant Function". *American Journal of Physiology-Heart and Circulatory Physiology*. DOI: 10.1152/ajpheart.00427.2019.

Gellner, B., L. Xin, R. V. P. Ribeiro, V. Bissoondath, P. Lu, M. B. Adamson, F. Yu, E. Paradiso, J. Zu, C. A. Simmons, and M. V. Badiwala (2020). "The Implementation of an Adjustable Afterload Module for Ex Situ Heart Perfusion". *Cardiovasc Eng Tech* **11**:1, pp. 96–110. DOI: 10.1007/s13239-019-00447-w.

Hatami, S., C. W. White, M. Ondrus, X. Qi, M. Buchko, S. Himmat, L. Lin, K. Cameron, D. Nobes, H.-J. Chung, J. Nagendran, and D. H. Freed (2019). "Normothermic Ex Situ Heart Perfusion in Working Mode: Assessment of Cardiac Function and Metabolism". *JoVE (Journal of Visualized Experiments)* 143, e58430. DOI: 10.3791/58430.

Kung, E. O. and C. A. Taylor (2011). "Development of a Physical Windkessel Module to Re-Create In Vivo Vascular Flow Impedance for In Vitro Experiments". *Cardiovasc Eng Tech* **2**:1, pp. 2–14. DOI: 10.1007/s13239-010-0030-6.

Messer, S. J., R. G. Axell, S. Colah, P. A. White, M. Ryan, A. A. Page, B. Parizkova, K. Valchanov, C. W. White, D. H. Freed, E. Ashley, J. Dunning, M. Goddard, J. Parameshwar, C. J. Watson, T. Krieg, A. Ali, S. Tsui, and S. R. Large (2016). "Functional assessment and transplantation of the donor heart after circulatory death". *The Journal of Heart and Lung Transplantation* **35**:12, pp. 1443–1452. DOI: 10.1016/j.healun.2016.07.004.

Monteagudo Vela, M., D. García Sáez, and A. R. Simon (2018). "Current approaches in retrieval and heart preservation". *Annals of Cardiothoracic Surgery* **7**:1, pp. 67–74. DOI: 10.21037/acs.2018.01.06.

Nilsson, J., V. Jernryd, G. Qin, A. Paskevicius, C. Metzsch, T. Sjöberg, and S. Steen (2020). "A nonrandomized open-label phase 2 trial of nonischemic heart preservation for human heart transplantation". *Nat Commun* **11**:1, p. 2976. DOI: 10.1038/s41467-020-16782-9.

Pigot, H., J. Hansson, A. Paskevicius, Q. Liao, T. Sjöberg, S. Steen, and K. Soltesz (2021). "Identification of cardiac afterload dynamics from data". *IFAC-PapersOnLine*. 11th IFAC Symposium on Biological and Medical Systems BMS 2021 **54**:15, pp. 508–513. DOI: 10.1016/j.ifacol.2021.10.307.

Ribeiro, R. V. P., J. S. Alvarez, F. Yu, M. B. Adamson, E. Paradiso, A. R. M. Hondjeu, L. Xin, B. Gellner, M. Degen, V. Bissoondath, M. Meineri, V. Rao, and M. V. Badiwala (2020). "Comparing Donor Heart Assessment Strategies During Ex Situ Heart Perfusion to Better Estimate Posttransplant Cardiac Function". *Transplantation* **104**:9, pp. 1890–1898. DOI: 10.1097/TP.0000000000003374.

Stamp, N. L., A. Shah, V. Vincent, B. Wright, C. Wood, W. Pavey, C. Cokis, S. Chih, L. Dembo, and R. Larbalestier (2015). "Successful Heart Transplant after Ten Hours Out-of-body Time using the TransMedics Organ Care System". *Heart, Lung and Circulation* **24**:6, pp. 611–613. DOI: 10.1016/j.hlc.2015.01.005.

Steen, S., T. Sjöberg, Q. Liao, G. Bozovic, and B. Wohlfart (2012). "Pharmacological normalization of circulation after acute brain death". *Acta Anaesthesiol Scand* **56**:8, pp. 1006–1012. DOI: 10.1111/j.1399-6576.2012.02721.x.

Steen, S., A. Paskevicius, and B. King (2019). "Afterload device for a beating heart during examination thereof". US10405756B2. (Visited on 2020-07-14).

Steen, S., A. Paskevicius, Q. Liao, and T. Sjöberg (2016). "Safe orthotopic transplantation of hearts harvested 24 hours after brain death and preserved for 24 hours". *Scandinavian Cardiovascular Journal* **50**:3, pp. 193–200. DOI: 10.3109/14017431.2016.1154598.

The European Parliament (2010). *On the Protection of Animals Used for Scientific Purpose*. Tech. rep. Council of Europe.

Westerhof, N., J.-W. Lankhaar, and B. E. Westerhof (2009). "The arterial Windkessel". *Med Biol Eng Comput* **47**:2, pp. 131–141. DOI: 10.1007/s11517-008-0359-2.

White, C. W., E. Ambrose, A. Müller, Y. Li, H. Le, B. Hiebert, R. Arora, T. W. Lee, I. Dixon, G. Tian, J. Nagendran, L. Hryshko, and D. Freed (2015). "Assessment of donor heart viability during ex vivo heart perfusion". *Can. J. Physiol. Pharmacol.* **93**:10, pp. 893–901. DOI: 10.1139/cjpp-2014-0474.

White, C. W., S. J. Messer, S. R. Large, J. Conway, D. H. Kim, D. J. Kutsogiannis, J. Nagendran, and D. H. Freed (2018). "Transplantation of Hearts Donated after Circulatory Death". *Frontiers in Cardiovascular Medicine* **5**, p. 8. DOI: 10.3389/fcvm.2018.00008.

Xin, L., B. Gellner, R. V. P. Ribeiro, G. M. Ruggeri, D. Banner, M. Meineri, V. Rao, J. Zu, and M. V. Badiwala (2018). "A New Multi-Mode Perfusion System for Ex Vivo Heart Perfusion Study". *J Med Syst* **42**:2, p. 25. DOI: 10.1007/s10916-017-0882-5.

Paper V

Actively controlled cardiac afterload

Henry Pigot **Ylva Wahlquist** **Kristian Soltesz**

Abstract

Ex vivo (outside of the body) working heart models enable the evaluation of isolated hearts. They are envisioned to play an important role in increasing the currently low utilization rate of donor hearts for transplantation. For the heart to work in isolation, an afterload (flow impedance) is needed. To date, afterload devices have been constructed by combining multiple constituent elements such as pumps, flow resistances, and flow capacitances (compliances), typically to replicate the structure of so-called Windkessel models. This limits active control to that achievable by varying these elements, making it slow and subject to the problem of dynamic coupling between parameters. Here we present a novel concept to achieve Windkessel dynamics through a very simple variable flow impedance. The impedance is actively controlled using feedback from a pressure measurement. Through simulations we demonstrate the ability to perfectly emulate Windkessel dynamics, while imposing tight pressure limits needed for safe operation—something not achievable with the verbatim implementation using constituent elements.

Originally published IFAC-PapersOnLine, 22nd IFAC World Congress (2023). Reprinted with permission.

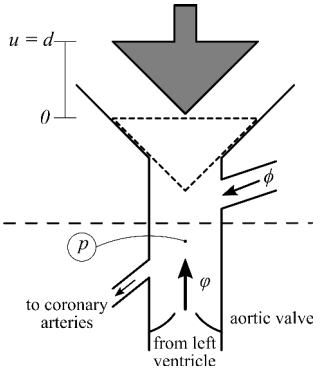

Figure 1. Schematic of the afterload mechanism (above dashed line) connected to the heart (below). The afterload consists of a plunger actively controlled to position $0 < u \leq d$. The flow through the device consists of the aortic flow φ, and an auxiliary contribution ϕ, chosen to ensure $\phi + \varphi > 0$. Plunger position control is based on measurements of aortic pressure p.

1. Introduction

Ex vivo working heart models enable the organ to be studied in isolation from other physiological systems. In addition to being a valuable tool in basic physiology and pharmacology research, such models show potential for use in functional evaluation of donor organs prior to transplantation, as described by [White et al., 2018; Gellner et al., 2020a]. Functional evaluation may facilitate the safe use of organs from marginal donors—organs that would otherwise go unused—by providing clinicians with concrete evidence of organ performance, thereby expanding the organ donor pool.

Cardiac afterload is the impedance the body poses to blood flow from the beating heart. *Ex vivo* working heart models rely on devices that emulate this load. Ideally, a cardiac afterload device mimics physiological afterload while also enabling beat-to-beat control of arterial pressure—pulmonary artery pressure, if used with the right side of the heart, or aortic pressure if used with the left side. Ensuring that arterial pressure remains between prescribed limits is critical for the safety of the organ under test. When beating outside of the body, the heart lacks the protective pleura that otherwise prevents over-extension of the ventricle in the event of high arterial pressures. Similarly, it is necessary to maintain a lower bound on aortic pressures to ensure sufficient perfusion of the coronary arteries during diastole despite variations in heart performance. These two factors make beat-to-beat control of cardiac afterload particularly important in *ex vivo* working heart models.

Cardiac afterload devices traditionally take one of two forms: a verbatim implementation of the common Windkessel lumped parameter models made

up of discrete resistive and compliant elements as in [Westerhof et al., 1971; Gellner et al., 2020b], described further in Section 2.2, or as a fixed resistive element supplemented by a centrifugal pump attached to the artery as in [White et al., 2015]. The latter are capable of maintaining a lower bound on diastolic aortic pressure as set by the pump speed, while systolic pressures are dependent on the geometry of the afterload. Windkessel-based afterload designs rely on the tuning of resistive and compliant elements to set diastolic and systolic pressures. However, the parameters in both these afterload concepts are only slowly adjustable, such as in [Fisher et al., 1984; Hatami et al., 2019; Gellner et al., 2020b], and the parameters are inherently coupled, making them unsuitable for beat-to-beat control of arterial pressures.

In [Pigot et al., 2022], a novel nonlinear afterload concept was introduced. The concept is based on a variable compliance chamber that enables diastolic and systolic limit control. Here, we propose a more versatile, actively controlled afterload concept designed to mimic physiological afterload and provide beat-to-beat arterial pressure control. The use of feedback control enables a much simpler operating principle, consisting of a constant flow source and variable flow conductance controlled at high bandwidth relative to hemodynamics. We describe the variable-conductance concept using first-principles models and provide a control strategy to emulate common afterload models with the addition of pressure limits. We then investigate the afterload concept using simulation.

2. Method

2.1 Variable-conductance afterload

We want to control a dynamic aortic flow impedance using a variable flow conductance. An ideal, time variable, flow conductor relates aortic pressure p to aortic volumetric flow φ through Ohm's law

$$p = \frac{\varphi}{Y}, \tag{1}$$

where the conductance Y is the reciprocal of the resistance $R = Y^{-1}$.

The conductance is varied by moving a plunger that changes the flow path cross section area between some small—but non-zero—minimum value and some larger maximal value, as shown in Figure 1. The plunger is designed so that its position u is directly proportional to the conductance throughout its range of motion $0 < u \leq d$:

$$Y = Y_0 \frac{u}{d} > 0. \tag{2}$$

While the heart is viewed as a flow source in the Windkessel model literature, see [Westerhof et al., 2009], it is arguably more physiologically correct

to consider it as a power source as discussed by [Pigot and Soltesz, 2022], providing a time-varying instantaneous power profile

$$w = p\varphi. \tag{3}$$

In normal physiology, a flow reversal can occur at the beginning of diastole, just before the aortic valve closes, after which the diastolic aortic pressure facilitates coronary perfusion until the start of systole. The coronary flow is small relative to total cardiac output, and thus not explicitly modeled in the Windkessel literature. From (2) we get that $u > 0 \Rightarrow Y > 0$. Taking this into account, (1) dictates $p < 0$ whenever $\varphi < 0$ (being the case during flow reversal) while $u > 0$. A problem with this is that unlike the arterial vasculature that can provide a reverse flow thanks to its compliance, our plunger cannot. To eliminate this problem, a mechanically forced auxiliary perfusate feed flow ϕ is introduced between the heart and the variable conductance, as schematically illustrated in Figure 1.

With the auxiliary flow in place, our conductance model (1) is extended into

$$p = \frac{\varphi + \phi}{Y}. \tag{4}$$

The auxiliary flow rate ϕ needs to be sufficiently large to ensure a positive aortic pressure. Let $w_{\min}$ be the smallest expectable instantaneous power. If $w_{\min} \geq 0$, we can omit the auxiliary flow and thus set $\phi = 0$. Otherwise, combining (3) and (4), we can write

$$pY = \frac{w}{p} + \phi. \tag{5}$$

Knowing that $Y > 0$, we can re-write (5) as

$$p^2 - \frac{\phi}{Y}p - \frac{w}{Y} = 0 \tag{6}$$

with solutions

$$p = \frac{\phi}{2Y} \pm \sqrt{\left(\frac{\phi}{2Y}\right)^2 + \frac{w}{Y}}. \tag{7}$$

There thus exists a positive real solution p if and only if

$$\frac{\phi^2}{4Y^2} + \frac{w}{Y} > 0. \tag{8}$$

Since $Y > 0$ according to (2), the condition (8) can equivalently be written

$$\phi^2 + 4wY > 0. \tag{9}$$

The case requiring the largest ϕ thus occurs when $-wY$ is maximal. Letting $w_{\min} < 0$ denote the smallest expected power, the worst case condition occurs at $w_{\min} Y_0$, making

$$\phi \geq 2\sqrt{-w_{\min} Y_0} \tag{10}$$

sufficient. Note, however, that (10) is only a necessary condition if $w_{\min}$ is attained while $Y = Y_0$.

2.2 Emulating dynamics

Linear time-invariant reference dynamics Our objective is to actively control the position u of the plunger in Figure 1 to emulate desired dynamics between aortic pressure p and flow φ. In a realistic scenario one could measure the aortic pressure p with either a sensor in the perfusate stream, or—knowing the plunger cross section area—by the force by which the perfusate pushes onto the plunger. However, accurate direct measurements of aortic flow φ or instantaneous cardiac power w at a sample rate matching the time scale of the involved cardiac dynamics (at least tens of Hertz) remain elusive. We will circumvent the need for such measurements, through using the combined actuation model of (4) and (2) as a very simple soft sensor providing an estimate

$$\varphi = \frac{Y_0}{d} up - \phi. \tag{11}$$

In (11) we use the same notation for measured and actual pressure, as well as for estimated and actual flow. This brings us to a set of assumptions that we make:

- Disturbances acting on the pressure measurement and plunger position control are negligible.
- Discrepancies between the plunger model (2) and the dynamics of the device implementing it are negligible. This allows us to utilize (2) in (11).
- Delay between obtaining a new pressure sample and updating plunger position is negligible. This allows us to update plunger position instantaneously based on fresh pressure measurements.
- The plunger can be moved fast compared to the time scale of the (cardiac) dynamics that the system is to emulate. This allows us to assume that there are no dynamics between change of plunger position reference and actual plunger position u.
- Pressure is equitemporally sampled at a constant rate h that is sufficiently faster than the emulated dynamics, and slower than the plunger position dynamics. This means that w does not change notably between consecutive sampling instances.

- The auxiliary flow ϕ is controlled to a known constant level, such that $\varphi + \phi > 0$, or equivalently by (4) $p > 0$ is maintained at every instance.
- Historic pressure-flow data are consistent with the reference dynamics. This means that it is sufficient for us to maintain this consistency from one sample to the next in order to perfectly track the reference dynamics.

We deem it realistic to approximate the above assumptions related to modeling and measurement well through adequate hardware design, and discuss the topic further in Section 4.

Let the reference dynamics that we wish to emulate be expressed through a continuous-time transfer function $G(s)$ (such as a Windkessel model) from aortic flow φ to pressure p. Zero-order-hold sampling of G at rate h, and subsequently applying the inverse z-transform then produces a difference equation

$$p_k = H(q^{-1})\varphi_k, \tag{12}$$

where subscript k indicates the time $t = kh$, so that for instance $p_k = p(kh)$, and where q^{-1} is the backward shift operator such that $q^{-m}p_k = p_{k-m}$.

If G is of order n, H can be parameterized as

$$H(q^{-1}) = \frac{b_0 + b_1 q^{-1} + \ldots + b_n q^{-n}}{1 + a_1 q^{-1} + \ldots + a_n q^{-n}}, \tag{13}$$

As a consequence of zero-order-hold sampling, there is no approximation error associated with (13) at the sampling instances. The constant coefficients b_k and a_k of (13) can be numerically (and in some cases analytically) determined based on G and h as described in for example [Åström and Wittenmark, 2011], and thus assumed to be known to us. For future convenience we also introduce the notation

$$B_1(q^{-1}) = b_1 q^{-1} + \ldots + b_n q^{-n}, \tag{14a}$$

$$A_1(q^{-1}) = a_1 q^{-1} + \ldots + a_n q^{-n}, \tag{14b}$$

that enable us to write

$$H(q^{-1}) = \frac{b_0 + B_1(q^{-1})}{1 + A_1(q^{-1})}. \tag{15}$$

Let $\tilde{p}_k$ denote the pressure measurement sampled at time $t = kh$, calculated in simulation using (7). We use (3) and (11) to reconstruct the (directly immeasurable) instantaneous power

$$w_k = \tilde{p}_k \tilde{\varphi}_k = \tilde{p}_k \left(\frac{Y_0}{d} u_k \tilde{p}_k - \phi \right). \tag{16}$$

where $\tilde{\varphi}_k$ is the actuation-model-based flow corresponding to $\tilde{p}_k$.

If (13) lacks direct term, signified by $b_0 = 0$, we can—assuming as stated above that we have historically matched the reference dynamics—solve for the pressure

$$p_k = \underbrace{B_1(q^{-1})\varphi_k - A_1(q^{-1})p_k}_{c_k}. \tag{17}$$

The right-hand-side, denoted c_k can be considered known at sampling instance k, since $A_1(q^{-1})p_k$ is a known linear combination of previously computed pressures, while $B_1(q^{-1})\varphi_k = B_1(q^{-1})(w_k/p_k)$ only relies on previously computed pressures and reconstructed instantaneous powers. One can note that in order for the reference dynamics to be trackable, it is required that $c_k > 0$. We will not go into details of analysing conditions for this, but suffice it to conclude that any reasonable LTI system (such as a Windkessel model) intended to describe the dynamics between aortic flow φ and pressure p will stay in the regimen of $p > 0$.

Thus p_k is known and the plunger can be moved to a new position u_k that is consistent with both the reconstructed instantaneous power w_k of (16) and the aortic pressure p_k of (17) dictated by the reference dynamics. This is done by combining (5) and (2), resulting in

$$u_k = \frac{d}{Y_0 p_k}\left(\frac{w_k}{p_k} + \phi\right). \tag{18}$$

If there is a direct term, signified by $b_0 \neq 0$, (13) instead gives us

$$p_k - b_0\varphi_k = \underbrace{B_1(q^{-1})\varphi_k - A_1(q^{-1})p_k}_{c_k}, \tag{19}$$

where c_k is the same as in (17) and thus can be considered known. Using (3) we can eliminate φ_k from (19) and arrive at the quadratic equation

$$p_k^2 - c_k p_k - b_0 w_k = 0 \tag{20}$$

with solutions

$$p_k = \frac{c_k}{2} \pm \sqrt{\frac{c_k^2}{4} + b_0 w_k}. \tag{21}$$

In order to honor continuity of the pressure profile, the positive solution that minimizes $p_k - p_{k-1}$ is chosen. We may also note that the solutions of (21) turn complex when $c_k^2 + 4b_0 w_k < 0$. For the concerned Windkessel models it holds that $b_0 \geq 0$, leading to complex solutions if and only if $w_k < -c_k^2/(4b_0)$.

As in the case without direct term, the computed reference pressure p_k is used to update the plunger position from u_{k-1} to u_k according to (18). This procedure is then repeated each time a new pressure measurement sample arrives.

Enforcing pressure limits Pressure limits can be imposed to ensure that the aortic pressure p remains within a safe span $p_{\min} \leq p \leq p_{\max}$. A simple way to achieve this is to clamp p_k to this span before applying (18). Doing so will of course violate the dynamics whenever the limits are active, but provide a practically feasible alternative to online adjustment of Windkessel model parameters to maintain pressure limits in presence of *e.g.* arrythmic events, as illustrated later in Section 3. Note that the Windkessel state (p,φ) must be tracked during clamping so as not to disrupt the desired dynamics.

Two-element Windkessel model Starting with the simplest Windkessel model, made up of two elements as described in [Frank, 1899; Westerhof et al., 2009], the dynamics from flow to pressure are expressed by the transfer function

$$G(s) = \frac{R_p}{1 + CR_p s}. \tag{22}$$

Zero-order-hold discretization and subsequent application of the inverse z transform, as outlined in Section 2.2, yields

$$H(q) = \frac{b_0 + b_1 q^{-1}}{1 + a_1 q^{-1}}, \tag{23}$$

where

$$\begin{aligned} b_0 &= 0, \\ b_1 &= R_p \left(1 - \tau_1\right), \\ a_1 &= -\tau_1, \end{aligned}$$

and

$$\tau_1 = e^{-h/(CR_p)}.$$

The lack of direct term means that we can employ (17) with

$$c_k = R_p \left(1 - \tau_1\right) q^{-1} \varphi_k + \tau_1 q^{-1} p_k. \tag{24}$$

Four-element Windkessel model Similarly, the 4-element Windkessel model as described in [Deswysen et al., 1980; Westerhof et al., 2009] is expressed by the transfer function

$$G(s) = R_c + \frac{R_p}{1 + CR_p s} - \frac{R_c}{1 + L/R_c s}. \tag{25}$$

The zero-order-hold discretized version has the structure

$$H(q^{-1}) = \frac{b_0 + b_1 q^{-1} + b_2 q^{-2}}{1 + a_1 q^{-1} + a_2 q^{-2}}, \tag{26}$$

Table 1. Windkessel model parameters used in the simulations.

Model	R_p $\frac{\text{mmHg}}{\text{L/min}}$	C $\frac{\text{L}}{\text{mmHg}}$	R_c $\frac{\text{mmHg}}{\text{L/min}}$	L $\frac{\text{mmHg·min}}{\text{L/min}}$
2-element	13.6	0.0996		
4-element	13.6	0.0743	0.952	0.0952

where

$$\begin{aligned} b_0 &= R_c, \\ b_1 &= R_p - R_c - \tau_1(R_p + R_c), \\ b_2 &= R_c\tau_1 - R_p\tau_2 + R_p\tau_1\tau_2, \\ a_1 &= -\tau_1 - \tau_2, \\ a_2 &= \tau_1\tau_2, \end{aligned}$$

and

$$\tau_2 = e^{-R_c h/L}.$$

The presence of direct term means that we can employ (21) with

$$c_k = \left(b_1 q^{-1} + b_2 q^{-2}\right)\varphi_k - \left(a_1 q^{-1} + a_2 q^{-2}\right) p_k. \tag{27}$$

2.3 Simulation examples

Simulations were performed to emulate 2- and 4-element Windkessel dynamics, with and without pressure limiting. The simulations were implemented in Julia, and the code and data used to generate the results published here are available on GitHub, see [Pigot, 2023]. Measured human aortic volumetric flow from [Stergiopulos et al., 1999] was used as input to discretized Windkessel models with parameters fit to the corresponding human aortic pressure measurements as described in [Pigot et al., 2021], provided

in Table 1. Both data sampling and model discretization were done with period $h = 5\,\text{ms}$. The product of the input flow and resulting pressures from each model were used as the driving cardiac power for the respective simulations.

Maximum plunger displacement d was set to 3 cm, and maximum conductance $Y_0 = 0.9\,(\text{L/min})/\text{mmHg}$ was tuned heuristically to yield displacements within this range. The lower bound $\phi \geq 49.6\,\text{L/min}$ given by (10) (for the 2-element model) is very conservative in practice, since w_{min} does not correspond to the fully open plunger position where $Y = Y_0$. Therefore, ϕ was set heuristically to a value below that, 21 L/min. The initial plunger position was set to $u = d/2$ to generate the first p and φ values used for plunger

position control, which avoids excessive loading of the heart during startup. After several beats, transient behavior caused by the initial conditions dies out and the simulation reaches steady-state. The simulation results reported in Section 3 show the last two of 20 cardiac cycles, long after initial condition transients become negligible.

3. Results

Figures 2 and 3 show afterload simulations where the plunger position is actively controlled to replicate the 2- and 4-element Windkessel dynamics in Table 1, respectively. The plots illustrate simulation with (blue, solid) and without (red, dashed) upper and lower pressure limits on aortic pressure p. The limits were set to 80 and 105 mmHg for illustrative purposes, though a wider range of admissible pressures would generally be considered.

Practical examples of pressure-limiting are shown in Figures 4 and 5, where two arrythmic events are simulated with pressure limits set at 50 and 120 mmHg using the the 4-element Windkessel dynamics in Table 1. In Figure 4 the third beat occurs early (shifted back by 70% of the cardiac period), as in [Pigot and Soltesz, 2022], causing the upper limit to be enforced. To illustrate the lower limit, the second beat in Figure 5 is delayed by one cardiac period.

In all mentioned examples, the afterload simulations without pressure limits resulted in p and φ that are indistinguishable from the corresponding discrete-time Windkessel model simulations (error less than single precision machine epsilon). The pressure-limit-imposed differences in aortic flow in Figures 2 and 3 appear subtle compared to the differences in pressure. This is due to the differences between the minimum and maximum values; the differences in pressure appear clearer as it is plotted from 70–110 mmHg while flow is plotted from −5–30 L/min.

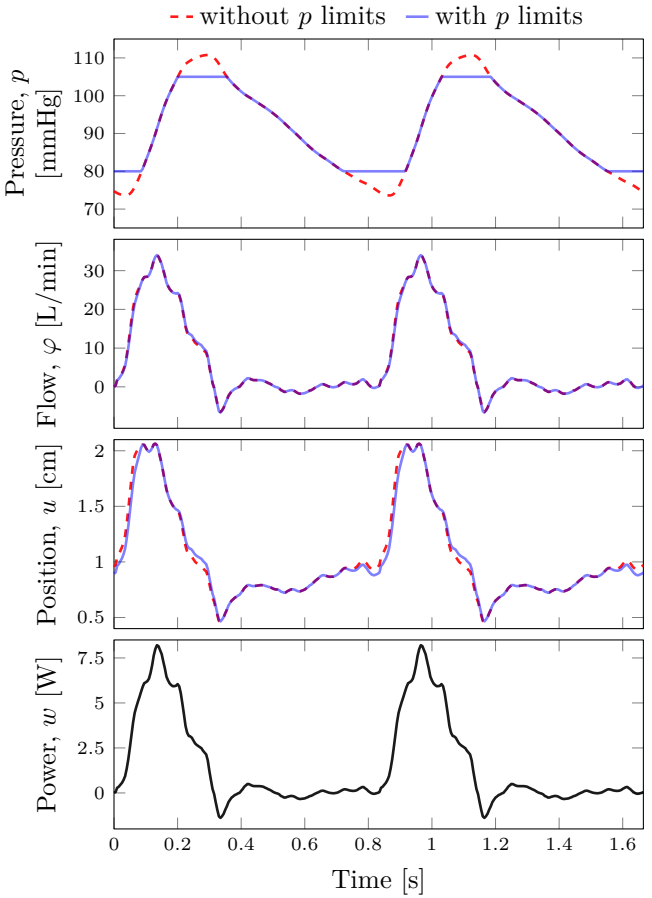

Figure 2. Afterload simulation with plunger position u actively controlled to replicate 2-element Windkessel dynamics with (blue, solid) and without (red, dashed) limits on aortic pressure p, driven by cardiac power w. The limits are 80 and 105 mmHg. The resulting p and φ without limits are indistinguishable from the 2-element Windkessel model simulation.

4. Discussion

The method presented here illustrates that it is in principle possible to replicate a wide range of dynamics relating pressure and flow, using the proposed afterload concept with auxiliary flow, schematically illustrated in Figure 1. However, in a viable implementation, the assumption made in Section 2.2 would require explicit attention. There will for example be noise on the pres-

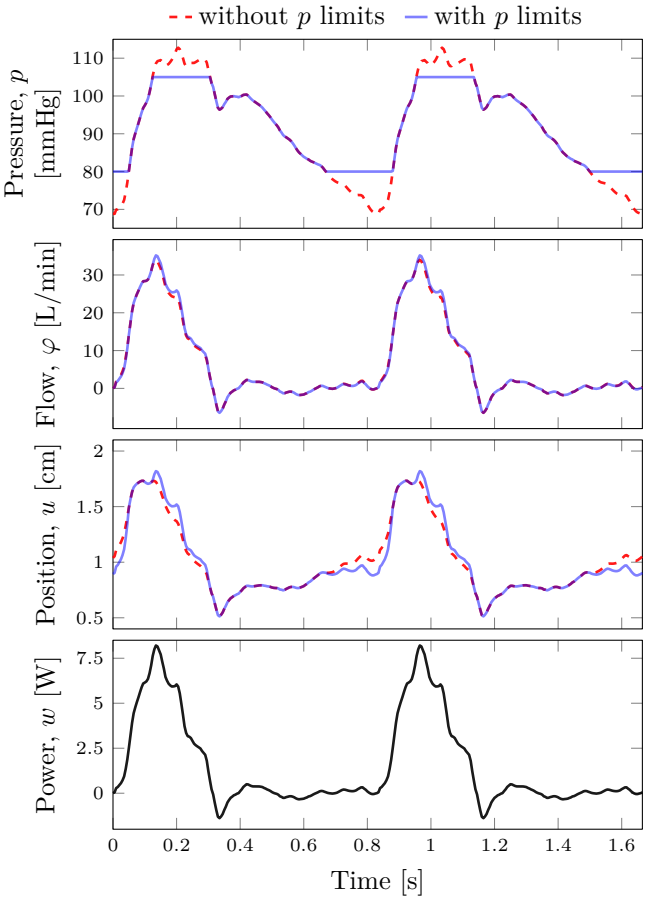

Figure 3. Afterload simulation with plunger position u actively controlled to replicate 4-element Windkessel dynamics with (blue, solid) and without (red, dashed) limits on aortic pressure p, driven by cardiac power w. The limits are 80 and 105 mmHg. The resulting p and φ without limits are indistinguishable from the 4-element Windkessel model simulation.

sure measurement $\tilde{p}$, and inaccuracies in the actuation model (2). Investigating the impact of deviations from the assumptions will be a central part of future work. A simple way would be to introduce stochastic noise models, such as additive or multiplicative Gaussian noise to the simulation and investigate the impact of its variance on tracking performance. To get a better understanding of where in the cardiac cycle the system is most sensitive to measurement noise one could instead assume perfect tracking up to sample k, then compute and plot $\partial(p_k - p_k^*)/\partial\tilde{p}_k$, where p_k^* is the pressure corresponding to the updated plunger position, based the noise-free measurement $\tilde{p}_k^*$, while p_k is the corresponding pressure that would arise if the measurement was instead $\tilde{p}_k$. Similar analyses can be conducted to map out the impact of actuation model inaccuracies. However, it can be expected that they are more difficult to accurately characterize than the pressure measurement noise. Depending on the outcome of the analyses mentioned above, it might be necessary to de-tune tracking performance to reduce sensitivities to these deviations from the assumptions.

When first attaching a cardioplegic heart to the afterload system, it could be set to a constant pressure target. In this mode, the afterload would provide a flow-controlled constant pressure source to perfuse the coronary arteries—so called Langendorff mode perfusion, see [Langendorff, 1895]—wherein any perfusate not entering the coronary arteries would be shunted through the afterload, as evidenced by the illustration in Figure 1. After the resumption of normal cardiac rhythm, the afterload dynamics could be controlled to the desired dynamics, such as 4-element Windkessel with pressure limits. Our aim is to perform such tests in large animal experiments using hearts procured from pigs. A cyber-physical implementation of mechanism of Figure 1 has been constructed. Experiments are planned to commence shortly, once the prototype has undergone dry run tests.

5. Acknowledgements

This research was funded by the Swedish Research Council (grant 2017-04989), the Swedish Foundation for Strategic Research (grant SM21-0037), the Hans-Gabriel and Alice Trolle-Wachtmeister foundation, and the ELLIIT Strategic Research Area. We extend special thanks to our collaborators with the Division of Thoracic Surgery at Lund University, in particular Stig Steen and Trygve Sjöberg.

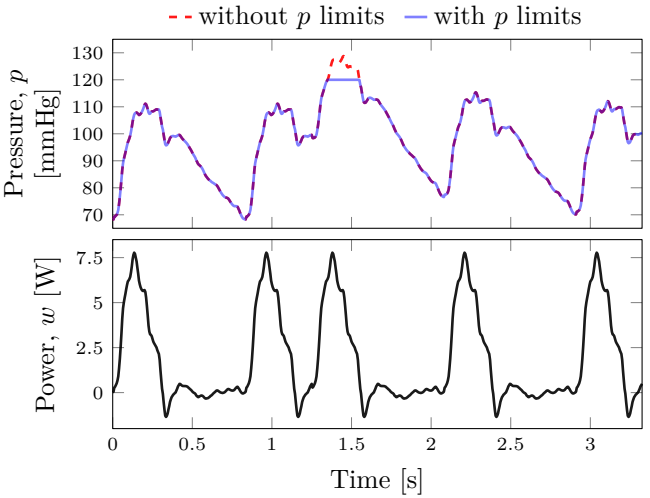

Figure 4. Afterload simulation with the third beat shifted back by 70% of the beat period. The afterload is controlled to replicate 4-element Windkessel dynamics with (blue, solid) and without (red, dashed) limits on aortic pressure p, with limits set to 50 and 120 mmHg.

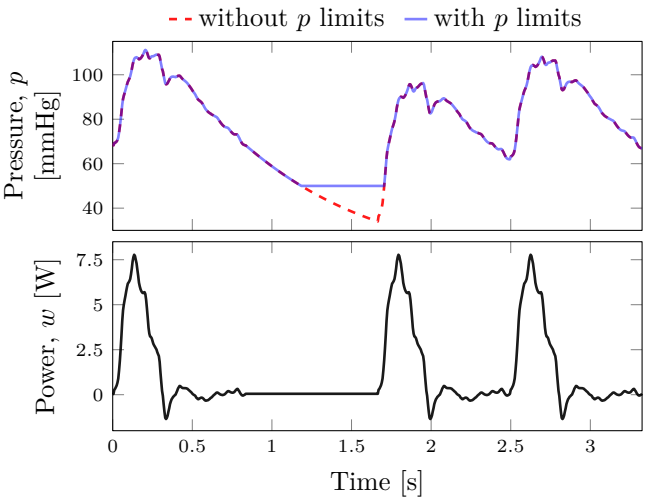

Figure 5. Afterload simulation with the second beat delayed by one beat period. The afterload is controlled to replicate 4-element Windkessel dynamics with (blue, solid) and without (red, dashed) limits on aortic pressure p, with limits set to 50 and 120 mmHg.

References

Åström, K. J. and B. Wittenmark (2011). *Computer-Controlled Systems: Theory and Design, Third Edition*. Dover Publications, Mineola, N.Y. ISBN: 978-0-486-48613-0.

Deswysen, B., A. A. Charlier, and M. Gevers (1980). "Quantitative evaluation of the systemic arterial bed by parameter estimation of a simple model". *Medical and Biological Engineering and Computing* **18**:2, pp. 153–166. DOI: 10.1007/BF02443290.

Fisher, A., R. E. Challis, and P. Swann (1984). "A controllable artificial afterload for isolated heart studies". *J Biomed Eng* **6**:4, pp. 305–310. DOI: 10.1016/0141-5425(84)90080-3.

Frank, O. (1899). "Die Grundform des arteriellen pulses. Erste Abhandlung. Erste Abhandlung." *Zeitschrift für Biologie* 37, pp. 485–526.

Gellner, B., L. Xin, R. V. Pinto Ribeiro, et al. (2020a). "The implementation of physiological afterload during ex situ heart perfusion augments prediction of posttransplant function". *American Journal of Physiology. Heart and Circulatory Physiology* **318**:1, H25–H33. DOI: 10.1152/ajpheart.00427.2019.

Gellner, B., L. Xin, R. V. P. Ribeiro, V. Bissoondath, P. Lu, M. B. Adamson, F. Yu, E. Paradiso, J. Zu, C. A. Simmons, and M. V. Badiwala (2020b). "The Implementation of an Adjustable Afterload Module for Ex Situ Heart Perfusion". *Cardiovasc Eng Tech* **11**:1, pp. 96–110. DOI: 10.1007/s13239-019-00447-w.

Hatami, S., C. W. White, M. Ondrus, X. Qi, M. Buchko, S. Himmat, L. Lin, K. Cameron, D. Nobes, H.-J. Chung, J. Nagendran, and D. H. Freed (2019). "Normothermic Ex Situ Heart Perfusion in Working Mode: Assessment of Cardiac Function and Metabolism". *JoVE (Journal of Visualized Experiments)* 143, e58430. DOI: 10.3791/58430.

Langendorff, O. (1895). "Untersuchungen am überlebenden Säugethierherzen". *Pflügers Arch.* **61**:6, pp. 291–332. DOI: 10.1007/BF01812150.

Pigot, H. and K. Soltesz (2022). "The Differential-Algebraic Windkessel Model with Power As Input". In: *American Control Conference, 2022 (in press)*. IEEE - Institute of Electrical and Electronics Engineers Inc.

Pigot, H. (2023). *Actively controlled cardiac afterload simulation*. URL: https://github.com/hpigot/controlled-cardiac-afterload (visited on 2023-03-10).

Pigot, H., J. Hansson, A. Paskevicius, Q. Liao, T. Sjöberg, S. Steen, and K. Soltesz (2021). "Identification of cardiac afterload dynamics from data". *IFAC-PapersOnLine*. 11th IFAC Symposium on Biological and Medical

Systems BMS 2021 **54**:15, pp. 508–513. DOI: 10.1016/j.ifacol.2021.10.307.

Pigot, H., K. Soltesz, A. Paskevicius, Q. Liao, T. Sjöberg, and S. Steen (2022). "A novel nonlinear afterload for ex vivo heart evaluation: Porcine experimental results". *Artificial Organs* **46**:9, pp. 1794–1803. DOI: 10.1111/aor.14307.

Stergiopulos, N., B. E. Westerhof, and N. Westerhof (1999). "Total arterial inertance as the fourth element of the windkessel model". en. *American Journal of Physiology-Heart and Circulatory Physiology* **276**:1, H81–H88. DOI: 10.1152/ajpheart.1999.276.1.H81.

Westerhof, N., G. Elzinga, and P. Sipkema (1971). "An artificial arterial system for pumping hearts." *Journal of Applied Physiology* **31**:5, pp. 776–781. DOI: 10.1152/jappl.1971.31.5.776.

Westerhof, N., J.-W. Lankhaar, and B. E. Westerhof (2009). "The arterial Windkessel". *Med Biol Eng Comput* **47**:2, pp. 131–141. DOI: 10.1007/s11517-008-0359-2.

White, C. W., E. Ambrose, A. Müller, Y. Li, H. Le, B. Hiebert, R. Arora, T. W. Lee, I. Dixon, G. Tian, J. Nagendran, L. Hryshko, and D. Freed (2015). "Assessment of donor heart viability during ex vivo heart perfusion". *Can. J. Physiol. Pharmacol.* **93**:10, pp. 893–901. DOI: 10.1139/cjpp-2014-0474.

White, C. W., S. J. Messer, S. R. Large, J. Conway, D. H. Kim, D. J. Kutsogiannis, J. Nagendran, and D. H. Freed (2018). "Transplantation of Hearts Donated after Circulatory Death". *Frontiers in Cardiovascular Medicine* **5**, p. 8. DOI: 10.3389/fcvm.2018.00008.

Erata

There was a unit error in time in Paper II. The input data, originally measured in seconds, were not converted to minutes when fitting parameters with minutes as their time-unit. Although this led to incorrectly scaled parameter values, first introduced in Table 2., the presented methods and conclusions remain valid. These incorrect parameter values were also used for the simulations in Paper III and V.

Utvärdering av donerade hjärtan inför transplantation

Henry Pigot
Institutionen för Reglerteknik

Populärvetenskaplig sammanfattning av doktorsavhandlingen *Afterload system design for functional donor heart assessment*, mars 2024. Avhandlingen kan laddas ner från: http://www.control.lth.se/publications

---

Denna avhandling strävar efter att förbättra utvärderingen av hjärtan donerade för transplantation, i syfte att möta bristen på användbara organ. Många donerade hjärtan kasseras i dagsläget på grund av osäkerhet kring deras tillstånd, vilket ofta är relaterat till syrebrist. Denna syrebrist kan orsakas av hjärtstillestånd hos donatorn eller uppstå under transport.

För närvarande saknas en pålitlig metod för att bedöma hjärtats funktion efter syrebristskadan och före transplantation. Att observera hjärtat under vanliga förhållanden, där det pumpar blod mot kroppens motstånd, är avgörande för en korrekt bedömning. Detta kan åstadkommas med ett utvärdingssystem där hjärtat slår mot ett mekaniskt motstånd som härmar kroppens.

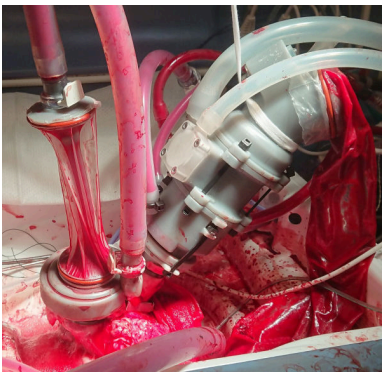

Ett motstånd (grått, till höger), som imiterar kroppen, används för att bedöma hjärtats (längst ner) pumpkapacitet under realistiska förhållanden. Foto från Artificial Organs, Pigot et al, 2022.

Utvecklingen av matematiska modeller och datorbaserade simuleringsverktyg som imiterar förhållandena ett hjärta upplever när det pumpar blod i människokroppen utgör en central del av avhandlingen. Fokus har legat på att skapa justerbara flödesmotstånd som noggrant återskapar dessa förhållanden. Eftersom varje hjärttransplantationspatient är unik, justeras motstånden automatiskt av en dator för att återspegla blodomloppet i den tilltänkta mottagaren och samtidigt säkerställa att skadligt höga eller låga blodtryck i hjärtat undviks. Detta uppnås genom återkoppling från tryckgivare och andra sensorer. Utöver simuleringar har en version av systemet med 3D-utskrivna flödesmotstånd framgångsrikt demonstrerats på grishjärtan. Detta är ett viktigt steg på vägen till kliniken där teknologin kan utgöra ett viktigt beslutsunderlag som möjliggör fler säkra transplantationer.

A system for improving heart assessment before transplantation

Henry Pigot

Department of Automatic Control

Popular science summary of the doctoral thesis *A Cyberphysical System for Donor Heart Assessment*, March 2024. The thesis can be downloaded from: http://www.control.lth.se/publications

---

This research aims to improve the assessment of donor heart quality for transplantation to address the shortage of viable organs. Many donor hearts are currently discarded due to uncertainties about their condition, often related to oxygen deprivation. This deprivation can occur due to cardiac arrest in the donor, or during transport of the heart from the donor to the recipient.

Currently, there is no reliable method for assessing heart function after oxygen deprivation damage and prior to transplantation. Observing the heart under normal conditions, where it pumps blood against the body's resistance, is crucial for an accurate assessment. This can be achieved using an evaluation system where the heart beats against a mechanical resistance that mimics the body.

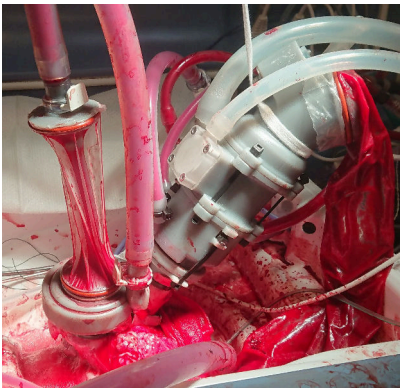

A resistance (right, grey), that imitates the body, is used to judge the heart's (bottom) pumping function under realistic conditions. Photo from Artificial Organs, Pigot et al, 2022].

The development of mathematical models and computer-based simulation tools that emulate the conditions a heart faces when pumping blood in the human body make up a central part of the thesis. Focus is also put on creating adjustable resistance devices that accurately replicate these conditions. Since all heart transplant patients are different, the devices are designed to adjust resistance to match a variety of potential recipients, while preventing harmful resistance levels. This is achieved through precise computer control, which continuously monitors the heart's condition and adjusts the resistance as needed. Beyond simulations, a version of the system with 3D-printed resistance devices are successfully demonstrated with pig hearts. This is an important step toward clinical implementation of the technology, where it can act as an important basis for decision-making that enables more safe transplants.